Lymphoid Tissue Damage in HIV and SIV Infections Depletes Naive T Cells and Limits Immune Reconstitution after Anti-retroviral Therapy

A DISSERTATION

SUBMITTED TO THE FACULTY OF THE GRADUATE SCHOOL

OF THE UNIVERSITY OF MINNESOTA

BY

Ming Zeng

IN PARTIAL FULFILLMENT OF THE REQUIREMENTS

FOR THE DEGREE OF

DOCTOR OF PHILOSOPHY

Ashley T. Haase, M.D., Advisor

May, 2012

Acknowledgements

First of all, I am heartily thankful to my supervisor, Dr. Ashley T. Haase for his encouragement, guidance and support from the initial to the final stage of my PhD studies. This enabled me to develop a solid understanding of the project and HIV research field, overcome obstacles in the research, and finally finish this dissertation. Without his insightful advice and persistent help, this dissertation would not have been possible. I am very also grateful to his wise and critical suggestions and support for my career development. He set a great example for me to follow in my academic career.

I also want to thank my PhD committee members: Dr. Peter Southern, Dr. David Masopust, and Dr. Brian Fife, for their consistent encouragement, motivation, enthusiasm, and intellectual input. These greatly enhanced the quality of my research and helped me to complete the research and write this dissertation.

I am very grateful to all my great lab mates and friends. They create a fun and stimulating research environment. I was fortunate enough to join such a wonderful lab. I appreciate their insightful discussions, advice, and (obscure) jokes very much. They are Dr. Jacob Estes, Dr. Anthony Smith, Steve Wietgrefe, Mary Zupancic, Lijie Duan, Dr. Kathy Staskus and Dr. Qingsheng Li. I also like to thank Colleen O'Neill and Timothy Leonard for their critical help in preparing the manuscripts and figures, Louise Shand for her help and advice for my graduate study, the whole MICaB graduate program for support, Dr. John Carlis for his extremely helpful advice on writing and logical thinking and our key collaborator Dr. Timothy Schacker for his continuous support and critical advice.

Lastly, I would like to sincerely thank my dear family and friends, particularly my parents Weiguang Zeng, Na Liang, my parents-in law Tiebing Shi, Sujie Gu, my grandparents Huaizhao Liang, Likun Gan, Peiqing Jian, Zhaojun Zeng and my wife Xiaolei Shi. Without their endless, unconditional, and dedicated love and support, this research and dissertation couldn’t be possibly finished.

Abstract

Human immunodeficiency virus (HIV) infection causes the Acquired Immunodeficiency Syndrome (AIDS), a condition in which progressive failure of the immune system allows life-threatening opportunistic infections (OIs) and cancers to thrive. HIV primarily infects and depletes CD4+ T cells, a cell type that is central to the maintenance of host's immunocompetency. The slow depletion of CD4+ T cells has been attributed to direct mechanisms such as viral killing and indirect mechanisms such as increased apoptosis accompanying the chronic immune activation associated with HIV infections. Highly active anti-retroviral therapy (HAART) can potently suppress HIV viral replication and largely normalize associated immune activation thereby significantly increasing the CD4+ T cell count and decreasing the morbidity and mortality in HIV infections. Yet more than a decade after the introduction of HAART, it is clear that relatively few individuals will achieve normal levels of peripheral blood CD4+ T cells, and up to 20% of the patients will have little or no increase at all despite the impact of HAART on the virological side of the equation. This limited immune reconstitution is most prevalent in patients starting HAART in the chronic stage of disease and in patients with older age and strongly correlates with significantly higher morbidity and mortality compared to uninfected populations. This suggests that there is a persistent defect in homeostasis in the CD4+ T cell population that is not fully corrected by HAART. However, the underlying mechanisms of this limited immune reconstitution after HAART are as yet unknown. More recently, there is increasing evidence showing that there is progressive fibrotic damage during HIV infection to the structure of lymphoid tissue (LTs) and the extent of this damage strongly correlates with the extent of depletion of naïve CD4+ T cells before HAART and the extent of immune reconstitution after HAART. Since LT structure is critical for the homeostasis of naïve T cells, we hypothesized that the LT damage during HIV infection contributes to CD4+ T cell depletion and limits immune reconstitution after HAART. In this dissertation, I tested this central hypothesis by providing experimental data to answer the following questions: 1) how does LT fibrosis deplete CD4+ T cells during HIV infection? 2) How does LT fibrosis limit the

restoration of CD4+ T cells? 3) What are mechanisms leading to LT fibrosis? 4) Could a therapeutic method be developed to avert/revert this pathological change? Collectively, the data presented here provide insights on the mechanisms of LT damage and how LT damage contributes to CD4+ T cell depletion and limited immune reconstitution. These insights point to novel avenues to improve immune reconstitution in HIV infected patients.

TABLE OF CONTENTS

List of Tables

List of Figures

Chapter 1 Literature Review

Introduction to HIV infection

HIV was first isolated and identified in 1983 as the cause of AIDS [1-2]. In the following three decades, HIV spread rapidly and globally to cause a severe public health crisis. To date, the Joint United Nations Program on HIV/AIDS (UNAIDS) estimates that more than 65 million people have been infected with HIV and about 25 million people have died from AIDS [3-4]. Currently, a total of 33.4 million [31.1 million–35.8 million] adults and children are living with HIV, and in 2008, an estimated 2.7 million [2.4 million–3.0 million] new HIV infections occurred with about 2 million [1.7 million–2.4 million] deaths from AIDS-related illnesses worldwide [4].

Sub-Saharan Africa is the most heavily affected region, accounting for 71% of all new HIV infections in 2008. An estimated 20.4 million adults and 2.1 million children younger than 15 years are currently living with HIV infection in sub-Saharan Africa [4]. These children, among whom less than 10% are receiving public support and services, often live in severe poverty and are vulnerable to abuse [5], thereby increasing their risk of HIV transmission.

Routes of HIV transmission

HIV can be transmitted through contact with body fluid from HIV infected patients. The majority of HIV infections are acquired through unprotected sex. This route accounts for about 85% of the global HIV burden [4]. Other routes of HIV transmission include mother-to-child transmission and blood transmission.

Stages of HIV infection

The course of HIV infection can be generally classified into three stages: acute/primary infection stage, clinically asymptomatic stage, and AIDS stage [6-7].

The first stage of HIV infection is called acute/primary infection stage and usually lasts for several weeks. This stage is characterized by rapid viral replication, leading to an abundance of virus in the peripheral blood called viremia. HIV plasma viremia usually

peaks at three to four weeks post exposure and can be as high as 10 million copies per µl [7-9]. The viral load then declines spontaneously, coincident with the cellular immune response, before reaching a steady state called the viral set point [10]. During the acute/primary infection stage, many patients develop an influenza or mononucleosis-like illness, whose symptoms may include fever, lymphadenopathy, pharyngitis, rash, myalgia, malaise, mouth and esophageal sores, and may also include, but less commonly, headache, nausea and vomiting, enlarged liver/spleen, weight loss, thrush, and neurological symptoms [11].

The second stage of HIV infection is the clinically asymptomatic stage. The length of this stage can vary between weeks and years among HIV-infected patients. As its name suggests, this stage is free from major symptoms, although there may be swollen lymph glands. Toward the middle and end of this period, the viral load begins to rise and the CD4+ cell count begins to drop.

AIDS is the final stage of HIV infection, defined by low CD4+ T cell counts (fewer than 200 cells/µl), various OIs, cancers and other conditions [12-13]. Common early OIs include oral candidiasis (thrush) caused by *Candida* species, pneumonia caused by the fungus *Pneumocystis jiroveci* infection, and tuberculosis due to *Mycobacterium tuberculosis* infection. Later, reactivation of latent herpes viruses, infection with or reactivation of cytomegalovirus or *Mycobacterium avium* complex, shingles, Epstein-Barr virus-induced B-cell lymphomas, or Kaposi's sarcoma become more prominent [14-15].

HIV pathogenesis

HIV replication cycle

HIV belongs to the family of *Retroviridae*. Viruses in this family are called retroviruses (literally, "reverse viruses") because of the unique step during their replication cycle

called reverse transcription in which the usual flow of genetic information in cells-DNA to RNA-is reversed- from the RNA viral genome to DNA o [1-2, 16-18].

More specifically, the HIV replication cycle can be divided into several major steps. These steps include viral entry into target cells, intracellular reverse transcription, integration and replication, assembly and budding from target cells [19]. The infection process starts from viral entry into target cells, mainly CD4+ T cells. When HIV virions meet target CD4+ T cells, the Env protein complex on the virions interacts with the CD4 molecules and CCR5 (or CXCR4) chemokine receptors on CD4+ T cells. This allows the release of the viral capsid containing viral genomic RNA into the cytoplasm [20-21]. After entry into target cells, HIV uses a viral enzyme called reverse transcriptase to convert its RNA into DNA and integrate the viral DNA into host cell's genome by another viral enzyme integrase [22-23]. Once integrated, the HIV DNA is known as a provirus. The provirus may lie dormant within a cell for a long time. But, when the infected CD4+ T cell becomes activated, it treats HIV genes in much the same way as human genes. First it converts HIV DNA into RNA by using the host cell enzyme RNA Pol III [24]. Then viral RNA is transported outside the nucleus to direct the translation of viral proteins while the full-length RNA itself serves as the genome for the production of new virions. Thereafter, viral genomic RNA, viral protein and enzymes are assembled together to form new virions and then released from the infected cell to begin the replication cycle anew. The viral protease plays a vital role at this stage of the HIV life cycle by cleaving viral structural protein into smaller pieces, which are used to construct mature viral cores [19, 25-29].

Anti-retroviral therapy

The understanding of these key steps of the HIV replication cycle provides a framework for the sites and mechanisms of action of anti-retroviral drugs. Based on the steps of HIV replication cycle that the drug inhibits, major anti-retroviral drugs can be classified as entry inhibitors, CCR5 receptor antagonists, reverse transcriptase inhibitors, protease inhibitors and integrase inhibitors [30-33].

Highly active anti-retroviral therapy (HAART) refers to the combination of several anti-retroviral drugs to treat HIV infected patients and is the current standard treatment for HIV infected patients. HAART has been a great advance in HIV infection clinical management as it significantly decreases morbidity and mortality in HIV infections [34-37]. In most industrialized nations, life expectancies associated with the infection have increased, and the rate of progression to AIDS has decelerated since the introduction of HAART [38-39].

Despite these beneficial effects on HIV infected patients by HAART, one important clinical issue with HAART is that the immune reconstitution in most HAART treated patients is very slow and usually incomplete for reasons yet fully understood [40-45]. I will discuss this issue in the following sections in greater detail.

Chronic immune activation and HIV infection

The slow depletion of CD4+ T cells during HIV infection ultimately leads without treatment to AIDS defining illnesses and death. It was originally thought that direct killing of CD4+ T cells by the HIV virus is the major mechanism that leads to the depletion of CD4+ T cells. However, this mechanism can not fully explain the observations that HIV can only infect a small proportion of CD4 T cells (estimated at 1 in 100 to 1 in 1,000) and yet still overwhelm the T cell renewal capacity of the immune system; and the observation that both naïve CD4+ and CD8+ T cells, rarely infected by HIV because their resistance to direct HIV infection, undergo severe depletion during HIV infection [46-48].

Recently, there is emerging evidence suggesting that chronic immune activation, the strongest correlate of HIV disease progression [49-50], plays a critical role in the pathogenesis of HIV infection. This chronic immune activation is believed to be caused by the high level of HIV viremia and translocation of microbial products from the intestinal mucosa into the circulation due to the loss of gut mucosal integrity [50-56]. It has been shown that persistent immune activation results in an increased turnover rate

and decrease in the overall half-life of T cells [50, 57]. Persistent immune activation also correlates with other immune defects, including exhaustion of CD8+ T cells [58-60]; hypergammaglobulinemia [56]; increased activation-induced cellular apoptosis of CD4+ and CD8+ T cells as well as B cells [61]; and increased susceptibility to the development of HIV-related malignancies, especially of the B cell type [62]. Furthermore, immune activation results in the generation of activated CD4+ T cell targets for the virus itself, further driving viral replication [63-64] and leading to further CD4+ T cell depletion [50, 63].

In support of the central role of immune activation in the pathogenesis of HIV infection, in natural SIV hosts (e.g., African green monkeys, sooty mangabeys), the avoidance of the chronic, generalized immune activation strongly correlates with the preservation of CD4+ T cells and immunocompetency [65-67]. Taken together, these findings suggest that the persistent immune activation plays a central role in the dysfunction of the whole immune system during HIV infection.

HAART and immune reconstitution

Based on the above observations, direct viral killing and persistent immune activation represent two principle mechanisms causing CD4+ T cell depletion and immune system dysfunction [50, 68-72]. In support of this view, HAART can efficiently control HIV plasma viremia and largely normalize the associated immune activation. These beneficial effects strongly correlate with a significant increase in CD4+ T cell count in most of the HAART treated patients. Yet more than a decade after the introduction of HAART, it is clear that relatively few individuals will achieve normal levels of peripheral blood CD4+ T cells, and up to 20% of these patients have little or no increase in CD4+ T cell count despite the impact of HAART on the virological side of the equation [40-45].

This limited immune reconstitution is most prevalent in patients starting HAART in the chronic stage of disease (CD4<350 cells/μl) and in patients with older age, and this failure of full immune reconstitution strongly correlates with significantly higher

morbidity and mortality compared to uninfected populations [40, 44-45, 73-75]. Further, the magnitude of CD4+ T cell reconstitution in peripheral blood does not reflect the real magnitude of immune reconstitution in LTs where CD4+ T cells mostly reside. Even with partial normalization of the peripheral blood CD4+ T cell count, populations of CD4+ T cells remain depleted by as much as 50% in secondary LNs and gut-associated lymphoid tissue (GALT) [76-79].

This limited reconstitution of T cells also correlates with important functional immunologic abnormalities including: 1) persistently poor vaccine responses [80-81]; 2) increased frequency of reactivation of latent herpes simplex infection and human papilloma virus infections [82-84]; 3) increased incidence of non-AIDS related clinical events such as cardiovascular disease, liver disease and non-AIDS-related cancer compared to uninfected population [85-88], and 4) increased susceptibility to bacterial infections [89]. Taken together, these observations suggest that there are persistent abnormalities in T cell homeostasis in patients receiving HAART and these abnormalities cannot be fully corrected by HAART itself.

Mechanisms of T cell homeostasis and survival

The homeostasis and survival of T cells heavily depend on the niche in which they live at different stages of their differentiation. In the central LTs such as thymus, the life of a T cell begins as a thymic progenitor cell from the bone marrow. In the thymus, $CD3^{-}CD4^{-}CD8^{-}$ triple negative thymocytes begin their differentiation and education through interaction with soluble and cellular components within thymic microenvironment such as self-peptide–MHC class I complexes signal as well as interleukin 7 (IL-7). Eventually, thymocytes become CD4 or CD8 single-positive naïve T cells and are exported to the periphery (reviewed in detail in [90] and [91]).

The newly generated naïve T cells emigrate from the thymus and form the long-lived pool of naive T cells that re-circulate within the confines of the secondary LTs, such as LNs and spleen, for many weeks or months [91]. Typical naive T cells have a phenotype

characterized by low expression of CD44 and high expression of the lymph node–homing receptors CD62L and CCR7. These receptors are necessary for naïve T cells to enter the T-cell zone of secondary LTs and access survival signals such as self-peptide–MHC class I complexes and IL-7 to maintain their survival [91-93]. These survival signals can sustain the expression of anti-apoptotic molecules such as Bcl-2, therefore allowing the naïve T cells to survive during circulation and residence in LTs [90-91, 94].

Collectively, the stable pool of mature naive T cells is maintained throughout life by both input from the thymus and homeostatic proliferation in the periphery. However, these two major mechanisms play different roles at different ages. Early in life, thymic export establishes the size and the diversity of the human naive T cell pool. By adolescence, thymopoiesis is greatly reduced. However, absolute numbers of naive T cells in young and elderly humans are relatively stable, despite decreased output from the thymus [95]. This implies that human naive T cells can proliferate in the periphery to balance the loss of production of naïve T cells from thymus during the aging process. In support of this view, experimental data derived from thymectomy experiments and analysis of T cell receptor excision circles (TRECs) (a marker of recent thymic emigrants) showed that the maintenance of the adult human naive T cell pool occurs almost exclusively through peripheral T cell division [96]. Collectively these observations show an age-dependent contribution of thymic emigrants and post-thymic T cell proliferation that maintains the peripheral T cell pool and contributes to T cell homeostasis. The thymus contributes relatively more at younger ages and peripheral T cell expansion contributes more in older subjects.

Mechanisms of limited immune reconstitution after HAART

Since thymopoiesis and the homeostasis of mature post-thymic T cells in peripheral LTs are both important for the maintenance of naïve T cells, mechanisms that affect thymopoiesis and the homeostasis of mature post-thymic T cells in peripheral LTs might

both contribute to the depletion of T cells and the limited immune reconstitution after HAART.

Impaired thymic output during HIV infection

Impairment of thymic T cell production was proposed as one of the causes of CD4+ T cell depletion. It has been shown that thymus undergoes significant pathological changes in AIDS patients involving destruction of the thymic structure, a lack of thymocytes and infiltration of activated T cells [95]. In late HIV infection, the HIV infected thymus undergoes premature atrophic changes that are similar to, but more severe than, normal thymic atrophy [95, 97-98]. In SIV infection, there is an early stage of suppressed thymopoiesis, reflected by the increased rate of thymocyte apoptosis and a decrease in thymocyte numbers [99]. In support of impaired thymopoiesis in HIV infection as one of the mechanisms leading to depletion of naïve T cells, it was shown that recent thymic emigrants, measured as TREC levels, were significantly lower in both CD4+ and CD8+ T cells in blood and LNs after HIV infection compared to age-matched uninfected controls [70]. Similar results were observed in non-human primate models in which the decrease of TREC level was correlated with the peripheral CD4+ T cell decline [100]. Furthermore, it has been shown that the TREC proportion among total peripheral blood mononuclear cells is a marker of disease progression [101]. Suppression of viral replication by HAART can also induce significant improvement for the TREC+ cells in younger HIV-infected patients and this improvement correlates with the CD4+ T cell restoration [70]. It has been shown that HIV directly kills thymocytes or dendritic cells required for normal thymocyte development and may damage thymic epithelial cells required for normal thymopoiesis [95]. Thus, impaired thymic production of T cells during HIV infection could be a cause of CD4 T cell depletion and limit immune reconstitution after HAART.

Peripheral maintenance of T cell populations and immune reconstitution

Another important mechanism accounting for the increase of CD4+ T cells after introduction of HAART is the proliferation of T cells in periphery [102-103]. This

process may be a more important mechanism of CD4+ T cell reconstitution than thymopoeisis. By comparing the kinetics of different subsets of CD4+ T cells in thymectomized and sham-operated juvenile rhesus macaques, Arron et al. found that thymic output in juvenile macaques has very little impact on the peripheral CD4+ T cell compartments, in both healthy and SIV-infected macaques [104]. Similar results were observed in HAART-treated HIV-infected humans thymectomized for myasthenia gravis [98]. It was further documented that the increases in CD4+ T cell number are mainly from the TREC-negative T cell population, and thus were likely due to peripheral T cell expansion [98]. Zhang et al. also showed that the quantity of newly generated TREC+ T cells is not sufficient to explain the post-HAART increase in peripheral T cells [105] and Walker et al. demonstrated that the CD4+ T cell pool in adults is maintained primarily by the proliferation of mature CD4+ T cells rather than by thymopoiesis [106]. Taken together, these findings suggest that homeostatic proliferation of CD4+ T cells in the periphery in response to viral suppression by HAART accounts for the more significant proportion of cells that contribute to immune reconstitution. As the homeostatic proliferation of CD4+ T cells is largely dependent on the microenvironment of peripheral LTs, I will review the microenvironment of peripheral LTs and its impact of T cell homeostasis in the following sections.

Structure and function of LTs

Secondary LTs are organized to promote immune responses and maintain normal sized populations of the principal players of immune responses: T cells, B cells and antigen presenting cells (APCs). The anatomic structures of LTs are uniquely suited to support this function. In general, secondary LTs such as LNs can be divided into three compartments: the B-cell zone, where most B cells reside; the T-cell zone where most T cells reside; and medullary sinuses, where plasma cells, APCs such as macrophages and dendritic cells (DCs) and other immune cells reside. Within LNs, the B-cell zone is located in the superficial cortex and is the site of development of effective memory B cell and high affinity antibody responses following immunization with T cell–dependent antigens [107-113]. The medullary sinuses are in the central part of LNs. The area

between B-cell zone and medullary sinuses is T-cell zone, where most naive CD4+ and CD8+ T cells reside and gain access to IL-7 and other survival signals required for their survival [93, 114-122].

The structure of T-cell zone is supported by a 3D network formed by a specialized stromal cell called the fibroblastic reticular cell (FRCs), and by collagen fibers. The FRCs ensheath collagen fibers to form a 3D conduit network system within T-cell zone. This network not only confers essential mechanical support to the LNs but also connects subcapsular and medullary sinuses with the perivascular spaces of high endothelial venules (HEVs). This conduit network transports soluble antigen, cytokines, and growth factors derived from the afferent lymph to the parenchyma of the LNs where APCs continuously sample the fluid content for lymph-borne antigens [114-115, 120, 123]. This FRC network is also critical for the migration and encounters between T cells and APCs, activation and homeostasis of lymphocytes within LTs [120].

T cell entry into LNs occurs via migration through the HEVs in the T-cell zone [124]. This process involves a cascade of selectin- (or integrin-) mediated rolling, chemokine-mediated integrin activation, and integrin-mediated adhesion regulated by the interaction between DCs and HEVs [125-128]. Once T cells migrate through HEVs, they enter the T-cell zone and migrate on the surface of FRC network. This process is dependent on the interactions between CCR7 on T cells and ligands of CCR7, namely CCL19 and CCL21 mainly expressed by the FRCs [93, 124, 127-129]. Interactions between CCR7 on T cells and chemokine cues on FRCs facilitate the movement of T cells over the FRC network in the T-cell zone and the interactions between T cells and APCs [93, 124, 127-130]. While cells move along the FRC network, T cells are also interacting with survival signals such as IL-7 and self-peptide–MHC class I complexes produced and presented on the surface the FRC network [93, 120, 124]. This interaction is critical for the survival of T cells, particularly naïve T cells. Blocking interactions with IL-7, either by adoptive transfer of T cells into IL-7-deficient hosts, by injection of IL-7 monoclonal antibody into normal mice or by blocking the chemokine receptors required for entry into LTs, significantly

impairs the survival of naive T cells in murine model. In contrast, over-expression of IL-7 increases the size of the naive T cell pool [91-92, 94, 118-119, 131]. Collectively, these findings suggest that the entry of naïve T cells into LTs and interaction with survival factors on the FRC network play a particularly critical role in maintaining populations of naïve T cells.

Chronic immune activation and LT damage

As mentioned above, HIV infection leads to persistent immune activation and inflammation, primarily in LTs. Similar to other chronic inflammatory diseases such as hepatitis C virus infection in the liver, the chronic inflammation caused by HIV infection in LTs has been shown to correlate with LT damage in the B-cell zone and T-cell zones.

LT structure damage during HIV infection was recognized soon after HIV was identified. The pathologic features of the severe lymphadenopathy in HIV infected patients begin with hyperplasia. This hyperplasia leads to B-cell zone lysis and eventually involution [54, 132]. These changes correlate with the clinical stages of HIV infection, with hyperplasia most often seen in the early and asymptomatic stage of HIV infection and lysis and involution seen as the patient progresses to AIDS stage [133-138]. By contrast, LNs from individuals referred to as long-term non-progressors, because of their relatively good control of viral replication and slower progression to disease, have less hyperplasia and the integrity of the architecture of LNs is better preserved [139-140].

The damage in the T-cell zone was first recognized in 1987. Damage was subsequently shown to be correlated with fibrotic deposition in LNs and GALT in a stage-dependent manner [77-78, 141-148]. But, the functional consequences of these changes have only recently been appreciated.

Since the highly organized structure of the T-cell zone is critical for the maintenance of naïve T cells, the damage in the T-cell zone should impair naïve T cell homeostasis. In support of this view, it has been shown that the extent of fibrosis within the T-cell zone

strongly correlates with the extent of loss of naïve CD4+ T cell population before HAART [77-78, 144-146] and the degree of reconstitution of the total CD4+ T cell population after 6 months of HAART [146]. These findings suggested that collagen-induced fibrotic damage in LTs might impair the normal homeostasis of naïve T cells during HIV infection and limit the immune reconstitution after HAART. However, several critical questions remained unanswered: 1) how does LT fibrosis deplete CD4+ T cells during HIV infection? 2) How does LT fibrosis limit the restoration of CD4+ T cells? 3) What are mechanisms leading to LT fibrosis? 4) Can therapies be developed to avert/revert this pathological change?

Studies presented in the following chapters will provide insights into these critical questions. Specifically, Chapter 2 is devoted to an investigation of the mechanisms by which LT fibrosis depletes naïve T cells and the mechanisms of LT fibrosis; Chapter 3 investigates the underlying mechanisms by which LT damage limits immune reconstitution; Chapter 4 provides data about the mechanisms that lead to the loss of LT structure; finally Chapter 5 discusses potential therapeutic interventions to revert/avert the pathological changes within LTs to enhance immune reconstitution after HAART.

Chapter 2

Originally published in J Clin Invest. 2011 Mar 1;121(3):998-1008. Reprinted with permission; the format has been adjusted.

Cumulative Mechanisms of Lymphoid Tissue Fibrosis and T Cell Depletion in Immunodeficiency Virus Infections

Ming Zeng[1*], Anthony J. Smith [1*], Stephen W. Wietgrefe[1], Peter J. Southern[1], Timothy W. Schacker[2], Cavan S. Reilly[3], Jacob D. Estes[4], Gregory F. Burton[5], Guido Silvestri[6], Jeffrey D. Lifson[4], John V. Carlis[7], Ashley T. Haase[1]

[1] Department of Microbiology, Medical School, University of Minnesota, MMC 196, 420 Delaware Street S.E., Minneapolis, MN 55455, USA.

[2] Department of Medicine, Medical School, University of Minnesota, MMC 250, 420 Delaware Street S.E., Minneapolis, MN 55455, USA.

[3] Division of Biostatistics, School of Public Health, University of Minnesota, MMC 303, 420 Delaware Street S.E., Minneapolis, MN 55455, USA.

[4] AIDS and Cancer Virus Program, Science Applications International Corporation–Frederick, Inc., National Cancer Institute, Frederick, MD 21702, USA.

[5] Department of Chemistry and Biochemistry, Brigham Young University, Provo, UT 84602, USA.

[6] Yerkes National Primate Research Center, and Emory University, Atlanta, GA, 30329, USA.

[7] Department of Computer Science and Engineering, Institute of Technology, University of Minnesota, 200 Union Street S.E., Minneapolis, MN 55455, USA.

Address correspondence to: Ashley T. Haase, Department of Microbiology, University of Minnesota, Box 196, 420 Delaware Street S.E., Minneapolis, Minnesota 55455, USA. Phone: (612) 624-4442; Fax: (612) 626-0623; E-mail: haase001@umn.edu.

*Authorship note: Ming Zeng and Anthony J. Smith contributed equally to this work.

Introduction

Depletion of CD4+ T cells, the defining characteristic for which the immunodeficiency viruses HIV and SIV were named, has been attributed to direct mechanisms of infection and cell killing and indirect mechanisms such as increased apoptosis accompanying the chronic immune activation associated with HIV and SIV infections. More recently, there is also increasing evidence that fibrosis induced by immune activation damages lymphoid tissue (LT) niches, thereby contributing to T cell depletion and impaired immune reconstitution upon institution of antiretroviral drug treatment [68, 78]. In HIV infection, fibrosis, measured as collagen deposition in LTs, strongly correlates with depletion of naïve CD4+ T cells and inversely correlates with the extent of immune reconstitution following suppression of viral replication by antiretroviral therapy [77-78, 144-147]. In pathogenic SIV infection as well, collagen deposition in the early stage of SIV infection of rhesus macaques (*Macaca mulatta;* RM) is associated with initial decreases in CD4+ T cells [143].

The mechanisms by which LT fibrosis depletes CD4+ T cells and impairs immune reconstitution in these immunodeficiency virus infections have not been well defined, but one previously advanced hypothesis [78], based on studies in mice [93, 124, 149-150], is that collagen deposition disrupts the architecture of the LT niche so that T cells have less access to self-antigen-major histocompatibility complex signals and IL-7 on the fibroblastic reticular cell (FRC) network on which they migrate. Since these factors are critical for T cell survival, particularly naïve T cells, decreased access to these homeostatic signals would result in increased apoptosis as a mechanism for T cell depletion associated with fibrosis in HIV and SIV infections.

We tested this hypothesis in SIV-infected RMs, an animal model in which we could analyze lymph node (LN) biopsies obtained in longitudinal and cross-sectional studies. We first show that FRCs are the major source of IL-7, the primary survival factor for naïve T cells in RMs, and that LN fibrosis limits lymphocyte access to FRC-derived IL-7, resulting in depletion, particularly of naïve CD4+ T cells, through apoptosis. T cell

apoptosis, along with other T cell killing mechanisms such as pathological immune activation that can lead to increased apoptosis of T cell, in turn diminishes the availability of T cell-derived lymphotoxin-β (LTβ) on which the FRC network depends. The decreased availability of LTβ-producing cells, along with collagen-restricted access to FRCs, results in loss of both the FRC network and IL-7 production. This further impairs the survival of naïve T cells, perpetuating a vicious cycle of continuous and cumulative loss of both T cells and the FRC network (diagrammed in Figure 2-19).

These results suggest that therapeutic interventions to avert or moderate this pathological process of fibrosis could improve immune reconstitution following highly active antiretroviral therapy (HAART). To design effective interventions, we investigated the underlying mechanisms of fibrosis in LTs during HIV infection and found that increases in transforming growth factor beta 1 (TGF-β1) expression in T regulatory cells activate the TGF-β1 signaling pathway in fibroblasts to trigger the increase of production of pro-collagen and chitinase 3-like-1 (CHI3L1), an enzyme that could enhance maturation of this pro-collagen into collagen fibrils in LT fibroblasts. We then show in vitro that targeting the TGF-β1 signaling pathway with the anti-fibrotic drug pirfenidone dramatically reduces collagen produced by primary human fibroblasts. These data suggest that the TGF-β1 signaling pathway plays a key role in progressive LT fibrosis during HIV infection. Therefore, early initiation of HAART to limit the viral replication-dependent inflammation that drives this process, along with complementary therapeutic interventions directed at the TGF-β1 signaling pathway, could potentially avert or moderate this pathological process and improve immune reconstitution post HAART.

Materials and Methods

Ethics statement

This human study was conducted according to the principles expressed in the Declaration of Helsinki. The study was approved by the Institutional Review Board of the University of Minnesota. All patients provided written informed consent for the collection of samples and subsequent analysis.

LN biopsy specimens

Inguinal LN (LN) biopsies from 4 HIV negative individuals and 23 untreated HIV-infected individuals at different clinical stages (Table 2-1) were obtained for this University of Minnesota Institutional Review Board-approved study. Viral load measurements were obtained the same day as biopsies. Each LN biopsy was immediately placed in fixative (4% neutral buffered paraformaldehyde or Streck's tissue fixative) and paraffin embedded.

Animals, SIV infection, & LN biopsy specimens

Adult RMs used in these studies were housed in accordance with the regulations of the American Association of Accreditation of Laboratory Animal Care and the standards of the Association for Assessment and Accreditation of Laboratory Animal Care International; all protocols and procedures were approved by the relevant Institutional Animal Care and Use Committee. LTs were obtained in longitudinal studies from five RMs who were inoculated intravenously with 10,000 $TCID_{50}$ of SIVmac239 (generous gift from R. Desrosiers), additional LTs from 11 RMs obtained in previously described cross-sectional studies [151]. Each LN biopsy was immediately placed in fixative (4% neutral buffered paraformaldehyde or Streck's tissue fixative) and paraffin embedded.

Immunofluorescence, Immunohistochemistry, in situ Hybridization (ISH), & Quantitative Image Analysis (QIA)

All staining procedures were performed as previously described [151-152] using 5-30 μm tissue sections mounted on glass slides. Tissues were deparaffinized and rehydrated in deionized water. Heat-induced epitope retrieval was performed using a high-pressure cooker (125^{o}C) in either DIVA Decloaker or EDTA Decloaker (Biocare Medical), followed by cooling to room temperature. Tissues for collagen type I staining required pre-treatment with 20 μg/ml proteinase K (Roche Diagnostics) in proteinase K buffer (0.2 M Tris, pH 7.4, 20 mM $CaCl_2$) for 15-20 min at room temperature. Tissue sections were then blocked with SNIPER Blocking Reagent (Biocare Medical) for 30 min at room

temperature. Primary antibodies were diluted in TNB (0.1M Tris-HCl, pH 7.5; 0.15M NaCl; 0.05% Tween 20 with Dupont blocking buffer) and incubated overnight at 4°C. After the primary antibody incubation, sections were washed with PBS and then incubated with fluochrome-conjugated secondary antibodies in TNB for 2 hr at room temperature. For sections using two mouse primary antibodies, one of the antibodies was first biotinylated using the One-step Antibody Biotinylation kit (Miltenyi Biotec) according to the manufacturer's instructions; an anti-biotin fluorophore-conjugated antibody was then used as the secondary reagent. Finally, sections were washed with PBS, nuclei counterstained blue with TOTO-3 or DAPI, and mounted using Aqua Poly/Mount (Polysciences Inc.). Immunofluorescent micrographs were taken using an Olympus FV1000 Fluoview confocal microscope with the following objectives: x20 (0.75 NA), x40 (0.75 NA), and x60 (1.42 NA); images were acquired and mean fluorescence intensity was analyzed by using Olympus Fluoview software (version 1.7a).

For combined immunohistochemistry/ISH, collagen type I (COL1alpha2) cDNA (I.M.A.G.E. clone 740269 from ATCC, Vector PT7T3D-Pac) was cut with *EcoR* I and transcribed with T3 polymerase (Promega) in the presence of S^{35} UTP to make the anti-sense probe. The cDNA was cut with *Not* I and transcribed with T7 polymerase to make the control sense probe according to the manufacturer's instructions. IL-7 cDNA (IMAGE clone 5748841) was cut with *Sal* I and transcribed with T7 polymerase (Promega) in the presence of S^{35} UTP. Tissues were deparaffinized in 60°C incubator for 2 hours and rehydrated through graded ethanols. Heat-induced epitope retrieval was performed using a water-bath (95°C for 25 min) followed by treatment with acetic anhydride. Sections were hybridized with S^{35}-labeled anti-sense or control sense RNA probes overnight at 45°C, washed in 2X SSC at 37°C, treated with RNase A at 37°C for 60 min, washed in 50% formamide/2X SSC at 50°C for 5 min, 1X SSC at 50°C for 10 min, and 0.5X SSC at 50°C for 15 min. Tissues were then blocked with SNIPER Blocking Reagent (Biocare Medical), incubated overnight at 4°C with the primary antibody. Tissues were then washed. Endogenous peroxidase inactivated with 3% (v/v) H_2O_2 in methanol and signal detected with Mach-3 (Biocare Medical) and DAB (Vector)

kits. Slides were dehydrated in ethanols containing 0.1M ammonium acetate and air dried. Slides were dipped in nuclear track emulsion, dried, exposed at 4°C, developed, fixed, counterstained with Harris Hematoxylin (Surgipath), and mounted with Permount (Fisher Scientific). Stained sections were examined by light microscopy at ambient temperatures. Light micrographs were taken using an Olympus BX60 upright microscope with the following objectives: x10 (0.3 NA), x20 (0.5 NA), and x40 (0.75 NA); images were acquired using a Spot color mosaic camera (model 11.2) and Spot acquisition software (version 4.5.9; Diagnostic Instruments). Isotype-matched IgG/IgM negative control antibodies in all instances yielded negative staining results (see Table 2-2, which lists the primary antibodies and antigen retrieval methodologies).

QIA was performed using 10–20 randomly acquired, high-powered images (X200 or X400 magnification) by either manually counting the cells in each image or by determining the percentage of LT area occupied by a positive chromagen or fluorescence signal using an automated action program in Adobe Photoshop CS with tools from Reindeer Graphics.

Ex vivo culture system

The experimental protocols used here for human tissue samples had full IRB approval (Institutional Review Board: Human Subjects Committee, Research Subjects' Protection Program, University of Minnesota) and informed written consent was obtained from individual patients, or the legal guardians of minors, for the use of tissue in research applications prior to the initiation of surgery. Fresh human palatine tonsil tissues were obtained from routine tonsillectomies and processed within 1–2 h of completion of surgery. Viable tonsil lymphocyte suspensions were prepared by forcing cut tissue pieces through a metal sieve and collecting the released single cell suspension in complete RPMI medium (10% heat inactivated fetal calf serum, 1x l-glutamine, penicillin & streptomycin; Invitrogen). The cells were washed and immediately cryopreserved. The remaining stromal cells left on the sieve were cultured in complete RPMI medium at 37°C / 5% CO_2 and adherent, proliferating fibroblasts were visible after 2–5 days in culture; confluent monolayers developed after 10–25 days. These primary stromal

populations were readily released with trypsin and further expanded/passaged using routine procedures for adherent cells.

Sub-confluent primary stromal cells (2 x 10^4 cells/well) were grown on Lab-Tek II chamber slides 2 day before experimental manipulation. TGF-β1, CHI3L1, and other agents were added to the culture and incubated for 48 h before analysis. For vimentin and p-smad2/3 staining, cells were first fixed by Streck's tissue fixative and then subject to secondary antibody staining as previously described. For live cell staining, samples were directly incubated with primary antibodies against collagen type I and/or CHI3L1 at 4°C overnight without antigen retrieval treatment; samples were then subject to secondary antibody staining as previously described. To quantify levels of collagen type I or CHI3L1, 10 randomly stained confocal images from each specimen and condition were captured and the mean fluorescence intensities calculated by FV10-ASW software.

Statistical analysis

All associations involving SIV-infected monkeys were tested using linear mixed models. Restricted maximum likelihood was used to obtain parameter estimates and Wald tests of regression coefficients were used to test for an association between each independent variable and the response variable of interest. Random intercepts were used to model the animal correlation in the response variable. More specifically, three different variables were used as response variables (percent area staining positive for IL-7, number of naïve T cells and number of naïve T cells undergoing apoptosis) and all other variables (namely percent area staining positive for desmin, the percent area staining positive for collagen and days post infection) were used as explanatory variables. Backward variable selection was used to remove non-significant covariates. This process led to models where: (i) days post infection and the percent area staining positive for desmin ($p<0.0001$) are predictive of percent area staining positive for IL-7; (ii) the percent area staining positive for collagen ($p=0.002$) and the percent area staining positive for desmin ($p=0.0004$) were predictive of the number of naïve T cells undergoing apoptosis; (iii) percent area staining positive for IL-7 is predictive of the number of naïve T cells ($p=0.0004$); and (iv) the

number of naïve T cells undergoing apoptosis is predictive of the number of naïve T cells ($p=0.0001$).

Associations between continuous variables involving HIV-infected humans were estimated using Pearson's correlation coefficient (after transforming to the log scale), and tests were conducted using the usual *t*-test for a correlation. Differences in CHI3L1 protein levels between HIV negative and positive subjects were tested using a 2 sample *t*-test (after transforming to the logarithmic scale to stabilize the variance). All calculations were performed with the software R, version 2.10.1

Results

The FRC network is the major source of IL-7 for T cells in the T cell zone

We investigated the hypothesis that the mechanism by which LT fibrosis causes depletion of T cells is by decreasing access to the survival factor IL-7 by first showing in uninfected RMs that the FRC network is the major source of IL-7 for T cells. We used antibodies to desmin to label both the FRC network in the T cell zone of LNs and the follicular dendritic cell (FDC) network in B cell follicles, antibodies to IL-7 to label IL-7-positive cells, and antibodies to desmin and in situ hybridization (ISH) to detect and quantify IL-7 mRNA. We found that both IL-7 mRNA and protein predominantly co-localize with not only the FRC and FDC cell bodies but also the dendritic processes that form their respective networks (Figure 2-1 and Figure 2-2, A-B), analogous to the localization of cytoskeletal and nervous system mRNAs and proteins [153-154]. Quantitatively, we conservatively estimate that ~70% of IL-7 mRNA co-localizes with the FRC network in the T cell zone and ~80% co-localizes with the FDC network in B cell follicles (Figure 2-3A). The co-localization of IL-7 protein and the FRC network is consistent with results reported in the mouse [93, 124], and the small portion of IL-7 we found associated with a subset of dendritic cells and macrophages (Figure 2-3B) is consistent with a study of human LTs [155].

Collagen deposition and loss of the FRC network impede access to IL-7 while also depleting its source

Under physiological conditions, FRCs ensheath collagen fibers to form a connective tissue and fibrous network on which lymphocytes, antigen presenting cells and other cells within LTs migrate [115, 117, 120, 124]. This architecture allows T cells to efficiently access chemokines and cytokines, including survival factors such as IL-7, “posted” on their path [93, 119, 150]. Thus, LT sections from uninfected RMs stained with antibodies to type I collagen, desmin and T cells reveal that the collagen and desmin co-localize and define the FRC network and three dimensional space in which the T cells migrate and

visibly contact the FRC network (Figure 2-4A and Figure 2-5A). In marked contrast, in chronically infected RMs (180 days post SIVmac239 infection, dpi), large deposits of collagen are evident outside the FRC network while the FRC network itself is greatly decreased (Figure 2-4B). As a consequence, few T cells visibly contact the FRC network and instead are only in contact with collagen (Figure 2-4B and Figure 2-5B).

Increased naïve T cell apoptosis

Since T cells migrate on the FRC network to access survival factors such as IL-7, the physical barrier created by collagen deposition and the loss of the FRC network itself would be expected to restrict IL-7 access and deplete the source of IL-7, thereby increasing apoptosis, particularly in the naïve T cell populations [93, 118-119]. We indeed found dramatic increases in apoptotic cells in the T cell zone in chronically infected animals. This is evident by comparison of an uninfected animal (SIV-) with an infected animal at 180 dpi, and is even more striking in an infected animal at 462 dpi (Figure 2-6, A-C). While there are cells clearly undergoing apoptosis even when they are close to the residual FRC network (Figure 2-6B), consistent with the well-established mechanism of increased apoptosis associated with chronic immune activation, the great majority of activated caspase3+ apoptotic cells are located in apparent ”black holes” where the FRC network has been lost and replaced by collagen. As predicted, we found significant increases in naïve T cell apoptosis (Figure 2-6D and 2-7B), which is inversely associated with the quantity of FRCs and positively associated with the quantity of collagen (p=0.0004 and p=0.002, respectively).

Depletion of naïve CD4+ and CD8+ T cell populations by increased apoptosis

The increased apoptosis in naïve T cell populations was significantly associated with their depletion (Figure 2-7, A and B, p=0.0001). Significant increases were detectable after the acute stage of SIV infection, and accelerated markedly in the later chronic stages of infection. In the acute stage of infection, the FRC network and IL-7 were slightly increased (Figure 2-7C and Figure 2-8, A and B), coincident with the LT hyperplasia in

this stage of infection (Figure 2-8B), potentially compensating for collagen deposition occurring during the acute phase so that there is only a small decrease in naïve T cell numbers. However, after 90 dpi, there is a rapid and parallel decline in the FRC network, IL-7 (Figure 2-7C and Figure 2-8, A and B, $p<0.0001$), and naïve T cells (Figure 2-7, D and E, $p=0.0004$). Most of the surviving naïve T cells reside at the border of B cell and T cell zones (Figure 2-8C), where the majority of the residual FRC network and IL-7 was still detectable (Figure 2-8, A and B, arrow). Lastly, as our hypothesis predicts, the destruction of LT architecture not only decreased the naïve CD4+ T cell number in LNs but also had a similar impact on naïve CD8+ T cells, with similar and parallel losses of both naïve CD4+ and CD8+ cells (Figure 2-8, D-F).

Survival interdependencies: Loss of FRCs caused by loss of LTβ+ T cells

Collagen deposition and loss of the FRC network decreased both access to IL-7 and the major source of IL-7 in the T cell zone, resulting in increased apoptosis and loss of T cells. However, what explains the loss of the FRC network itself? We hypothesized that the loss of the FRC network was reciprocally related to depletion of T cells as a major source of lymphotoxin β (LTβ) [156], based on ex vivo studies in the mouse in which maintenance of the FRC network has been shown to be dependent on LTβ signaling from T cells [157]. We confirmed this dependency in vivo by documenting loss of the FRC network in mice by separately blocking either the LTβ pathway or by depleting T cells (Figure 2-9), and then showed that T cells are a major source of LTβ (~80% of the LTβ+ cells are T cells) in the T cell zone of RMs (Figure 2-10A). Furthermore, the loss of LTβ+ T cells followed a parallel time course, consistent with the loss of the FRC network in SIV infection (Figure 2-10, B-D), further supporting the conclusion that the loss of FRCs is a consequence of the loss of LTβ-producing T cells.

Fibroblasts are the major producers of collagen

These findings establish a cooperative and cumulative mechanism of collagen deposition and naive T cell depletion, but leave unanswered the questions of the cellular sources and

mechanisms of collagen production and deposition. For answers to these questions that could provide insights to design interventions in HIV infection to minimize depletion and improve immune reconstitution, we turned to HIV infection in studies of LT and in vitro models.

To determine the cellular source of collagen within LT in HIV infection, we utilized antibodies to CD3 (T cells), CD68 (macrophages), CD20 (B cells), CD11c (dendritic cells), and vimentin (fibroblasts) to identify which cell types were producing pro-collagen, the precursor of mature collagen fibers [158-160]. As shown in a representative image in Figure 2-11A, pro-collagen mainly co-localized with vimentin+ fibroblasts. To corroborate this finding, we used in situ hybridization combined with immunohistochemistry to show that type I collagen mRNA primarily co-localized with vimentin+ fibroblasts (Figure 2-11B). Lastly, we isolated leukocyte and fibroblast subpopulations from human tonsil and compared their ability to produce collagen in an ex vivo culture system. As shown in Figure 2-11C, cultured primary fibroblasts were able to synthesize type I collagen while leukocytes produced very little type I collagen (data not shown). Taken together, these data confirm that fibroblasts are the major producers of collagen within LTs.

Enhanced TGF-β1 signaling leads to increased production of collagen

The TGF-β signaling pathway is a known, key mediator of fibrosis [161-163] while TGF-β1+ regulatory T cells have been shown to be an important factor in increased fibrosis of LT during acute SIV infection [143]. We therefore examined the expression of various components of the TGF-β1 signaling pathway in the LTs from a cohort of HIV infected patients (Table 2-1), including TGF-β1, TGF-β1 receptor (R) II, and downstream signaling molecules such as phosphorylated smad2/3 (p-smad2/3). We did detect an increase in TGF-β1+ T cells during HIV infection (Figure 2-12, A and B and Figure 2-13A), identified mainly as CD3+/CD4+/Foxp3+ regulatory cells (Figure 2-13A and Figure 2-14). This increase in TGFβ1+ regulatory T cells was accompanied by a parallel

increase in TGF-β1 RII expression in vimentin+ fibroblasts and increases in the downstream signaling molecules p-smad2/3 (Figure 2-12A and Figure 2-13, B and C).

The increased frequency and spatial proximity of TGF-β1+ regulatory T cells and TGF-β1 R+ fibroblasts (Figure 2-13D) suggested a potential mechanism for increased collagen deposition in which interactions between T cells and fibroblasts activate the TGF-β1 signaling pathway. In support of this hypothesis, we found a significant association between TGF-β1+ cells and fibrosis as measured by collagen type I deposition ($r = 0.68$, $p = 0.0001$) (Figure 2-12C). Moreover, addition of TGF-β1 to primary fibroblasts cultured ex vivo resulted in increased production of type I collagen over basal levels (Figure 2-15).

Blocking TGF-β1 signaling decreases production of collagen

These results, linking LT fibrosis to activation of the TGF-b1 pathway from viral replication-related inflammation, with consequent disruption of the FRC and depletion of naïve T cells, suggested that interventions that disrupt these processes, even without directly affecting viral replication, might confer therapeutic benefits. To begin to evaluate approaches for inhibition of LT fibrosis as a possible adjunctive therapy in HIV infection, we investigated the effects of the ant-fibrotic drug, pirfenidone, on the TGF-β1 signaling pathway. Addition of pirfenidone to TGF-β1-stimulated fibroblasts effectively blocked this signaling pathway and concomitantly decreased collagen production in an ex vivo culture system (Figure 2-15).

Role of CHI3L1 in collagen deposition and relationship to TGF-β1 signaling

In a previous microarray analysis of HIV-infected LT [164], we identified CHI3L1 as one of the genes with the greatest increase in expression during HIV infection. Since CHI3L1 has been shown to play an important role in collagen formation, both by increasing the rate of fibrillogenesis during the collagen maturation process [165-166] and decreasing the rate of collagen degradation by inhibiting matrix metalloproteinase-1 (MMP-1) [166], we explored the role that CHI3L1 might play in increasing collagen

deposition during HIV infection. We found significant increases in the CHI3L1 expression in LTs during HIV infection, consistent with the previously documented increases in mRNA ($p = 0.034$) (Figure 2-16, A and B) and identified vimentin+ fibroblasts as the cells that express CHI3L1 (Figure 2-16C). As a number of cytokines induce CHI3L1 expression [167-168], we asked whether increased TGF-β1 expression was associated with increased CHI3L1 expression during HIV infection, and found that there was a significant positive association between TGF-β1+ cells and CHI3L1 expression in LT ($r = 0.49$, $p = 0.0092$) (Figure 2-17A). In addition, TGF-β1 treatment of primary LT fibroblasts resulted in enhancement of CHI3L1 expression compared to untreated cultures (Figure 2-17, B and C).

As we had now shown that CHI3L1 and pro-collagen are both produced in LT fibroblasts and both increased during HIV infection, we hypothesized that CHI3L1 directly contributed to collagen deposition by facilitating the formation of collagen fibrils [165-166]. Consistent with this hypothesis, we found: 1) CHI3L1 levels and collagen type I in LT are significantly correlated ($r = 0.85$, $p < 0.0001$) (Figure 2-18A); 2) addition of exogenous CHI3L1 to cultures of primary fibroblasts enhanced the formation of mature collagen type I (Figure 2-18B); and 3) CHI3L1-specific blocking antibodies reduced this effect. We also found that pirfenidone treatment blocked the effects of CHI3L1 on collagen formation (Figure 2-18B), suggesting that the anti-fibrotic effects of the drug are cooperative: blocking the TGF-β1 signaling pathway inhibits both production of pro-collagen and CHI3L1, thereby blocking fibril formation.

Discussion

The hallmark of untreated immunodeficiency virus infections is the cumulative depletion of CD4+ T cells that is most marked in the later stages of infection by the predominant depletion in blood and LT of naïve CD4+ T cells [46, 105, 144]. This has been attributed to impaired output from the thymus [69-70, 169] combined with loss in the periphery, where T cells die by direct and indirect mechanisms related to chronic immune activation: 1) activated naïve T cells become memory T cells that are susceptible to

infection in which they succumb or are killed by virus-specific CD8+ T cells; and 2) activated cells undergo activation-induced cell death [68, 71-72].

To these established mechanisms we now add another indirect mechanism of T cell depletion in which chronic immune activation elicits a T regulatory counter response with the adverse consequence of increased collagen production and deposition. This, in turn, sets in motion cooperative and cumulative mechanisms that contribute to the depletion of T cells, particularly naïve T cells in SIV-infected RMs (Figure 2-19A): Collagen disrupts T cell access to IL-7 provided on the FRC network, leading to increased apoptosis of T cells, particularly naïve T cells. The depletion of LTβ+ T cells, in turn, deprives the FRC network of the major source of LTβ+ [156] on which it depends [157]. This, along with the collagen-restricted access of LTβ+ T cells to the FRC network, results in loss of the FRC network and further decreases in IL-7 availability for T cells. Thus, a positive loop mechanism (Figure 2-19) is established that progressively and cumulatively causes T cell depletion, particularly in the naïve T cell populations.

This mechanism provides a broadened perspective on the preferential depletion of naïve CD4+ T cells in late HIV infection in both peripheral blood and LTs [46, 48, 144] and helps explain why both naïve CD4+ and CD8+T cells are depleted in HIV infection [46, 170], thereby impairing the ability to respond to new infections and malignancies. Because of resistance to viral infection by naïve CD8+ T cells and relative resistance to viral infection and killing of naïve CD4+ T cells [47, 171] compared to memory CD4+ T cells [172-173], depletion of these populations has heretofore been attributed to indirect mechanisms of apoptosis associated with chronic immune activation [68, 71-72], and to decreased thymic output [69-70, 169], rather than direct mechanisms. However, these indirect mechanisms do not fully account for the continued apoptosis and slow and incomplete restoration of the naïve CD4+ T cell populations after HAART has largely suppressed direct losses attributable to viral infection, and after immune activation has largely subsided with commensurate decreases in activation induced cell death [48] (Figure 2-19A). On the other hand, collagen deposition, which impairs access to IL-7 on

the FRC network and causes loss of the FRC network itself as an important source of IL-7, provides mechanisms for: 1) depletion of both naïve CD4+ and CD8+ T cells [46, 170]; 2) continued high level of apoptosis in LTs while on HAART; and 3) the correlation between the extent of fibrosis of LTs before the initiation of HAART and the extent of restoration of naïve CD4+ T cells after long term HAART [146] (Figure 2-19B).

Our findings suggest the potential benefit of IL-7 treatment during HIV infection. Indeed, studies have shown that complementing HAART with IL-7 during both SIV and HIV infection significantly increases the circulating naïve CD4+ T cell number [174-176]. Furthermore, ex vivo and in vivo studies with T cells from HIV infected patients showed that IL-7 treatment could significantly up-regulate Bcl-2 levels to normalize the extent of apoptosis in CD4+ and CD8+ T cells from HIV-infected individuals [177-178]. These data consistently suggest that insufficient IL-7 is a key contributor in the impaired T cell homeostasis in SIV/HIV infection.

However, the immediate decline of the absolute numbers of both naïve CD4+ and CD8+ T cells after termination of IL-7 therapy [174-176] suggests that complementing IL-7 only provides transient survival benefit for naïve CD4+ and CD8+ T cells and strongly argues for the development of therapeutic interventions to provide long-term survival benefit for naïve T cells. Our findings here clearly suggest that collagen deposition and the loss of FRCs as the major source of IL-7 play critical roles in compromising homeostasis of naïve T cells and thus restoration of the LT niche could potentially provide long-term survival benefit for naïve T cells.

Our findings on mechanisms of fibrosis in LTs during HIV infection also support a cooperative and cumulative mechanism of collagen deposition driven by immune activation (Figure 2-19A). The increased expressions of both TGF-β1 in regulatory T cells (responding to immune activation) and its cognate receptor in spatially proximate fibroblasts chronically activate the TGF-β1 signaling pathway. This results in increased expression of pro-collagen, the immature, unprocessed form of collagen (Figure 2-20).

TGF-β1 also enhances the expression of CHI3L1, so that in this model, TGF-β1 plays a dual role—a cytokine which increases both an upstream substrate (pro-collagen) and its downstream effector (CHI3L1) within the same cell type (fibroblast), thereby establishing a cooperative process of collagen deposition and cumulative fibrosis in LT during HIV infection.

The link established here between fibrosis, damage to the LT niche through loss of access and a source of IL-7 on the FRC network, and naïve T cell depletion clearly argues for therapeutic approaches targeting fibrosis and maintaining and restoring a functional FRC network. Because the underlying mechanisms of both fibrosis and damage to the FRC network operate cumulatively, the most straightforward way to do this would be through earlier initiation of HAART to limit the inflammation associated with viral replication that drives the process. In addition, development of adjunctive anti-fibrosis treatment might additionally avert or lessen the consequences of damage to the LT niche and improve immune reconstitution. As a proof of principle, we targeted the TGF-β1 signaling pathway with the anti-fibrotic drug pirfenidone, currently in a phase II clinical trial in the treatment of pulmonary fibrosis [179], and showed that we could dramatically reduce collagen production by primary human fibroblasts. Thus, therapeutic interventions directed at theTGF-β1 signaling pathway, or other pathways involved in collagen formation, deposition, and degradation could potentially avert or moderate LT fibrosis and improve immune reconstitution post HAART.

Acknowledgements

We thank the Yerkes National Primate Research Center (Atlanta, GA); D. Masopust and V. Vezys for providing CD3 depleting antibodies; C. O'Neill and T. Leonard for help in preparing the manuscript and figures; Jeffrey Browning for providing soluble LTβR-Ig and control IgG; and Dr. Ben Ng from Carl Zeiss for help in generating the 3D images. We also thank all of the donor participants in this study. This work was supported in part by NIH research grants AI028246, AI048484 and AI056997 to A.T.H., in part by Yerkes

base grant P51-00165 to G. S. and in part by federal funds from the National Cancer Institute, National Institutes of Health, under Contract No. HHSN261200800001E.

Figure 2-1.

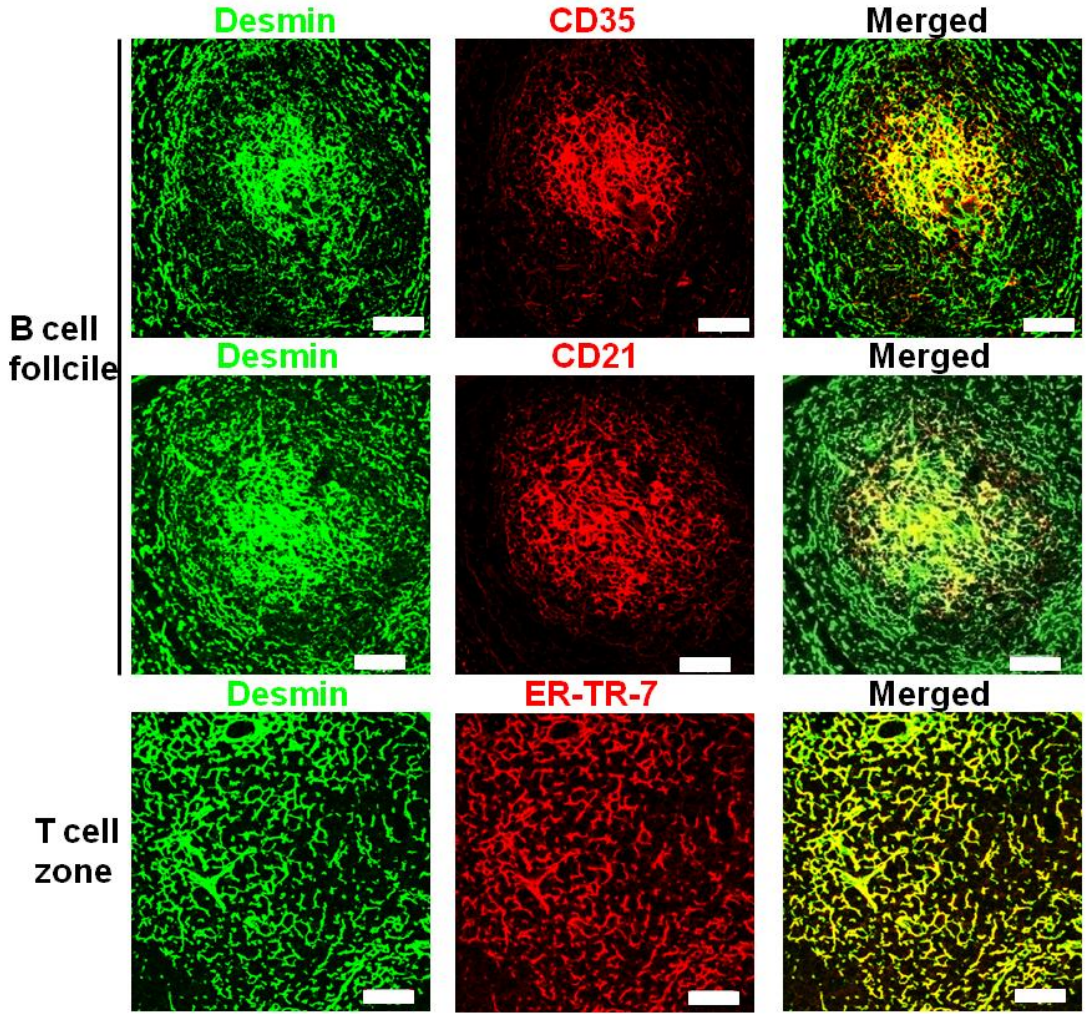

Figure 2-1. Desmin is a marker of FRCs and FDCs. Confocal images of LN sections from uninfected RMs (representative image for one animal of 9) stained for desmin (green) and markers (red) for FDCs (CD35, CD21) and FRCs (ER-TR-7). Desmin staining co-localizes respectively with FDC markers and FRC marker. FDCs form a network with higher density than the FRC network in T cell zone. Scale bars, 50 μm.

Figure 2-2.

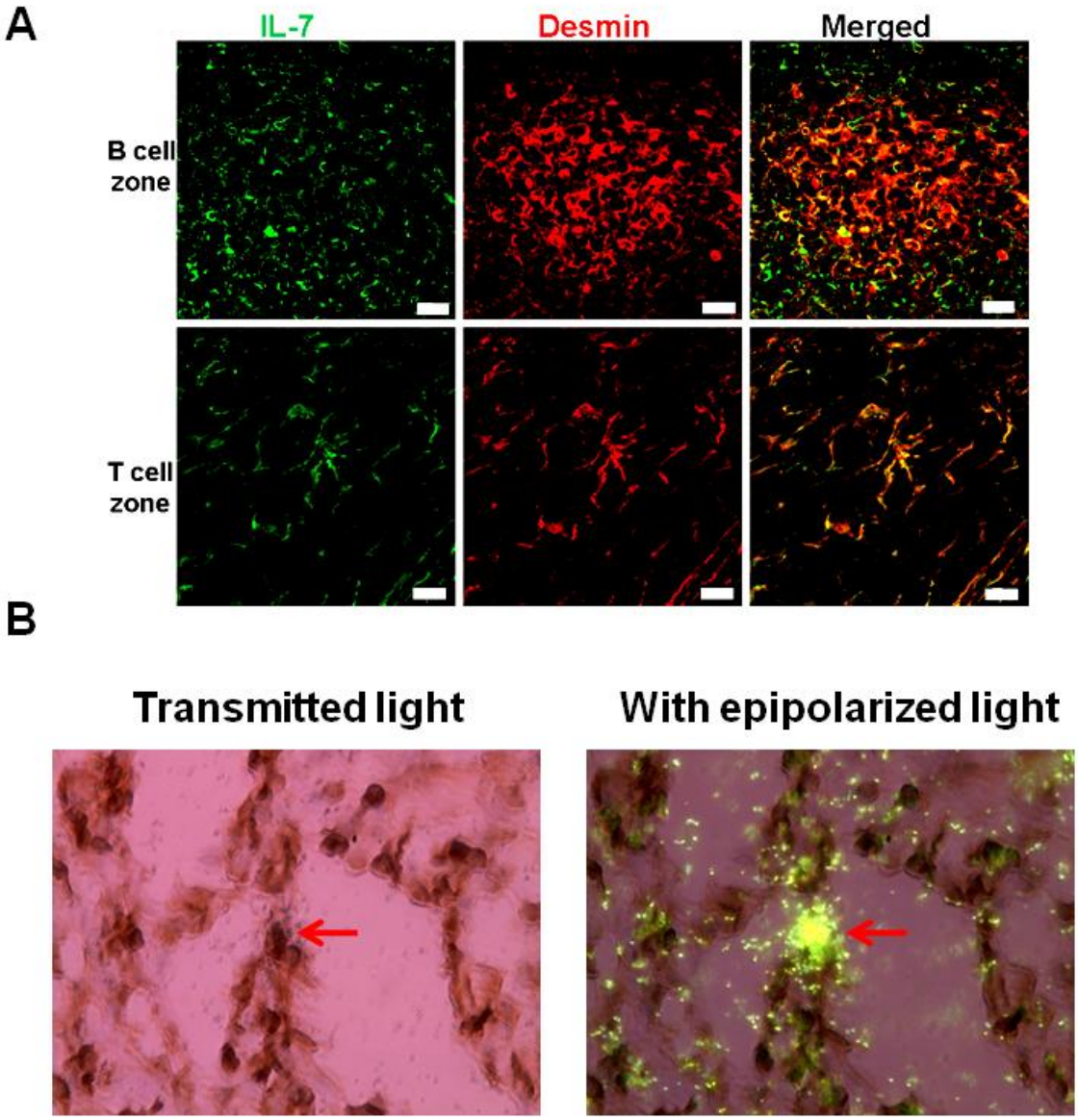
A
IL-7
Desmin
Merged
B cell zone
T cell zone
B
Transmitted light
With epipolarized light

Figure 2-2. FRC and FDC networks are the major producers of IL-7. (**A**) LN sections (representative image for one animal of 3) stained for desmin (red) and IL-7 (green). Merged confocal image shows co-localization of IL-7 and FRC and FDC networks in B cell follicle and T cell zones respectively. Scale bar, 20 μm. (**B**) ISH for IL-7 mRNA combined with desmin immunohistochemical staining (brown), showing the co-localization of IL-7 mRNA and FRCs. In the image taken in transmitted light (left panel), the FRCs and their processes have been stained brown. The red arrow points to the position of IL-7 mRNA shown in the right panel. In developed radioautographs, after hybridization to a S^{35} -labelled IL-7 specific riboprobe, the signals (with epipolarized light) are yellow appearing silver grains overlying the stained FRCs and FRC processes (red arrow). Magnification, 600x.

Figure 2-3.

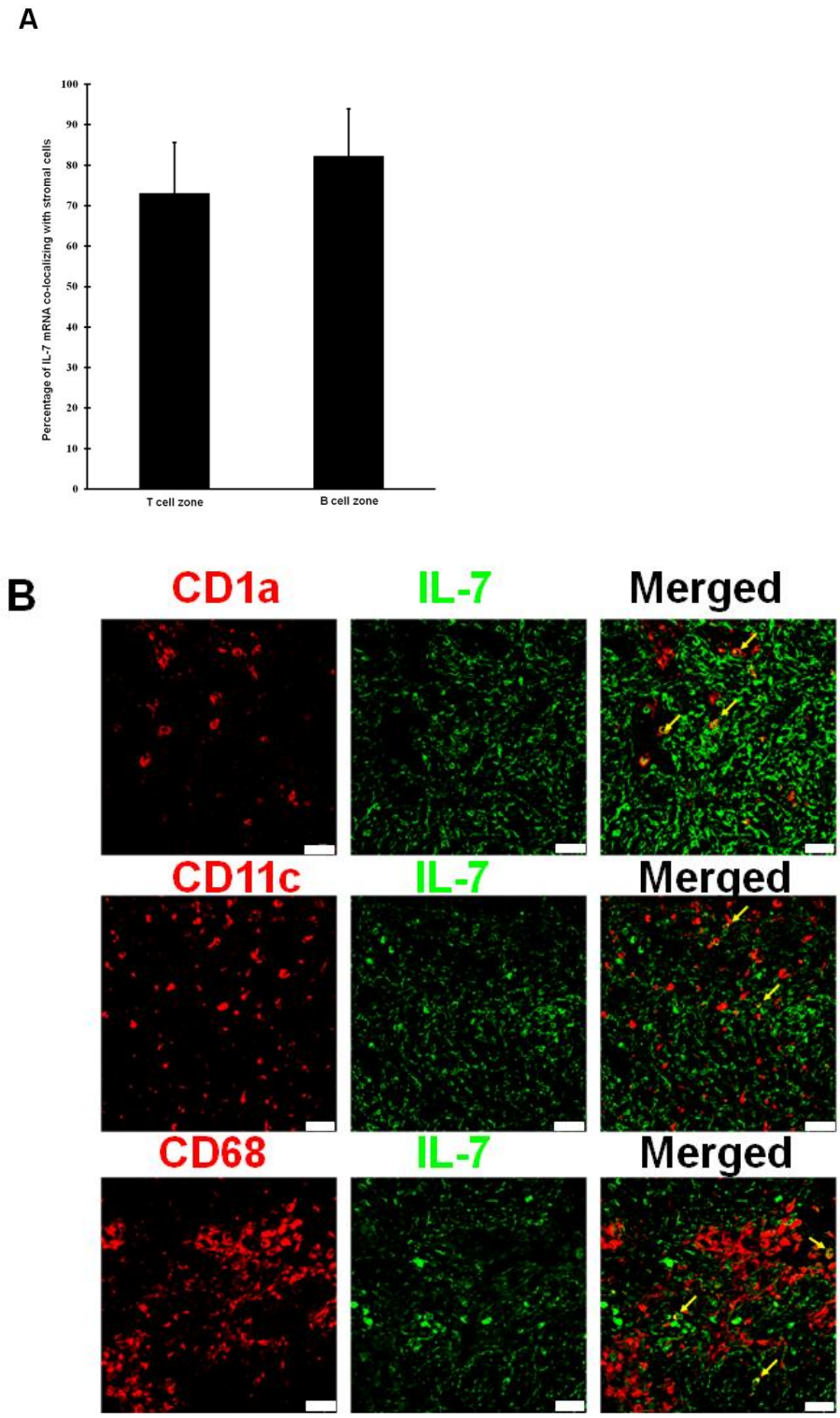
A
Percentage of IL-7 mRNA co-localizing with stromal cells
100
90
80
70
60
50
40
30
20
10
0
T cell zone
B cell zone
B
CD1a
IL-7
Merged
CD11c
IL-7
Merged
CD68
IL-7
Merged

Figure 2-3. FRCs and FDCs are the major sources of IL-7 in LTs. (**A**) Quantitative image analysis of the percentage of the IL-7 mRNA signal that co-localizes with desmin+ FRCs in T cell zone and FDCs in the B cell follicles. Values are the mean of the percentage of the IL-7 mRNA signal that co-localizes with desmin+ cells ± s.d. (**B**) Confocal image of LN sections from uninfected RMs (representative image for one animal of 3) double immunofluorescently stained for IL-7 (green) and CD1a, CD11c or CD68 (red), showing a small portion of IL-7 is produced by a subset of dendritic cells or macrophages. Scale bar, 30 μm.

Figure 2-4.

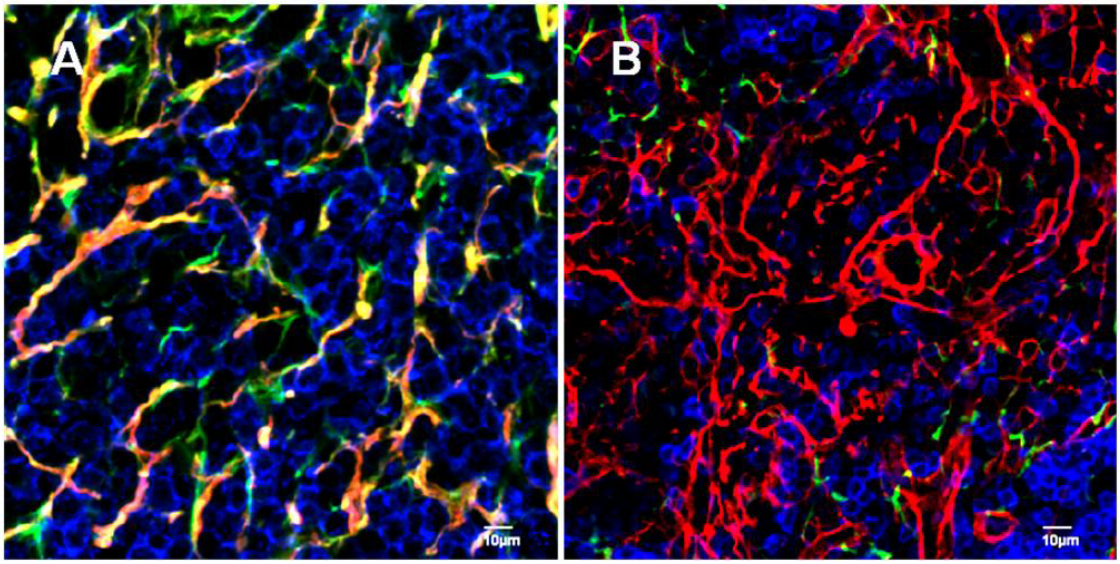

Figure 2-4. Collagen deposition and loss of the FRC network lead to loss of contact between T cells and FRCs. (**A**) In the merged confocal image in an uninfected RM (representative image for one animal of 9), collagen (red) co-localizes with the FRC network (green), and the CD3+ T cells (blue) are in contact with the FRC network. (**B**) In an animal at 180 dpi (representative image for one animal of 4), there is abundant collagen staining that does not co-localize with the FRC network. Note the FRC network (green) is also greatly decreased, so that large numbers of T cells are not in contact with the FRC network, but instead mainly contact extra-FRC collagen. Scale bar, 10 μm.

Figure 2-5.

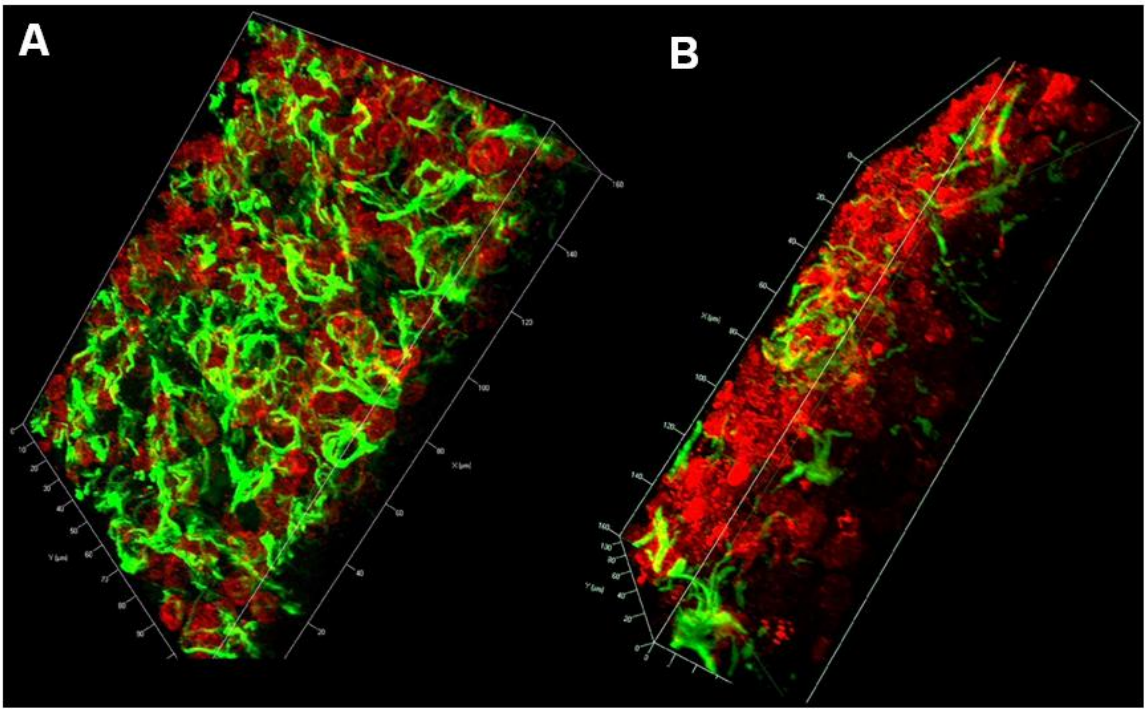

Figure 2-5. T cells lose contact with FRCs during SIV infection. (**A-B**) Optical 3D slice showing green stained FRC network and red-stained CD3 T cells in (**A**) an uninfected RM (representative image for one animal of 3) and (**B**) a SIV-infected RM at 180 dpi (representative image for one animal of 4). In the infected animal, much of the FRC network has been lost and T cells are not in contact with FRCs. Scale bar, 20 μm per divide.

Figure 2-6.

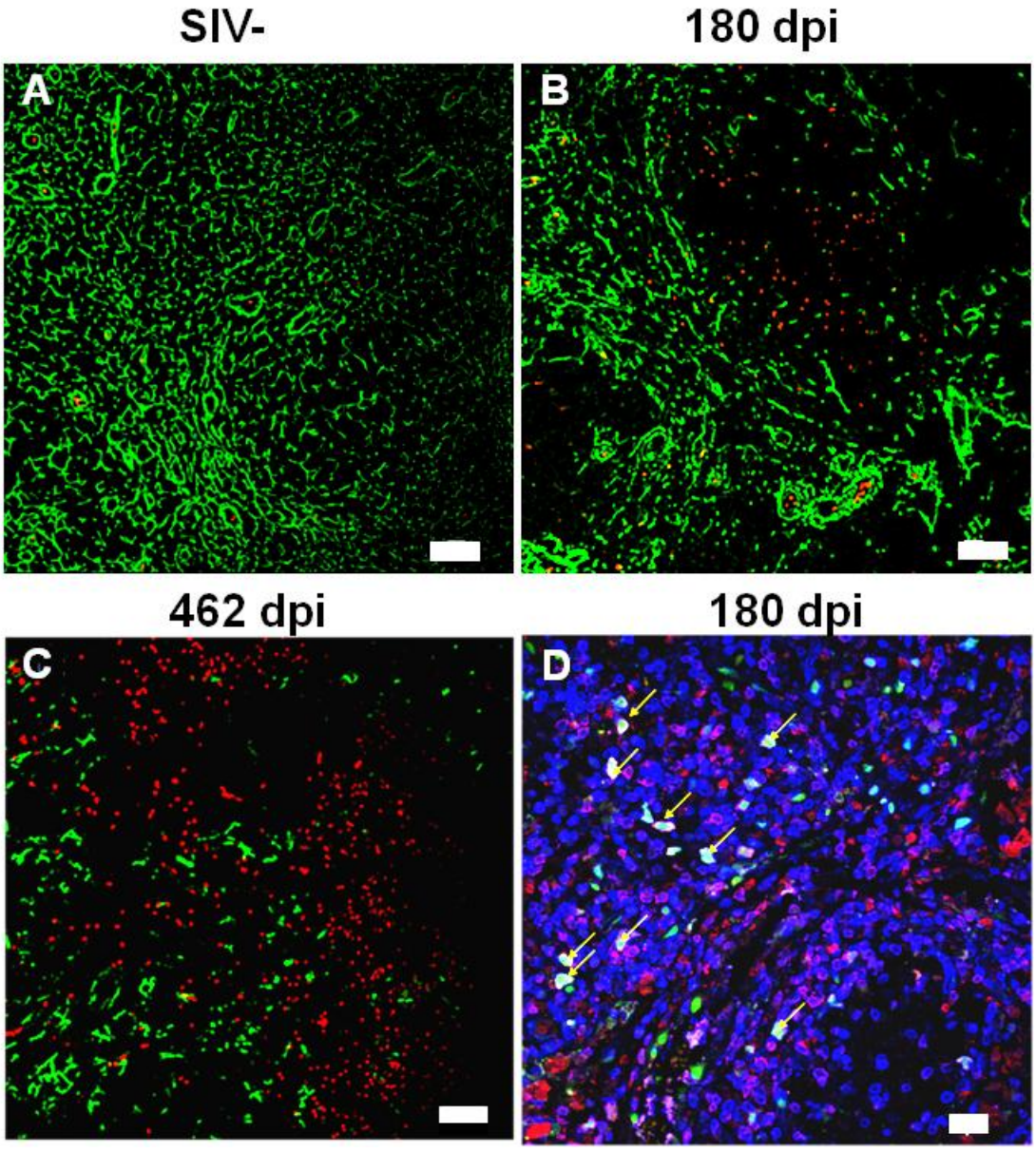

Figure 2-6. Loss of FRC network leads to increased apoptosis of naïve T cells. (**A-C**) Confocal images of LN sections from RMs at different time points post SIV infection double immunofluorescently stained for desmin (green) and activated caspase 3 (red), showing increased apoptosis associated with loss of the FRC network at (**B**) 180 dpi (representative image for one animal of 5) and (**C**) 462 dpi (representative image for one animal of 5 animals infected longer than 200 days) compared with (**A**) uninfected RMs (representative image for one animal of 9). Scale bar, 20 μm. (**D**) Confocal image of a LN section showing apoptotic naïve T cells (yellow arrows) (TUNEL+ (green) CD45RA+ (Red) CD3+ (blue)) at 180 dpi (representative image for one animal of 5). Scale bar, 20 μm.

Figure 2-7.

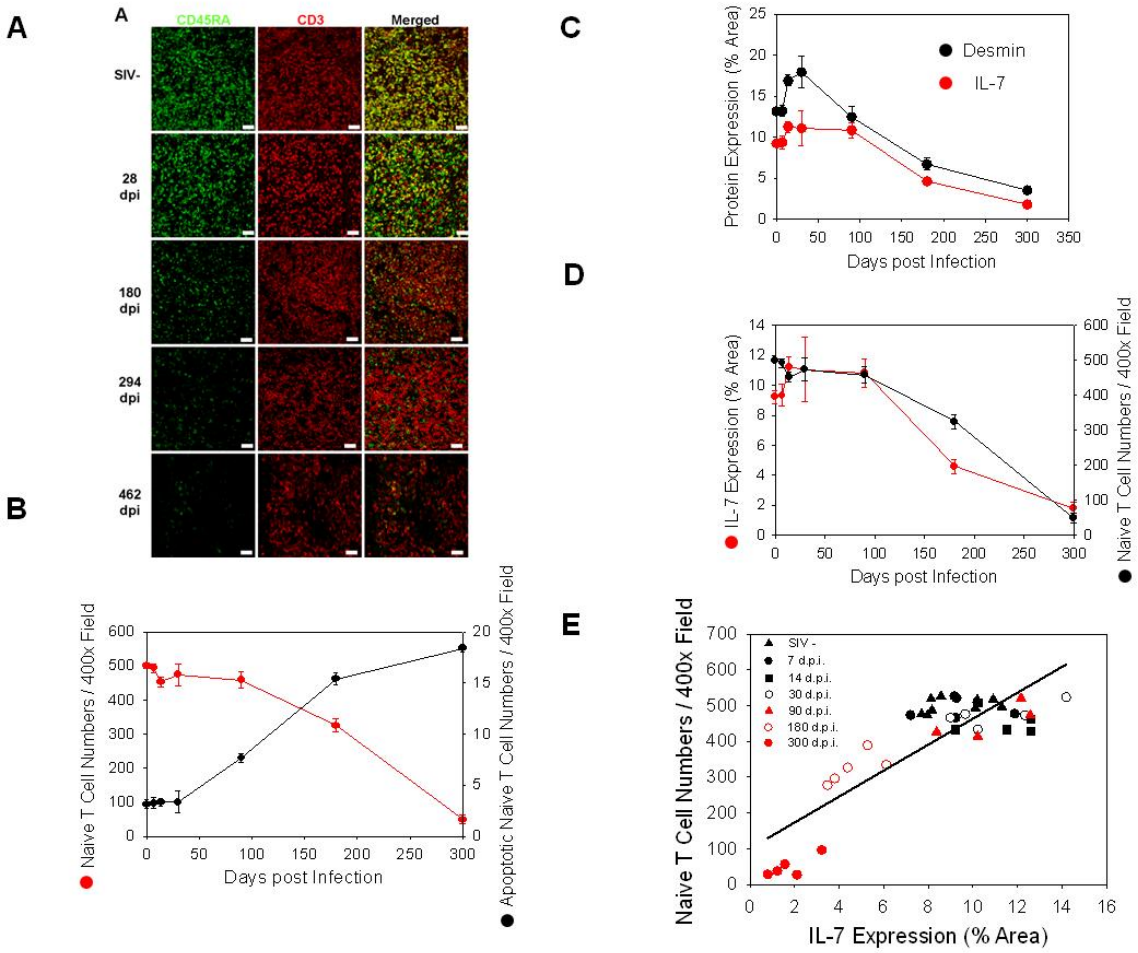
A
CD45RA
CD3
Merged
SIV-
28 dpi
180 dpi
294 dpi
462 dpi
B
Naive T Cell Numbers / 400x Field
Apoptotic Naive T Cell Numbers / 400x Field
Days post Infection
C
Desmin
IL-7
Protein Expression (% Area)
Days post Infection
D
IL-7 Expression (% Area)
Naive T Cell Numbers / 400x Field
Days post Infection
E
SIV -
7 d.p.i.
14 d.p.i.
30 d.p.i.
90 d.p.i.
180 d.p.i.
300 d.p.i.
Naive T Cell Numbers / 400x Field
IL-7 Expression (% Area)

Figure 2-7. Loss of FRCs is associated with loss of naïve T cells within LTs. (**A**) Confocal images of LN sections from RMs at different time points post SIV infection double immunofluorescently stained for CD45RA (green) and CD3 (red), showing the gradual loss of CD45RA+CD3+ naïve T cells within LTs during SIV infection (total n=38, n=9 for uninfected RMs, n=5 for 7 dpi, n=5 for 14 dpi, n=5 for 30 dpi, n=4 for 90 dpi, n=5 for 180 dpi, n=5 for 300 dpi). Scale bar, 30 μm. (**B**) Quantification of the number of apoptotic naïve T cells (TUNEL+CD45RA+CD3+) and the number of naïve T cells (CD45RA+CD3+), showing the statistically significant inverse association (total n=38, p=0.0001). Time point shown as 300 dpi represents the mean measurement of 5 animals which were infected for 222 days, 280 days, 294 days, 462 days and 560 days respectively. (**C**) Quantitative image analysis of the percent area staining positive for desmin and the percent area staining positive for IL-7, showing the statistically significant association between the quantity of IL-7 and the quantity of the FRC network (total n=38, p<0.0001). (**D**) Quantitative image analysis of percent area staining positive for IL-7 and the number of CD45RA+CD3+ naïve T cells within LTs, showing the kinetics of IL-7 and the kinetics of naïve T cell number. Error bars represent the s.d. (**E)** Quantitative image analysis of percent area staining positive for IL-7 and the number of CD45RA+CD3+ naïve T cells for each animal, showing that the loss of naïve T cells is associated with loss of IL-7 production (total n=38, p=0.0004).

Figure 2-8.

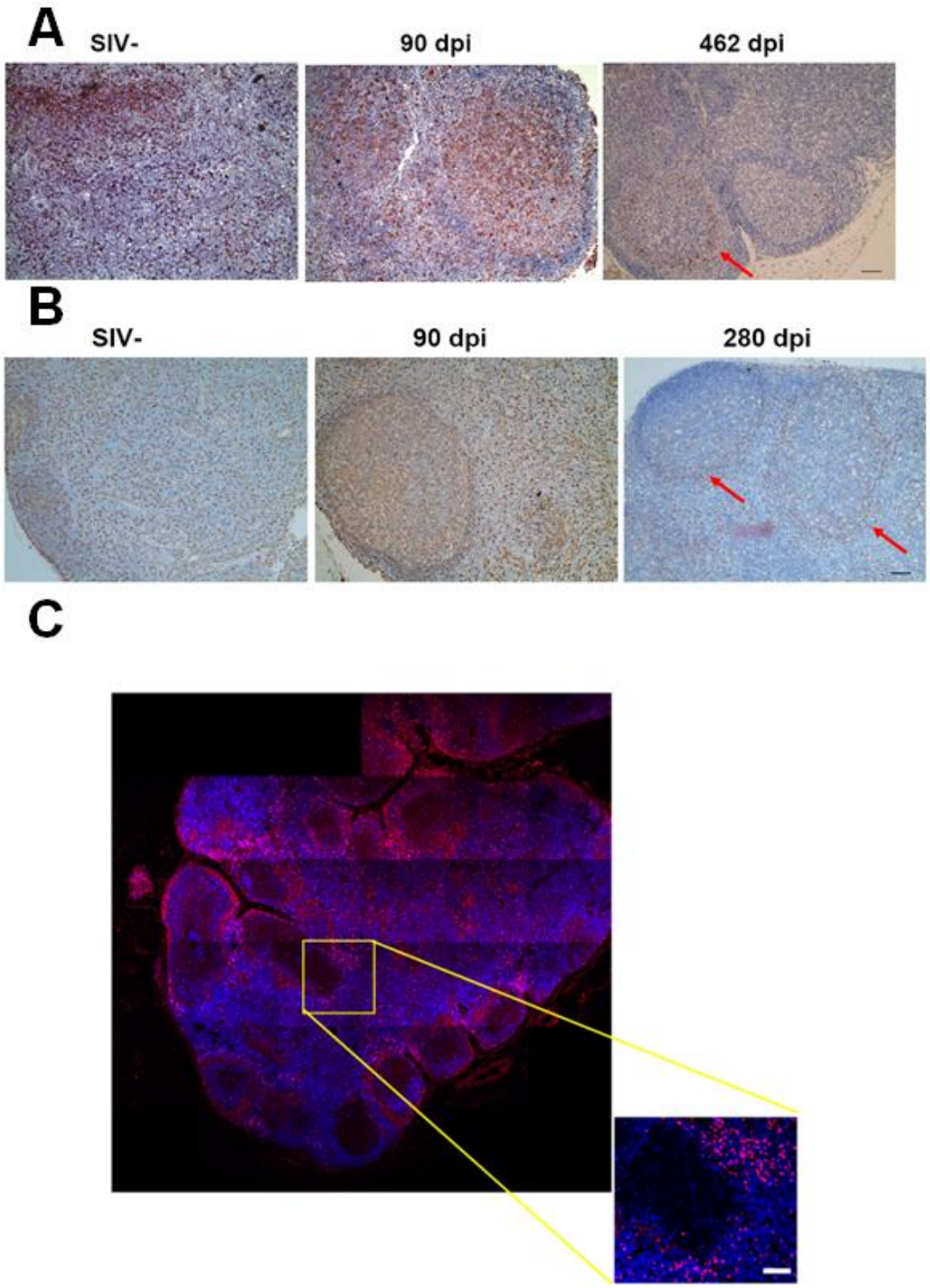

D

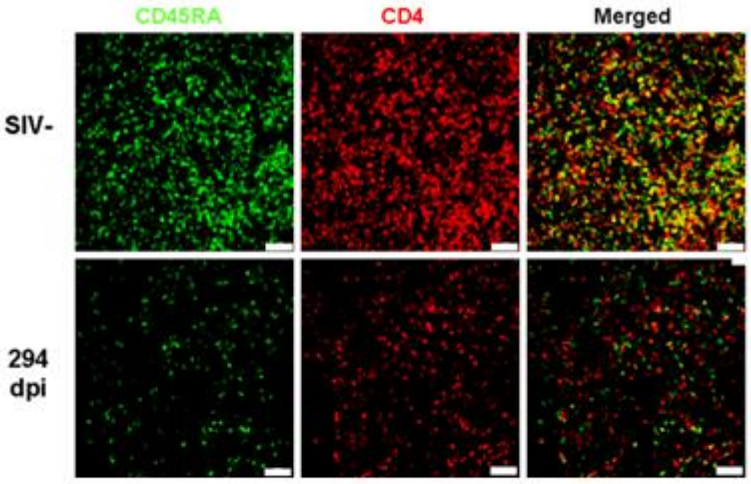
CD45RA
CD4
Merged
SIV-
294 dpi

E

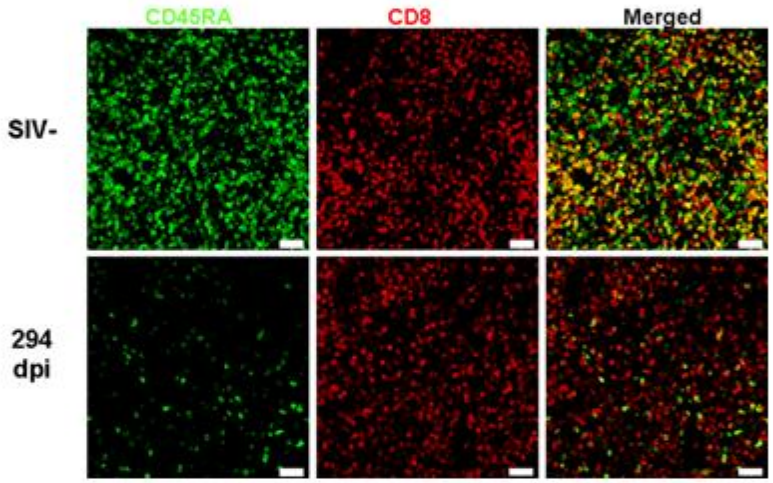
CD45RA
CD8
Merged
SIV-
294 dpi

F

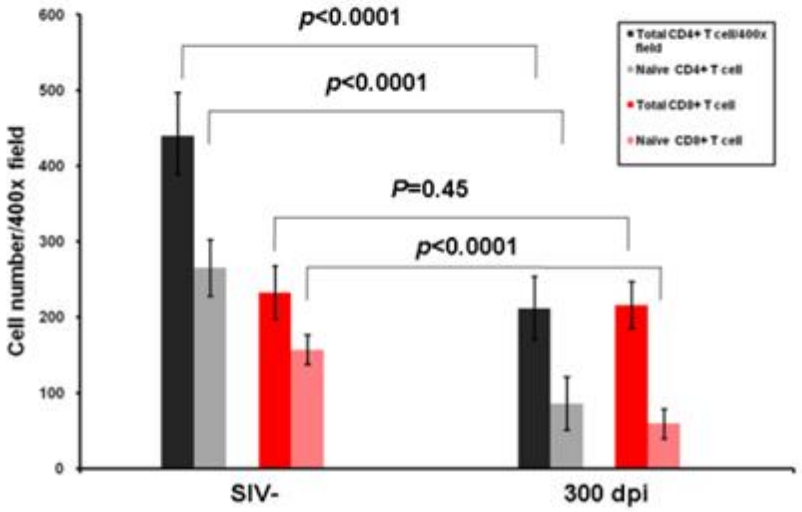
p<0.0001
p<0.0001
P=0.45
p<0.0001
Total CD4+ T cell/400x field
Naïve CD4+ T cell
Total CD8+ T cell
Naïve CD8+ T cell
Cell number/400x field
600
500
400
300
200
100
0
SIV-
300 dpi

Figure 2-8. Loss of FRCs is associated with decreased IL-7 and depletion of naïve T cells within LNs in SIV infection. (**A-B**) Immunohistochemical staining of (**A**) IL-7 and (**B**) desmin in LNs from RMs at different time points post infection. Red arrow points to residual IL-7 and residual FRCs at the B-T cell zone border (representative image for one of 4 animals at each time point). Scale bar, 40 μm. (**C**) Montage image of confocal images of LN section from RMs at 294 dpi stained for CD45RA (red) and CD3 (blue) showing that the residual naïve T cells reside at the B-T border. Scale bar in the inset, 20 μm. (**D-E**) Confocal image of LN sections from uninfected RMs (representative image for one of 4 animals) and RM at 294 dpi stained for CD45RA (green) and CD4 or CD8 (red), showing the progressive and parallel loss of naïve CD4+ and CD8+ T cells within LTs during SIV infection. Scale bar, 30 μm. (**F**) Quantification of the number of total CD4+ and CD8+ T cells and CD45RA+ naïve CD4+ and CD8+ T cells before and in the chronic phase of infection. Note the rate of the loss of naïve CD8+ T cells is parallel to the loss of naïve CD4+ T cells. (Two-tailed *t* test, n=5, values are the mean of the number of cells ± s.d.)**.**

Figure 2-9.

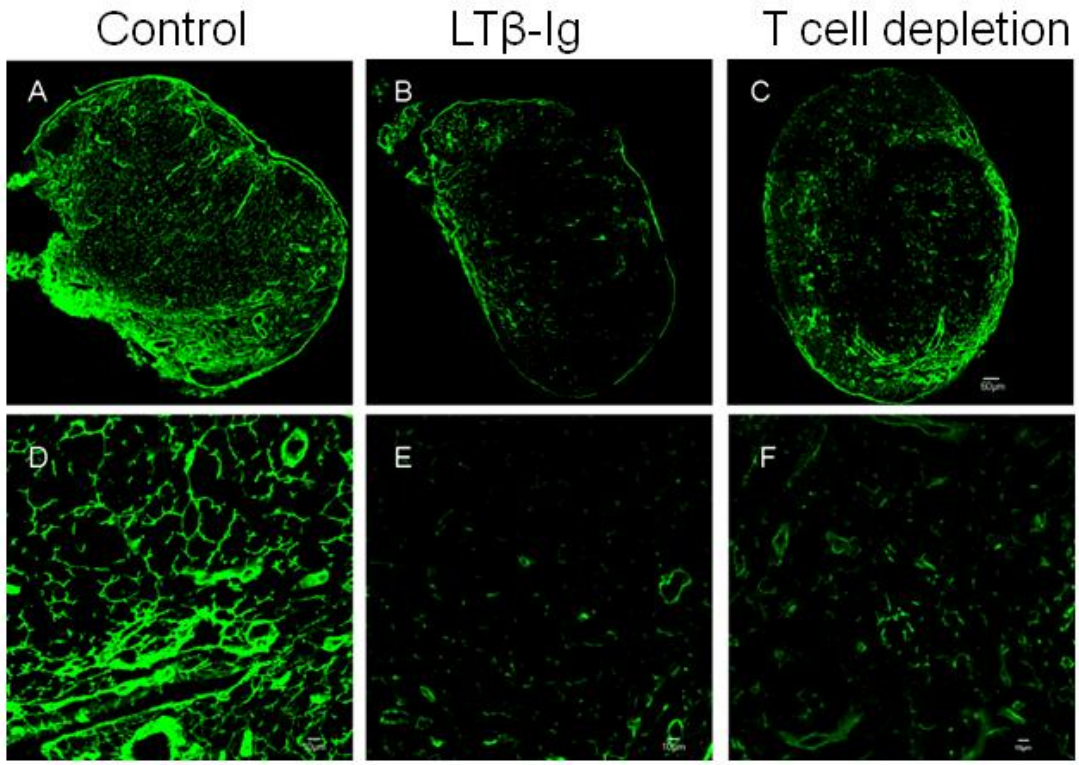
Control
LTβ-Ig
T cell depletion
A
B
C
D
E
F

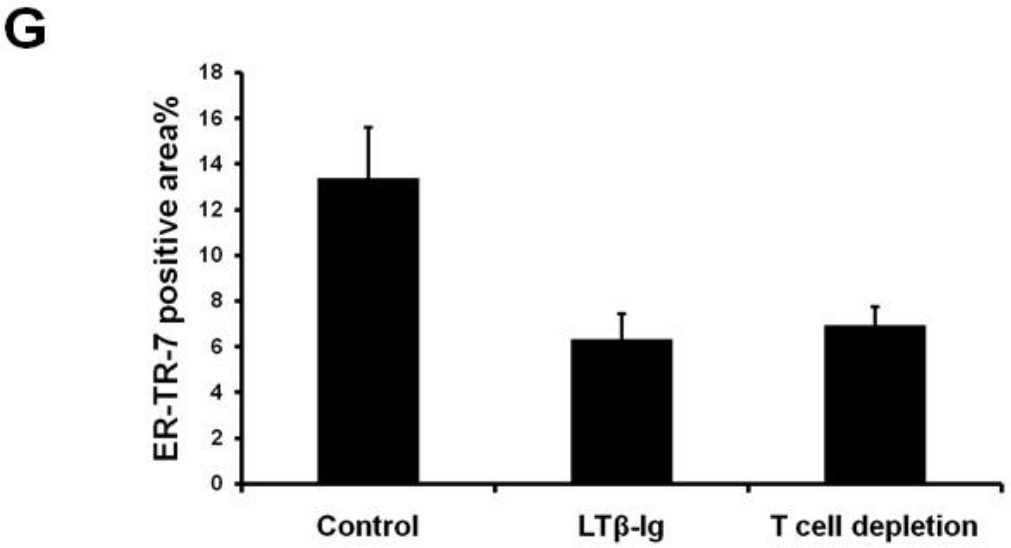
G
ER-TR-7 positive area%
18
16
14
12
10
8
6
4
2
0
Control
LTβ-Ig
T cell depletion

Figure 2-9. LTβR-Ig treatment and T cell depletion leads to FRC depletion in mouse LNs. (**A-C**) ER-TR-7 staining in LN sections from mice (representative image for one animal of 3) treated with two weekly injections of control IgG (**A**), two weekly injections of LTβR-Ig (**B**), or with 8 weekly injections of CD3 depleting antibody (**C**). Scale bar, 300 μm. (**D-F**) Magnified images of (**A-C**) respectively. Scale bar, 30 μm. (**G**) Quantification of percent area of FRCs in control, LTβR-Ig treated or CD3 depleting antibody-treated mice. Data are expressed as the mean ± s.d..

Figure 2-10.

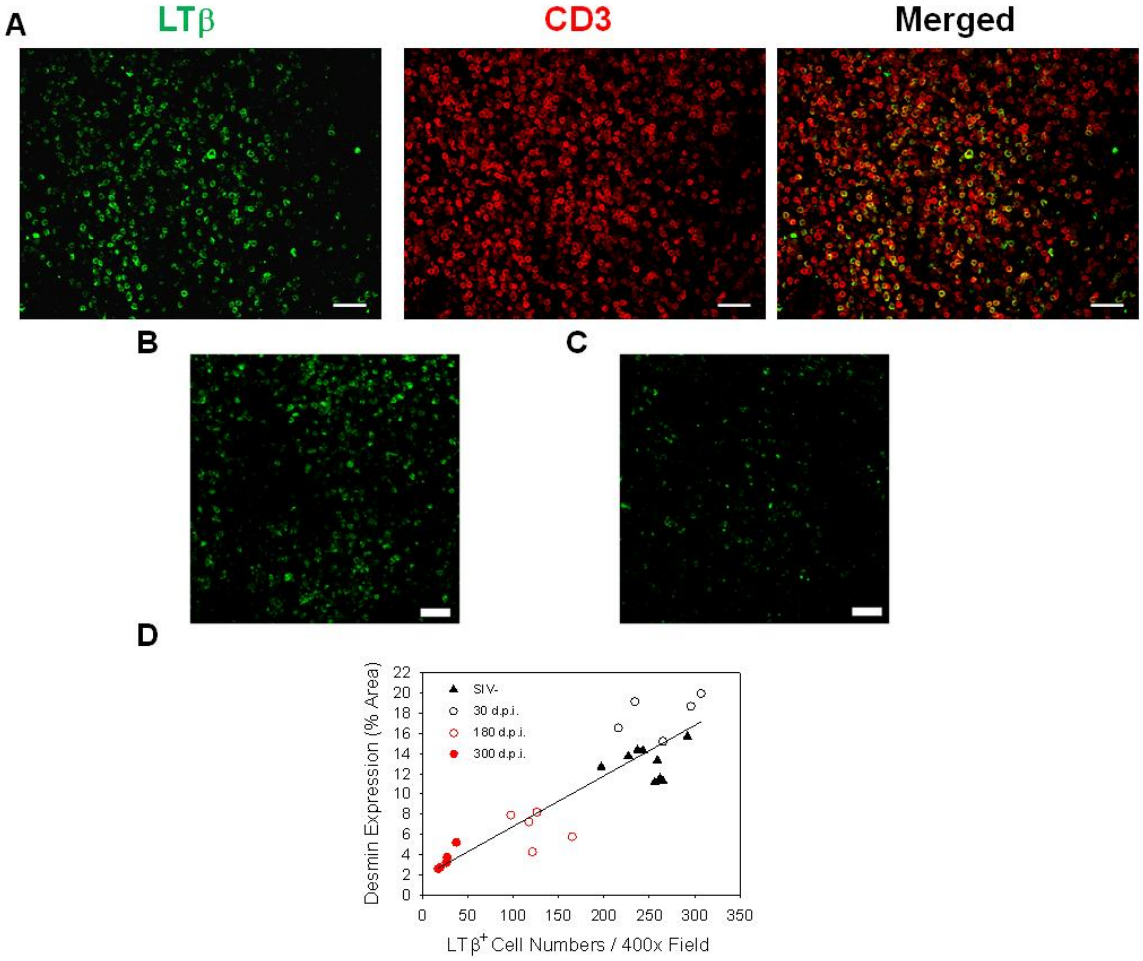
A
LTβ
CD3
Merged
B
C
D
SIV-
30 d.p.i.
180 d.p.i.
300 d.p.i.
Desmin Expression (% Area)
LTβ+ Cell Numbers / 400x Field
0
2
4
6
8
10
12
14
16
18
20
22
0
50
100
150
200
250
300
350

Figure 2-10. LTβ+ T cells are depleted during SIV infection in RMs. (**A**) Confocal images (representative image for one animal of 5) showing CD3+ T cells (red) are the major producers of LTβ (green) in the T cell zone in an uninfected RM LN. (**B-C**) Progressive depletion of LTβ+ T cells (green) in RM LTs at (**C**) 180 dpi (representative image for one animal of 5) compared to (**B**) 30 dpi and (**A**) uninfected animal. Scale bar, 30 μm. (**D**) Quantitative image analysis of number of LTβ+ T cells and the percent area staining positive for desmin for each animal, showing the correlation between LTβ+ T cells and FRCs ($p<0.0001$. n=9 for uninfected RMs, n=5 for 30 dpi, n=5 for 180 dpi, n=5 for 300 dpi).

Figure 2-11.

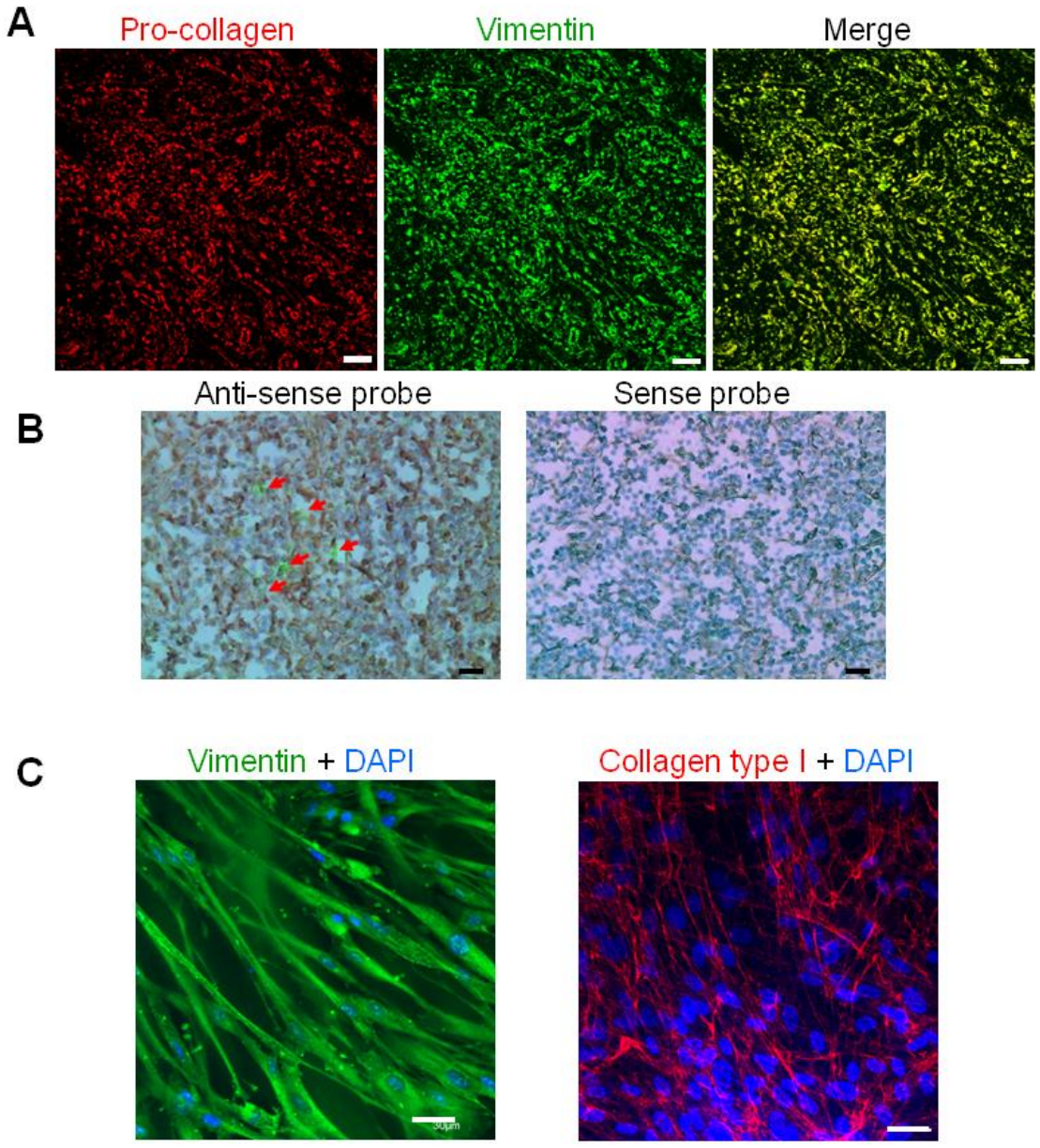
A
Pro-collagen
Vimentin
Merge
B
Anti-sense probe
Sense probe
C
Vimentin + DAPI
Collagen type I + DAPI

Figure 2-11. Fibroblasts are the major producers of type I collagen within LT during HIV infection. (**A**) Immunofluorescent images of pro-collagen (red staining) and vimentin (green staining) in the LT from an HIV infected individual in the presymptomatic stage of disease, showing co-localization between pro-collagen and vimentin+ fibroblasts (representative image for one of 4 subjects). Scale bars: 50 μm. (**B**) Immunohistochemical images of vimentin staining (brown) combined with ISH of type I collagen mRNA (yellow/green appearing silver grains due to epipolarized reflected light). Red arrows indicate co-localization between vimentin+ fibroblasts and collagen type I mRNA (representative image for one of 4 subjects in presymptomatic stage). Sense probe shows the negative control staining. Scale bars: 20 μm. (**C**) Immunofluorescent images of vimentin (green staining) and type I collagen (red staining) in primary human fibroblasts isolated from tonsillar tissue from an uninfected individual, revealing basal levels of extracellular type I collagen from an ex vivo culture system 2 days post isolation. Cell nuclei appear blue (DAPI). Scale bars: 30 μm.

Figure 2-12.

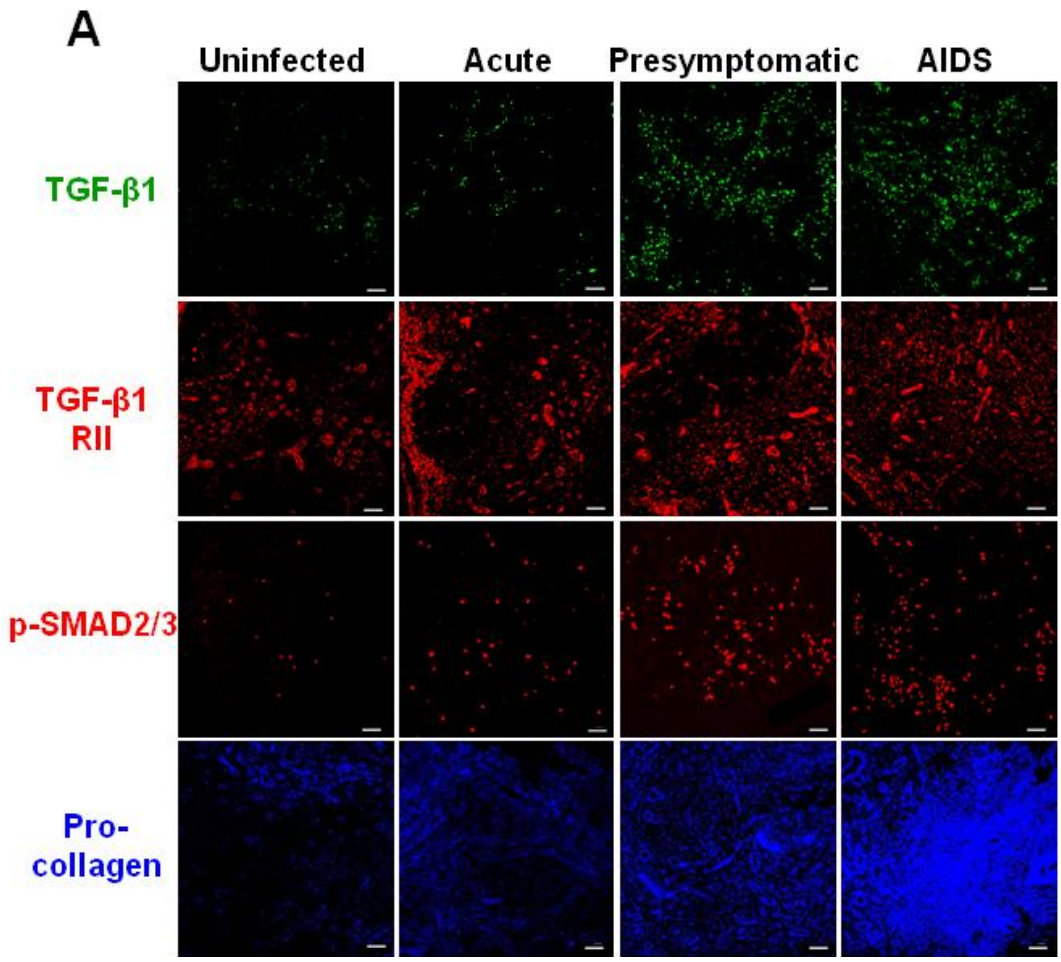
A
Uninfected
Acute
Presymptomatic
AIDS
TGF-β1
TGF-β1 RII
p-SMAD2/3
Pro-collagen

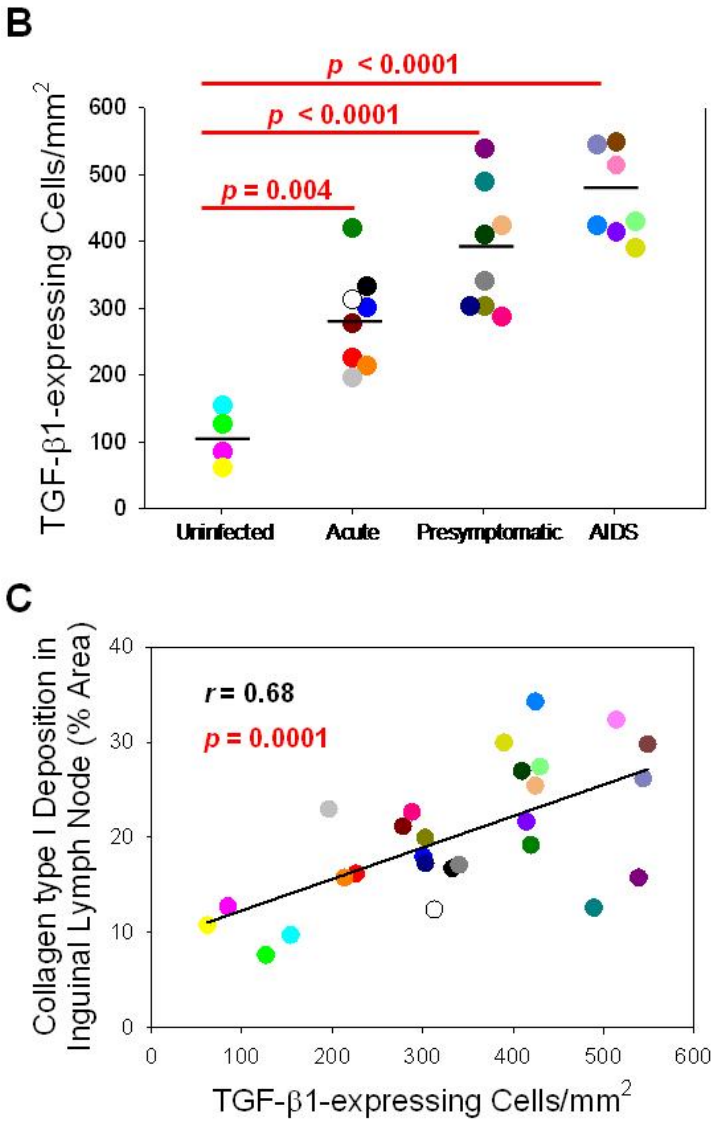
B
p < 0.0001
p < 0.0001
p = 0.004
TGF-β1-expressing Cells/mm2
600
500
400
300
200
100
0
Uninfected
Acute
Presymptomatic
AIDS
C
Collagen type I Deposition in Inguinal Lymph Node (% Area)
r = 0.68
p = 0.0001
40
30
20
10
0
0
100
200
300
400
500
600
TGF-β1-expressing Cells/mm2

Figure 2-12. The TGF-β1 signaling pathway is activated in LTs during HIV infection. (**A**) Immunofluorescent images of TGF-β1 (green staining, top panels), TGF-β1 RII (red staining, upper-middle panels), p-SMAD2/3 (red staining, lower-middle panels), and pro-collagen (blue staining, bottom panels) in LTs from HIV infected individuals, showing a parallel increase in TGF-β1 and its cognate receptor, leading to activation of the TGF-β1 signaling pathway (p-SMAD2/3) and resulting synthesis of pro-collagen (representative image for one of 4 subjects at each stage). Scale bars: 50 μm. (**B**) TGF-β1+ cells were quantified in each LN biopsy and reported as number of TGF-β1-expressing cells per mm^2 of tissue. Mean values for each group are indicated by horizontal black bars. (**C**) TGF-β1-expressing cells were significantly correlated with collagen type I deposition in the inguinal LN.

Figure 2-13.

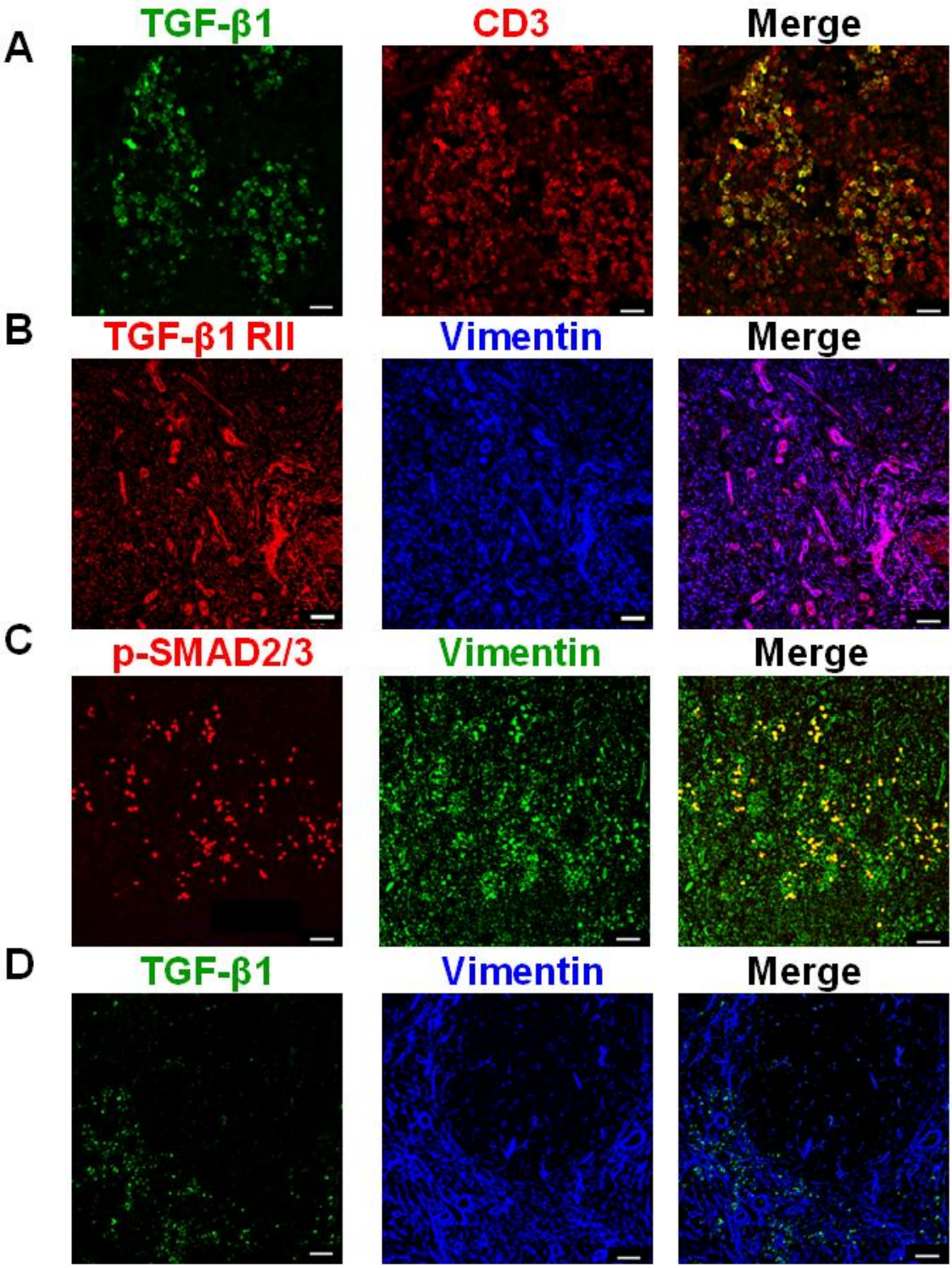
A
TGF-β1
CD3
Merge
B
TGF-β1 RII
Vimentin
Merge
C
p-SMAD2/3
Vimentin
Merge
D
TGF-β1
Vimentin
Merge

Figure 2-13. TGF-β1 expression occurs predominantly in CD3+ T cells while components of the TGF-β1 signaling pathway (TGF-β1 RII, p-SMAD2/3) are expressed in vimentin+ fibroblasts. Immunofluorescent images of (**A**)TGF-β1 (green staining) and CD3 (red staining), (**B**) TGF-β1 RII (red staining) and vimentin (blue staining), (**C**) p-SMAD 2/3 (red staining) and vimentin (green staining) and (**D**) TGF-β1 (green staining) and vimentin (blue staining) in LT from HIV infected individuals (representative image for one of 4 subjects), showing the close spatial proximity between TGF-β1-expressing $CD3^+$ T cells and vimentin+ fibroblasts expressing the TGF-β1 RII. Scale bars: 20 μm.

Figure 2-14.

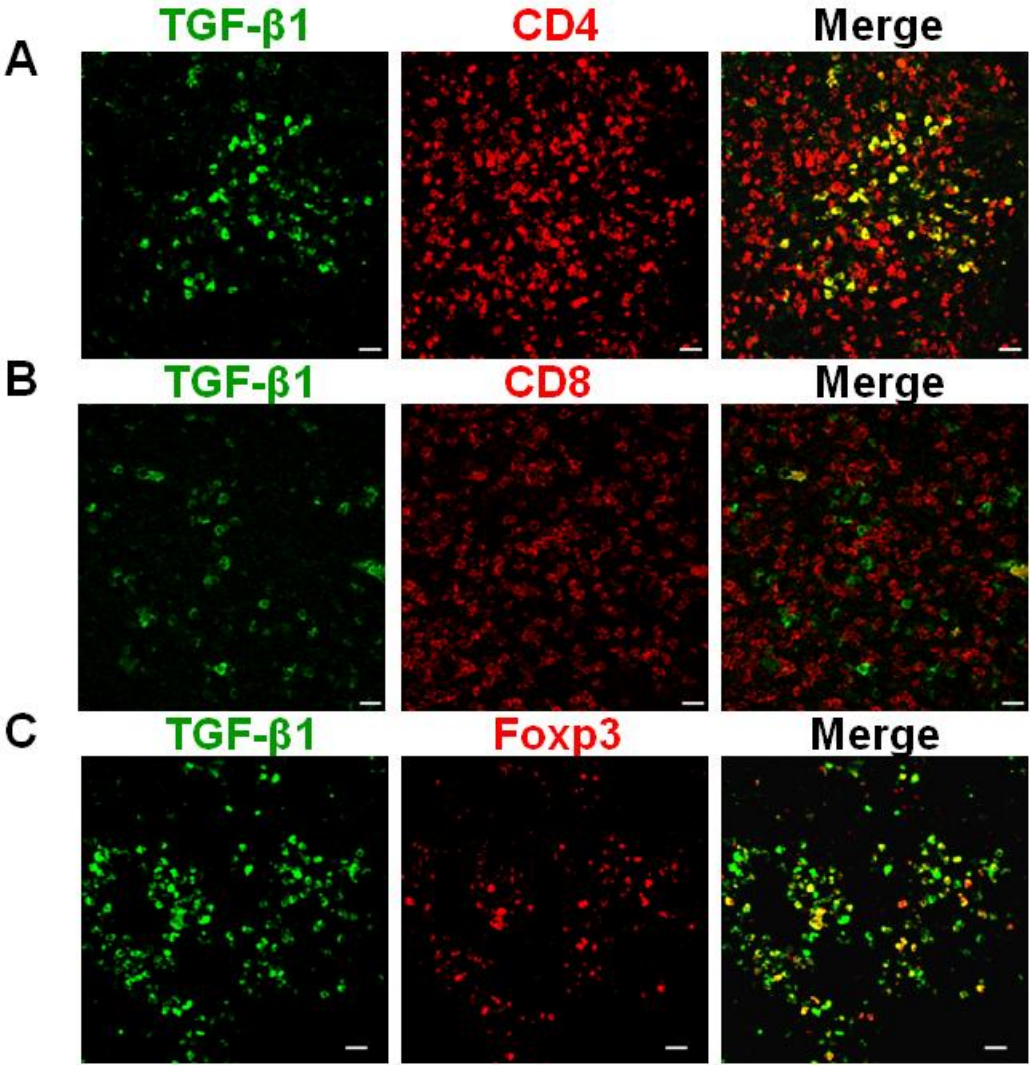

Figure 2-14. TGF-β1 is mainly produced by CD4+ / Foxp3+ T regulatory cells. (**A**) Immunofluorescent images of TGF-β1 (green staining) and CD4 (red staining), (**B**) TGF-β1 (green staining) and CD8 (red staining), (**C**) TGF-β1 (green staining) and Foxp3 (red staining) in LTs from HIV infected individuals (representative image for one of 4 subjects), showing TGF-β1 expression primarily in CD4+ Foxp3+ T regulatory cells. Scale bars: 20 μm.

Figure 2-15.

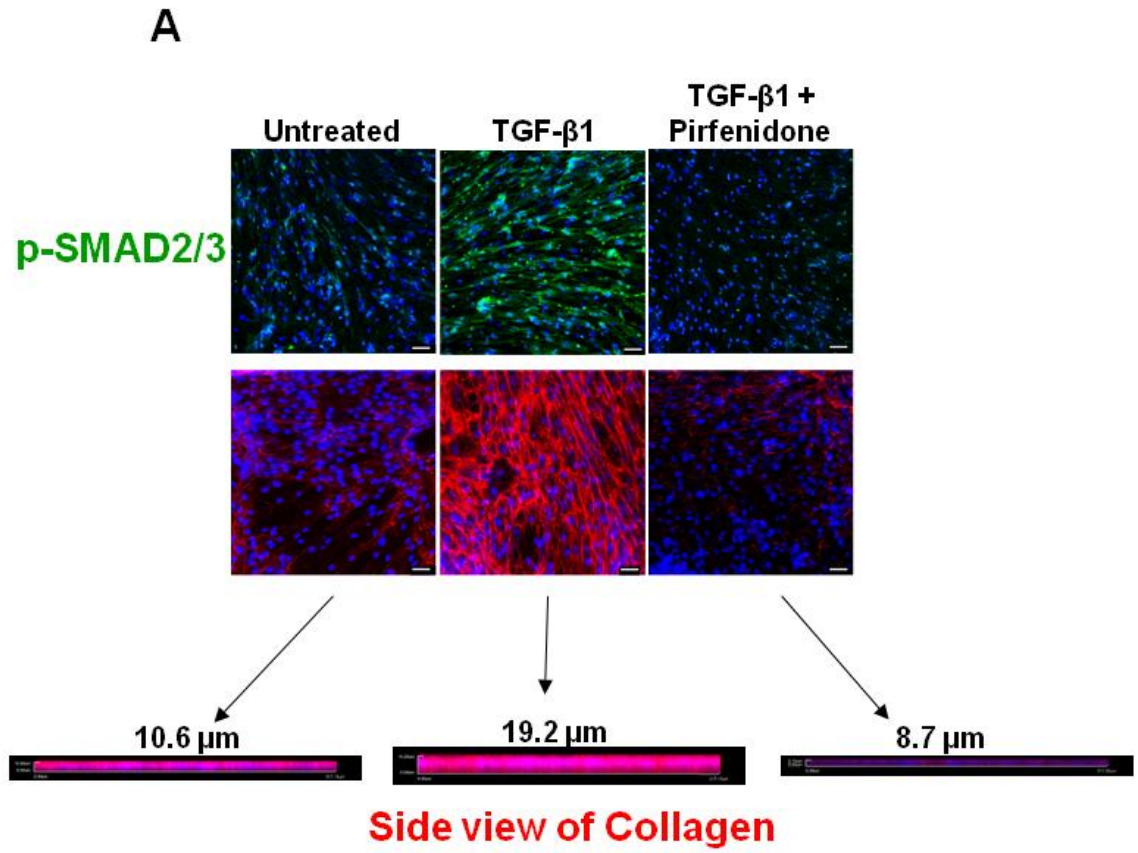
A
Untreated
TGF-β1
TGF-β1 +
Pirfenidone
p-SMAD2/3
10.6 µm
19.2 µm
8.7 µm
Side view of Collagen

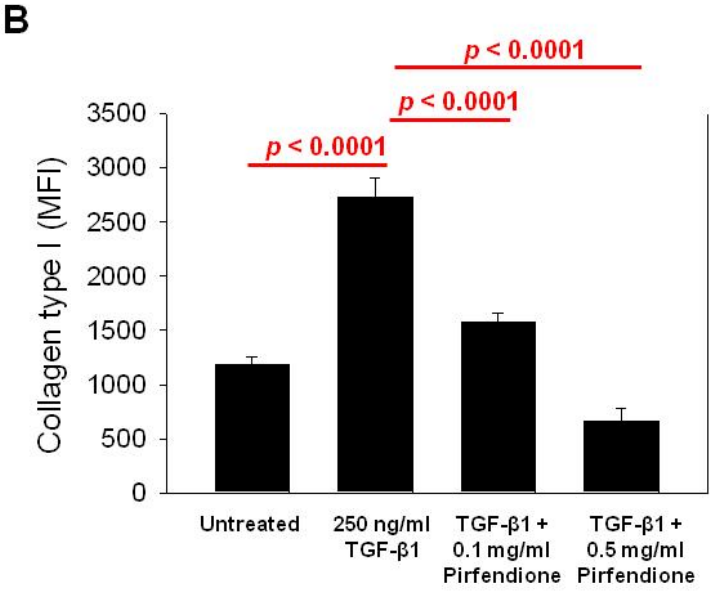
B
p < 0.0001
p < 0.0001
p < 0.0001
Collagen type I (MFI)
3500
3000
2500
2000
1500
1000
500
0
Untreated
250 ng/ml TGF-β1
TGF-β1 + 0.1 mg/ml Pirfendione
TGF-β1 + 0.5 mg/ml Pirfendione

Figure 2-15. TGF-β1 stimulates the production of type I collagen by LT fibroblasts. (**A**) Immunofluorescent images of p-SMAD2/3 (green staining) and collagen type I (red staining) in primary human fibroblasts treated with or without TGF-β1 (250 ng/ml) for 48 hr. Addition of the anti-fibrotic drug, pirfenidone (0.1 or 0.5 mg/ml), inhibits the TGF-β1 signaling pathway and decreases collagen type I production (representative image of 10 images). Cell nuclei appear blue (DAPI). Side views of individual collagen type I fibers were captured to display the relative thickness of the extracellular collagen networks in primary LT fibroblasts. Scale bars: 50 μm. (**B**) The extracellular collagen type I networks of primary human fibroblasts were quantified for each condition and reported as collagen type I Mean Fluorescence Intensity (MFI). Data are expressed as the mean ± s.d., where 3 independent experiments were performed in quadruplicate. The results are shown with significance where applicable ($p < 0.05$).

Figure 2-16.

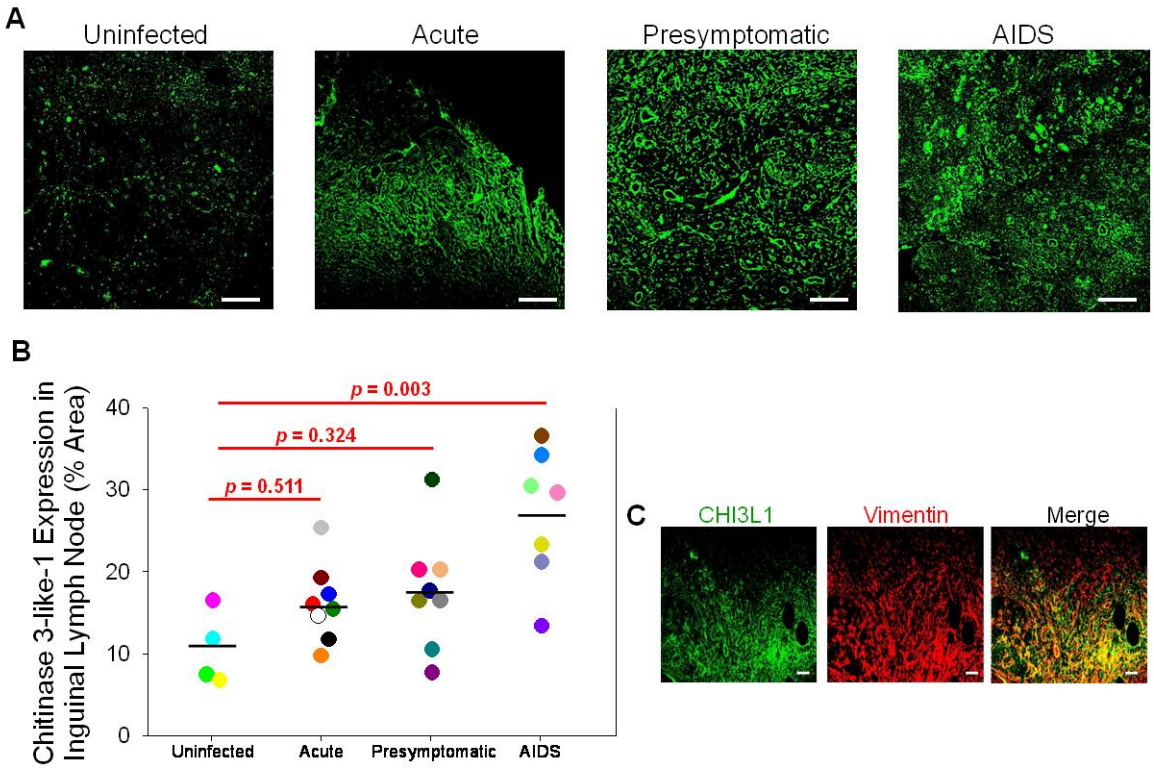
A
Uninfected
Acute
Presymptomatic
AIDS
B
Chitinase 3-like-1 Expression in Inguinal Lymph Node (% Area)
p = 0.003
p = 0.324
p = 0.511
0
10
20
30
40
Uninfected
Acute
Presymptomatic
AIDS
C
CHI3L1
Vimentin
Merge

Figure 2-16. CHI3L1 progressively increases within LTs during HIV infection. (**A**) Immunofluorescent images reveal progressive increases in CHI3L1 (green staining) within LT during HIV infection (representative image for all the subjects at each stage). Scale bars: 200 μm. (**B**) CHI3L1 expression was quantified in each LN biopsy and reported as percent tissue area positive for CHI3L1. The results are shown with significance where applicable ($p < 0.05$). Mean values for each group are indicated by horizontal black bars. (**C**) Immunofluorescent images of CHI3L1 (green staining) and vimentin (red staining) in the LT from an HIV infected individual in the presymptomatic stage of disease (representative image for one of 4 subjects), showing co-localization between CHI3L1 and vimentin+ fibroblasts. Scale bars: 50 μm.

Figure 2-17.

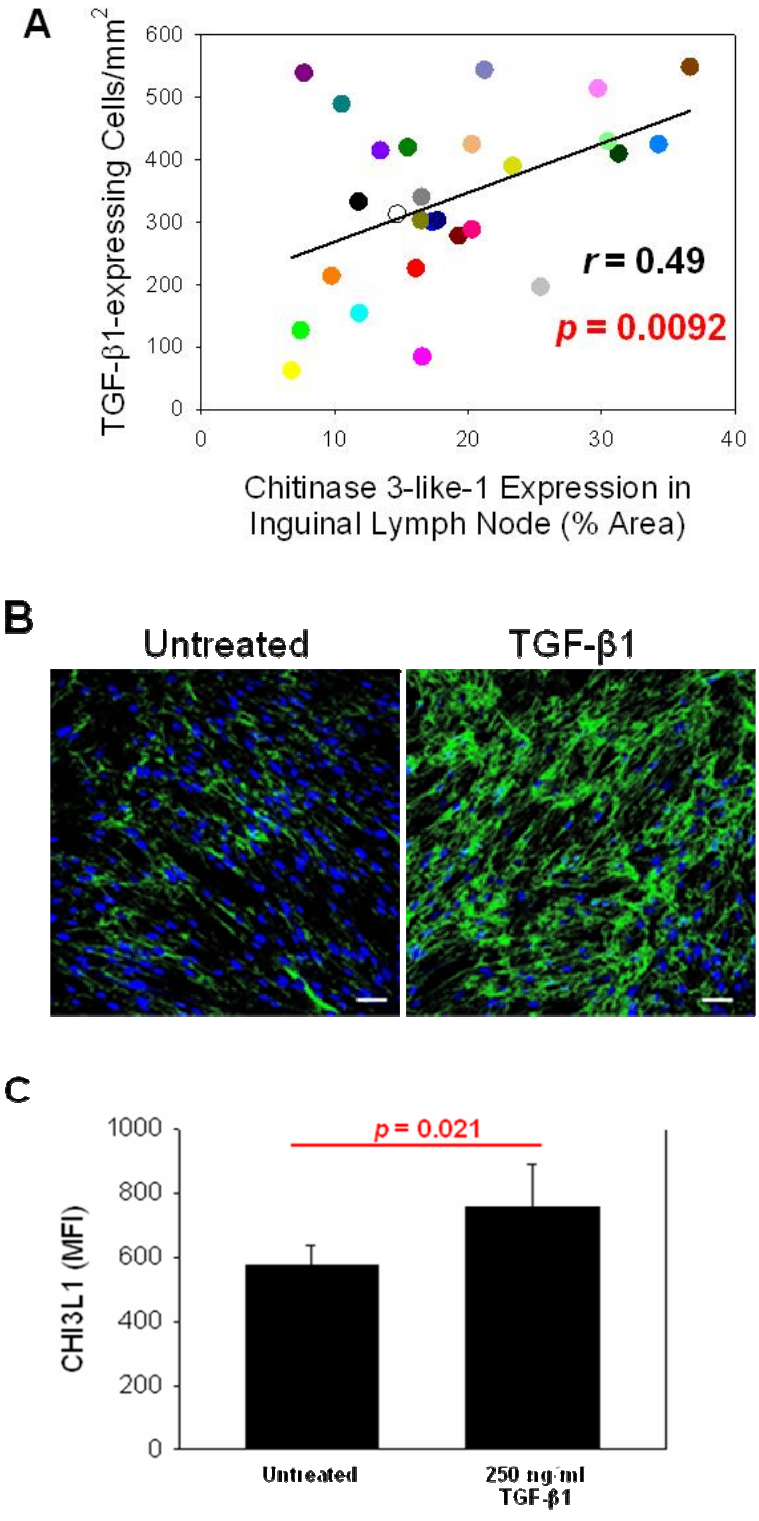
A
TGF-β1-expressing Cells/mm2
600
500
400
300
200
100
0
0
10
20
30
40
r = 0.49
p = 0.0092
Chitinase 3-like-1 Expression in Inguinal Lymph Node (% Area)
B
Untreated
TGF-β1
C
p = 0.021
CHI3L1 (MFI)
1000
800
600
400
200
0
Untreated
250 ng/ml TGF-β1

Figure 2-17. TGF-β1 stimulates the production of CHI3L1 by LT fibroblasts. (**A**) TGF-β1-expressing cells were significantly correlated with CHI3L1expression in the inguinal LN. (**B**) Immunofluorescent images of CHI3L1 (green staining) in primary human fibroblasts treated with or without TGF-β1 (250 ng/ml) for 48 hr (representative image of 10). Cell nuclei appear blue (DAPI staining). Scale bars: 50 μm. (**C**) The extracellular CHI3L1 networks of primary human fibroblasts were quantified for each condition and reported as CHI3L1 Mean Fluorescence Intensity (MFI). Data are expressed as the mean ± s.d., where 3 independent experiments were performed in quadruplicate. The results are shown with significance where applicable ($p < 0.05$).

Figure 2-18.

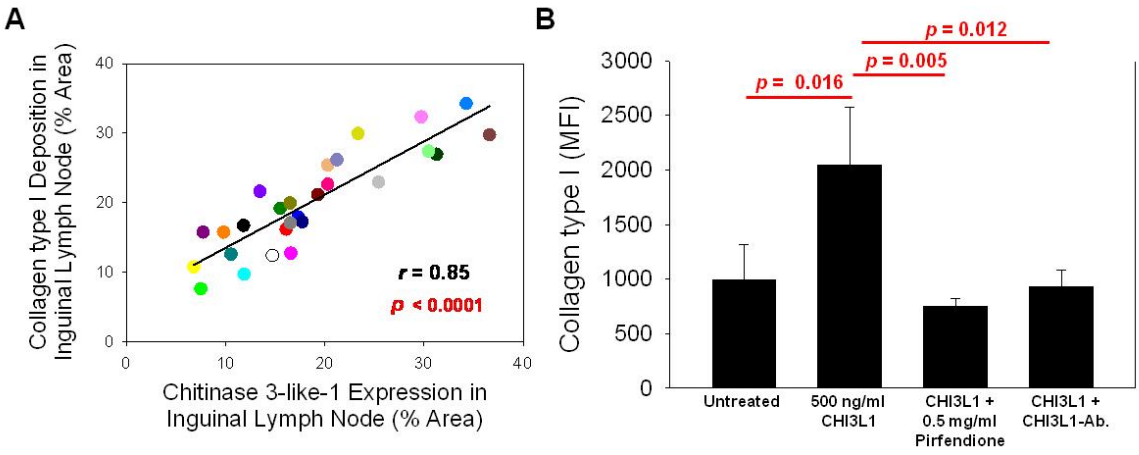
A
Collagen type I Deposition in Inguinal Lymph Node (% Area)
Chitinase 3-like-1 Expression in Inguinal Lymph Node (% Area)
r = 0.85
p < 0.0001
B
Collagen type I (MFI)
p = 0.016
p = 0.005
p = 0.012
Untreated
500 ng/ml CHI3L1
CHI3L1 + 0.5 mg/ml Pirfendione
CHI3L1 + CHI3L1-Ab.

Figure 2-18. CHI3L1 facilitates type I collagen formation. (**A**) CHI3L1 expression was significantly correlated with collagen type I deposition in the inguinal LN. (**B**) The extracellular collagen type I networks of primary human fibroblasts were quantified for fibroblasts treated with or without CHI3L1 (500 ng/ml) for 48 hr. Addition of the anti-fibrotic drug, pirfenidone (0.5 mg/ml), or a CHI3L1-blocking antibody decreased collagen type I production. The extracellular collagen type I networks were quantified for each condition and reported as collagen type I Mean Fluorescence Intensity (MFI). Data are expressed as the mean ± s.d., where 3 independent experiments were performed in quadruplicate. The results are shown with significance where applicable ($p < 0.05$).

Figure 2-19.

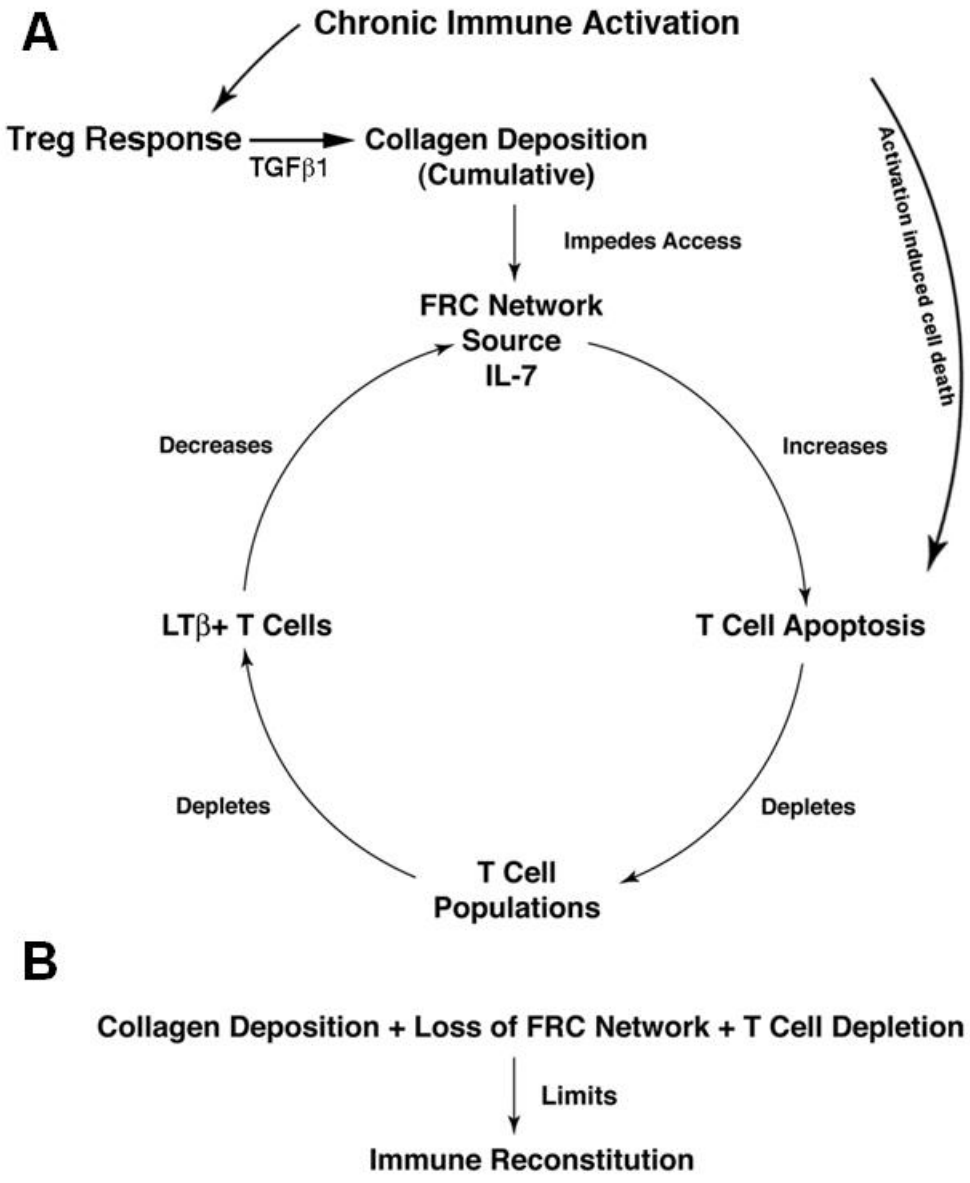
A
Chronic Immune Activation
Treg Response
TGFβ1
Collagen Deposition
(Cumulative)
Impedes Access
FRC Network
Source
IL-7
Activation induced cell death
Decreases
Increases
LTβ+ T Cells
T Cell Apoptosis
Depletes
Depletes
T Cell
Populations
B
Collagen Deposition + Loss of FRC Network + T Cell Depletion
Limits
Immune Reconstitution

Figure 2-19. Mechanisms of LT fibrosis and damage to the LT niche and depletion of T cells. (**A**) Chronic immune activation in HIV and SIV infections is thought to deplete T cells through increased activation-induced cell death, but immune activation also elicits a T regulatory response that activates TGF-β1 signaling in fibroblasts resulting in cumulative collagen deposition. Collagen deposition impedes access of T cells to the survival factor IL-7 on the FRC network to cause increased apoptosis, which, along with activation- induced cell death, depletes T cells. Depletion of T cells decreases LTβ, which, along with collagen-impeded access to LTβ for FRCs, results in loss of FRC network and IL-7. This vicious cycle of survival interdependencies and collagen deposition cause progressive T cell depletion, particularly in the naïve T cell populations. (**B**) HAART can suppress the loss of CD4+ T cells due to the direct effects of infection and normalize immune activation to reduce losses of CD4+ T cells due to activation-induced cell death. However, pre-existing collagen, loss of FRC network and T cell depletion will limit immune reconstitution by the continued cyclical mechanisms shown in (**A**).

Figure 2-20.

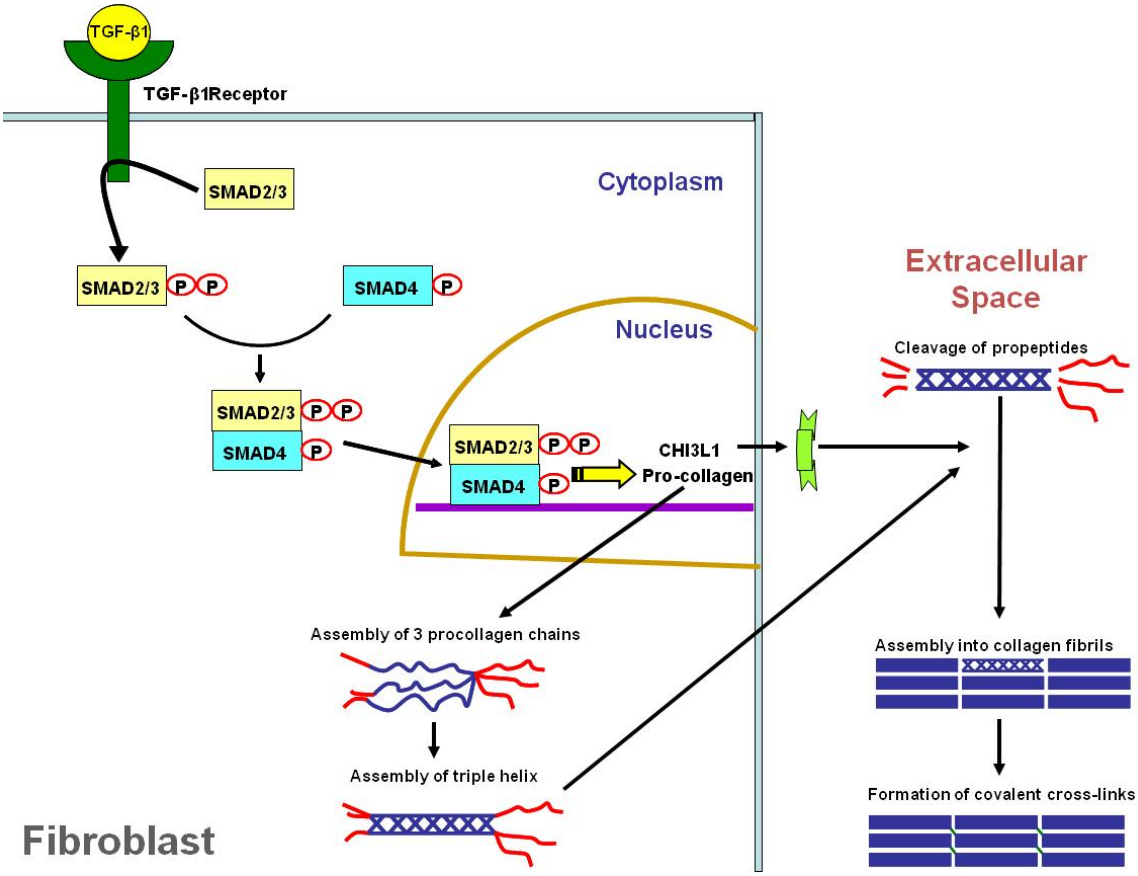
TGF-β1
TGF-β1Receptor
SMAD2/3
Cytoplasm
SMAD2/3 P P
SMAD4 P
Nucleus
Extracellular Space
Cleavage of propeptides
SMAD2/3 P P
SMAD4 P
SMAD2/3 P P
SMAD4 P
CHI3L1
Pro-collagen
Assembly of 3 procollagen chains
Assembly into collagen fibrils
Assembly of triple helix
Formation of covalent cross-links
Fibroblast

Figure 2-20. A model of fibrosis within LT during HIV infection. Increases in TGF-β1-expressing T regulatory cells and its cognate receptor in fibroblasts result in amplification of the TGF-β1 signaling pathway. This leads to increased production of pro-collagen and CHI3L1, a protein which can enhance the maturation of pro-collagen into collagen fibrils. Collectively, these changes accelerate the pathological process of fibrosis.

Tables

Table 2-1 Demographic characteristics and clinical information of subjects

Patient	Disease Stage	Gender	Age	Race	Peripheral Blood $CD4^+$ T Cell Count (Cells/µl)	Plasma HIV RNA Levels (Copies/ml)
1425	Uninfected	Male	43	Caucasian	1,351	Undetectable
1442	Uninfected	Female	45	Caucasian	485	Undetectable
1476	Uninfected	Female	28	Caucasian	704	Undetectable
1472	Uninfected	Female	52	Caucasian	837	Undetectable
1455	Acute	Male	23	African American	209	19,400
1391	Acute	Male	37	African American	234	24,718
1389	Acute	Male	32	Caucasian	824	32,173

1449	Acute	Male	30	Caucasian	333	> 100,000
1484	Acute	Male	49	Caucasian	301	23,721
1469	Acute	Male	44	Caucasian	201	>100,000
1458	Acute	Male	51	Caucasian	400	439,000
1435	Acute	Male	42	Caucasian	410	> 100,000
1086	Asymptomatic	Male	30	Caucasian	512	20,562
1293	Asymptomatic	Male	36	Caucasian	905	14,225
1419	Asymptomatic	Male	37	Caucasian	245	61,432
1428	Asymptomatic	Male	30	Caucasian	363	38,600
1436	Asymptomatic	Male	63	Caucasian	248	46,400
1459	Asymptomatic	Male	36	Caucasian	286	> 100,000
1317	Asymptomatic	Male	31	Caucasian	399	120,469
1479	Asymptomatic	Male	42	Caucasian	273	1,650

1413	AIDS	Male	50	African American	42	59,401
1438	AIDS	Male	49	Caucasian	147	4,960
1462	AIDS	Male	43	Caucasian	81	35,000
1327	AIDS	Female	40	African American	112	12,046
1446	AIDS	Female	45	Caucasian	200	150,500
1474	AIDS	Male	40	African American	98	10,000
1263	AIDS	Male	44	Caucasian	3	> 100,000

Table 2-2 List of primary antibodies and antigen retrieval methodologies

Antibody	Clone/ Manufacturer & Catalog #	Antigen-retrieval Pretreatment	Antibody Dilution	Species
Desmin	D33 / Lab Vision & # MS-376-S1	Diva Decloaker; High pressure cooker for 30 seconds at 125°C.	1/200	Mouse
Desmin	Polyclonal / Lab Vision & # RB-9014-P1	Diva Decloaker; High pressure cooker for 30 seconds at 125°C.	1/200	Rabbit
CD35	Ber-MAC-DRC / Dako & # M0846	Diva Decloaker; High pressure cooker for 30 seconds at 125°C.	1/100	Mouse

CD21	1F8 / Dako / # M0784	Diva Decloaker; High pressure cooker for 30 seconds at 125°C.	1/100	Mouse
ER-TR7	ER-TR7 / Acris Antibodies & # BM4018	Frozen tissue, Diva Decloaker; Water bath for 5 min at 95°C.	1/200	Rat
CD3	MCA147 / AbD Serotec & # MCA1477	Diva Decloaker; High pressure cooker for 30 seconds at 125°C.	1/200	Rat
CD3	SP7 / Thermo Scientific & # RM-9107-S1	Diva Decloaker; High pressure cooker for 30 seconds at 125°C.	1/100	Rabbit

IL-7	7417 / R & D Systems & # MAB207	Diva Decloaker; High pressure cooker for 30 seconds at 125°C. Proteinase K treatment for 15 min	1/100	Mouse
CD45RA	4KB5 / Dako & # M0754	Diva Decloaker; High pressure cooker for 30 seconds at 125°C.	1/100	Mouse
Activated Caspase-3	8G10 / Cell Signaling Tech. & # 9665	1mm EDTA (ph 8); High pressure cooker for 30 seconds at 125°C.	1/100	Rabbit
Collagen 1	COL-1 / Sigma & # C2456	Diva Decloaker; High pressure cooker for 30	1/100	Mouse

		seconds at 125°C. Protease K (10 µg/ml).		
Lymphotoxin-β	135105 / R & D Systems & # MAB1684	Diva Decloaker; High pressure cooker for 30 seconds at 125°C.	1/100	Mouse
CD4	Polyclonal / R & D Systems & # AF-379-NA	Diva Decloaker; High pressure cooker for 30 seconds at 125°C.	1/100	Goat
CD4	1F6 / Novacastra & # NCL-CD4–1F6	Diva Decloaker; High pressure cooker for 30 seconds at 125°C.	1/100	Mouse
CD8	SP16 / Neomarkers &	Diva Decloaker; High pressure	1/100	Rabbit

	# RM-9116-s	cooker for 30 seconds at 125°C.		
Lymphotoxin-β	Polyclonal / Santa Cruz Biotech. & # sc-23561	Diva Decloaker; High pressure cooker for 30 seconds at 125°C.	1/100	Goat
Vimentin	Vim 3B4 / DAKO & # M7020	Diva Decloaker; High pressure cooker for 30 seconds at 125°C.	1/100	Mouse
Vimentin	Polyclonal / Neomarkers & # Rb-9063-P1	Diva Decloaker; High pressure cooker for 30 seconds at 125°C.	1/100	Rabbit
TGF-β1	Polyclonal / Santa Cruz &	Diva Decloaker; High pressure cooker for 30	1/100	Goat

	# SC-146-G	seconds at 125°C. Protease K (10 µg/ml).		
Collagen I	Polyclonal / Abcam & # ab292	Diva Decloaker; High pressure cooker for 30 seconds at 125°C. Protease K (10 µg/ml).	1/200	Rabbit
Pro-collagen	M-58 / Millipore & # MAB1912	Diva Decloaker; High pressure cooker for 30 seconds at 125°C. Protease K (10 µg/ml).	1/50	Rat
TGF-β RII	Polyclonal / R & D Systems & # AF-241-NA	Diva Decloaker; High pressure cooker for 30 seconds at 125°C.	1/100	Goat

		Protease K (10 µg/ml).		
Ki-67	SP6 / Neomarkers & # RM-9106-S1	Diva Decloaker; High pressure cooker for 30 seconds at 125°C.	1/200	Rabbit
p-SMAD2/3	Polyclonal / Santa Cruz & # SC-11769	Diva Decloaker; High pressure cooker for 30 seconds at 125°C. Protease K (10 µg/ml).	1/50	Goat
CHI3L1	Polyclonal / Quidel & # 4815	Diva Decloaker; High pressure cooker for 30 seconds at 125°C. Protease K (10 µg/ml).	1/200	Rabbit

IgG Isotype Controls	Dako, Jackson ImmunoResearch	Diva Decloaker; High pressure cooker for 30 seconds at 125°C. Protease K (10 µg/ml).	1/50-1/200	Mouse, Rabbit, Rat, Goat

Chapter 3

Originally published in PLoS Pathog. 2012 Jan;8(1):e1002437. Reprinted with permission; the format has been adjusted.

Lymphoid Tissue Damage in HIV-1 Infection Depletes Naïve T Cells and Limits T Cell Reconstitution after Antiretroviral Therapy

Ming Zeng[1], Peter J. Southern[1], Cavan S. Reilly[2], Greg J. Beilman[3], Jeffrey G. Chipman[3], Timothy W.Schacker[4], Ashley T.Haase[1*].

[1]Department of Microbiology, Medical School, University of Minnesota, MMC 196, 420 Delaware Street S.E., Minneapolis, MN, USA, 55455,

[2] Division of Biostatistics, School of Public Health, University of Minnesota, MMC 303, 420 Delaware Street S.E., Minneapolis, MN 55455, USA.

[3] Department of Surgery, Medical School, University of Minnesota, MMC 195, 420 Delaware Street S.E., Minneapolis, MN, USA, 55455

[4] Department of Medicine, Medical School, University of Minnesota, MMC 250, 420 Delaware Street S.E., Minneapolis, MN, USA, 55455

Address correspondence to: Ashley T. Haase, Department of Microbiology, University of Minnesota, MMC 196, 420 Delaware Street S.E., Minneapolis, Minnesota 55455, USA. Phone: (612) 624-4442; Fax: (612) 626-0623; E-mail: haase001@umn.edu.

Introduction

The hallmark of HIV infection, depletion of CD4+ T cells, has been largely attributed to direct mechanisms of infection and cell death from viral replication or killing by virus-specific cytotoxic T-lymphocytes (CTLs), and to indirect mechanisms such as increased apoptosis accompanying chronic immune activation associated with HIV infections [68]. It is thus puzzling that if these were the sole mechanisms responsible for CD4+ T cell depletion, why 20% of HIV infected patients have no significant increase in their peripheral blood CD4 count after initiation of HAART, since treatment can suppress viral replication to undetectable levels and normalize much of the chronic immune activation associated with infection [48, 180]. Moreover, even among patients with significant increases in peripheral blood CD4+ T cells, few reconstitute to normal levels after years of HAART, and this incomplete immune reconstitution is associated with significantly higher rates of malignancy and other morbidities compared with HIV-uninfected individuals [181-188].

The preferential depletion of naïve T cells in blood and lymphoid tissues (LT) [48], where they mainly reside, also poses particular difficulties for attributing depletion simply to direct mechanisms of viral infection or indirect mechanisms of activation induced cell death (AICD), since (1) naïve CD4+ T cells are resistant to HIV infection and (2) AICD should primarily affect the activated effector and memory populations [47, 171, 173]. Furthermore, the similar extent of depletion of not only naïve CD4+ T cells but also naïve CD8+ T cells that are not usually infected by HIV[46, 170], suggests that there is a general mechanism impacting naïve T cell populations unrelated to direct infection.

The incomplete restoration of naïve T cell populations with HAART also points to mechanisms in addition to AICD in depletion of CD4+ T cells, since suppression of this "drain" should enable repopulation of naïve CD4+ T cell populations by thymopoiesis and homeostatic proliferation of existing naïve T cells in secondary LT, but this does not happen [70, 98, 106, 189]. Cumulative observations therefore suggest that there may be additional mechanisms that impair the survival of naïve T cells, thereby restricting immune reconstitution [48, 68].

To account for the preferential loss of naïve T cells, and failure of HAART to restore both naïve and memory populations by thymopoesis and homeostatic proliferation, we have proposed a damaged LT niche hypothesis in which collagen deposition disrupts the FRC network on which naïve T cells migrate and gain access to survival factors such as interleukin-7 (IL-7). This results in elevated levels of naïve T cell apoptosis [93, 119, 124] before treatment and impairs the reconstitution of naïve T cells after treatment. We recently showed in the SIV-rhesus macaque animal model that the critical disruption in LT architecture caused by collagen deposition and decreased access of T cells to survival factor IL-7 "posted" on the FRC network was in fact associated with increased apoptosis and depletion of both naïve CD4+ and CD8+ T cells. We also showed that this mechanism is a cooperative and cumulative vicious cycle in which the mutual interdependencies for survival of naïve T cells on IL-7, and the FRC network on lymphotoxin-beta (LTβ) supplied by the T cells, perpetuate depletion of both T cells and the FRC network [190].

One implication of this model is that because the impact of LT fibrosis on CD4+ T cell depletion is progressive and cumulative, initiating HAART in the early stages of infection should improve immune reconstitution because there should be less collagen deposition and loss of the FRC network at this stage. We tested this hypothesis by examining LTs from HIV infected individuals at baseline and 6 months after initiating HAART in the acute, pre-symptomatic and AIDS stages of infection. We first document the same damaged LT niche mechanism described in the SIV-rhesus macaque model of collagen deposition and loss of the FRC network with depletion of naïve T cells through increased apoptosis as a consequence of decreased access to IL-7. We then show that the extent of loss of the FRC network and collagen deposition predict the extent of inhibition of naïve T cell apoptosis and restoration of the naïve T cell population in LT after 6 months of HAART, and total CD4+ T cell counts in peripheral blood after 12 months of HAART. Furthermore, we find that the extent of restoration of FRC network after 6 months of HAART is highly dependent on the stage of disease at which the therapy is initiated, with greatest restoration only when HAART is initiated during the early stage of infection. This directly correlates with optimal inhibition of naïve T cell apoptosis and

restoration of naïve T cells in the patients receiving HAART during the early stage of infection. This mechanism explains why initiation of HAART during the early stage of infection is associated with more rapid and complete CD4+ T cell restoration, and thus strongly argues for early initiation of HAART [44, 191]. It also argues for a potential use of adjunctive therapies such as anti-fibrotic therapy to avert and/or revert the LT structure to improve immune reconstitution.

Materials and Methods

Ethics statement

This human study was conducted according to the principles expressed in the Declaration of Helsinki. The study was approved by the Institutional Review Board of the University of Minnesota. All patients provided written informed consent for the collection of samples and subsequent analysis.

LN biopsy specimens

Inguinal LN (LN) biopsies from HIV negative individuals and HIV-infected individuals at different clinical stages (7 at acute/early stage, 18 at presymptomatic stage and 8 at AIDS stage. Table 3-1) were obtained for this University of Minnesota Institutional Review Board-approved study. Viral load measurements were obtained the same day as biopsies. Each LN biopsy was immediately placed in fixative (4% neutral buffered paraformaldehyde or Streck's tissue fixative) and paraffin embedded.

Immunofluorescence staining and Quantitative Image Analysis (QIA)

All staining procedures were performed as previously described [151, 190] using 5-30 μm tissue sections mounted on glass slides. Tissues were deparaffinized and rehydrated in deionized water. Heat-induced epitope retrieval was performed using a high-pressure cooker (125^{o}C) in either DIVA Decloaker or EDTA Decloaker (Biocare Medical), followed by cooling to room temperature. Tissues for collagen type I staining required pre-treatment with 20 μg/ml proteinase K (Roche Diagnostics) in proteinase K buffer (0.2 M Tris, pH 7.4, 20 mM $CaCl_2$) for 15-20 min at room temperature. Tissue sections were

then blocked with SNIPER Blocking Reagent (Biocare Medical) for 30 min at room temperature. Primary antibodies were diluted in TNB (0.1M Tris-HCl, pH 7.5; 0.15M NaCl; 0.05% Tween 20 with Dupont blocking buffer) and incubated overnight at 4^{o}C. After the primary antibody incubation, sections were washed with phosphate buffered saline (PBS) and then incubated with fluorochrome-conjugated secondary antibodies in TNB for 2 hr at room temperature. Finally, sections were washed with PBS, nuclei were counterstained blue with DAPI, and mounted using Aqua Poly/Mount (Polysciences Inc.). Immunofluorescent micrographs were taken using an Olympus BX61 Fluoview confocal microscope with the following objectives: x20 (0.75 NA), x40 (0.75 NA), and x60 (1.42 NA); images were acquired and mean fluorescence intensities were analyzed using Olympus Fluoview software (version 1.7a).

Isotype-matched negative control antibodies in all instances yielded negative staining results (see Table 3-2, which lists the primary antibodies and antigen retrieval methodologies).

Quantitative image analysis (QIA) was performed using 10–20 randomly acquired, high-powered images (X200 or X400 magnification) by either manually counting the cells in each image or by determining the percentage of LT area occupied by positive fluorescence signal using an automated action program in Adobe Photoshop CS with tools from Reindeer Graphics.

Ex vivo culture system

The experimental protocols used here for human tissue samples had full IRB approval (Institutional Review Board: Human Subjects Committee, Research Subjects' Protection Program, University of Minnesota) and informed written consent was obtained from individual patients, or the legal guardians of minors, for the use of tissue in research applications prior to the initiation of surgery. Fresh human palatine tonsil tissues were obtained from routine tonsillectomies and processed within 1–2 h of completion of surgery. Viable tonsil lymphocyte suspensions were prepared by forcing cut tissue pieces through a metal sieve and collecting the released single cell suspension in complete RPMI medium (10% heat inactivated fetal calf serum, 1x l-glutamine, penicillin, and

streptomycin solution; Invitrogen). The cells were washed and immediately cryopreserved. By culturing the stroma left on the metal sieve in complete RPMI medium, adherent proliferating fibroblasts were first visible after 2–5 days in culture, and confluent monolayers developed after 10–25 days. These primary stromal populations were readily released with trypsin, and the cells were further expanded and passaged using routine procedures for adherent cells. Some stromal cells were fixed in Streck's tissue fixative at one day prior to co-culture for analysis of intracellular desmin and IL-7 expression. For live stromal cells staining and imaging, stromal cells were directly incubated with antibody against IL-7 at 4°C without heat antigen retrieval and subject to secondary fluorochrome-conjugated-antibody staining. For co-culture of lymphocytes and stromal cells, $2x10^5$ lymphocytes isolated from human tonsil were cultured in chamber slides without stromal cells, with autologous stromal cells ($2x10^4$cells/well), with stromal cells and IL-7 blocking antibody or with stromal cells but separated by transwells for 2 to 3 days. After co-culture, the slides were fixed in Streck's tissue fixative and stained for activated caspase3, CD45RA and CD3 to quantify the number of apoptotic naïve T cells by QIA as described above.

Statistical analysis

To test for differences in FRCs and collagen across all stages a 1-way ANOVA was used and post-hoc comparisons were made with Welch's modified 2 sample *t*-tests with a Bonferroni correction (hence *p*-values are reported for differences between stages). A similar analysis was used to test for differences from the data that arose from the *ex vivo* culture system.

To test for associations between FRCs and apoptotic naïve cell counts mixed models were used with FRCs as the explanatory variable in addition to clinical stage of infection (since it is associated with both FRCs and apoptotic naïve cell counts). Random effects were included in these models since all of the data (i.e. all time points) were used to fit these models and random effects provide a simple way to incorporate correlation among measurements from the same subject into the model. Continuous variables were log transformed prior to fitting the model and restricted maximum likelihood was used to

obtain parameter estimates. The same approach was used to test for an association between apoptotic naïve cell counts and naïve counts. A similar approach was used to test for an association between both Ki67 levels and viral load and apoptotic naïve cell counts and naïve counts except that FRCs and collagen were included in the model in addition to clinical stage of infection.

To test if baseline FRCs or collagen are predictive of apoptotic naïve cell counts and naïve counts at 6 months post initiation of HAART, linear regression models were used that included the baseline value of the variable we were trying to predict at 6 months since such baseline values are potentially related to the value of the variable at 6 months and the baseline levels of FRCs or collagen. All continuous variables were first log transformed and standard model diagnostics were conducted.

One sample *t*-tests were used to test for changes over the first 6 months of therapy for each stage. Spearman's rank correlation was used to test for associations that were potentially nonlinear (but monotone).

Results

Collagen deposition and loss of the FRC network impede access to and source of IL-7 in HIV infection

To evaluate this hypothesis, we first show that the FRC network is the major source of IL-7 for T cells in human LTs, as has been demonstrated in mice and monkeys [93, 190]. In LT sections from uninfected individuals stained for IL-7 and desmin, a marker for FRCs, IL-7 largely co-localizes with the FRC network on which lymphocytes, antigen presenting cells and other cells within LTs migrate (Figure 3-1A). This architecture allows T cells to efficiently access survival factors such as IL-7 and self-antigen-major histocompatibility complex as well as chemokines "posted" on their path. Thus, in the lymph node (LN) sections from HIV-uninfected individuals stained for type I collagen, desmin and T cells, the collagen within the FRC network co-localizes with desmin, and the T cells visibly contact the FRC network (Figure 3-1B). In contrast, HIV infection is associated with stage-specific progressive decreases in the FRC network (Figure 3-1D-E) and thus the available source of IL-7 (Figure 3-1F). The depletion of FRCs correlates with a parallel increase in collagen deposited outside the FRC network, so that as infection progresses, fewer and fewer T cells are in contact with and have access to IL-7 on the FRC network (Figure 3-1C) compared with uninfected populations (Figure 3-1B).

T cell apoptosis increases with decreased availability of IL-7

Because survival of naïve T cells is dependent on access to IL-7 [93, 119, 124], the collagen deposition-restricted access to and loss of the FRC network itself should result in an increase in apoptosis proportional to the extent of collagen deposition and decreased IL-7 source as infection progresses. We first demonstrate that contact with FRCs as a source of IL-7 is critical for T cell survival in an ex vivo culture system. We established monolayers of desmin+ IL-7+ FRC-like cells from stromal cells isolated from human tonsils (Figure 3-2A-B), and show that IL-7 localizes to the surfaces of live cells stained without permeabilization (Figure 3-2C) . Only about 10% of naïve T cells underwent apoptosis if co-cultured with autologous IL-7+FRC-like cells compared to about 30-40% of naïve T cells cultured for 2-3 days without stromal cells. We show that the enhanced

survival is contact dependent and is mediated mainly via IL-7, as antibody blocking of IL-7 or separation of T cells and the FRCs by transwells leads to increased apoptosis in naïve T cells (Figure 3-2D-E). However, the blockade of IL-7 does not fully recapitulate the apoptosis level in the naïve T alone culture, suggesting that other survival factors such as CCL19 produced by FRCs may independently support the survival of naïve T cells [93].

These ex vivo co-culture results support the concept that naïve T cells need to contact FRCs in order to gain access to IL-7 to maintain their survival. Therefore, the loss of FRCs as well as the loss of the contact between naïve T cells and FRCs together in vivo would be expected to increase apoptosis and thereby deplete naïve T cells. We tested this hypothesis in LTs from HIV infected patients and found that the stage-dependent increases in naïve T cell apoptosis (Figure 3-3A) were associated with depletion of both naïve CD4+ and CD8+ T cells (Figure 3-3B-C), and that stage-dependent decreases in the FRC network (Figure 3-1D) were associated both with apoptosis and naïve T cell depletion (Figure 3-3D-E).

Restoration of LT structure and increases in naïve T cells depend on the timing of initiation of HAART

Because the LT damage-mediated naïve T cell depletion mechanism now documented in both HIV infection and SIV infection [190] is cumulative and progressive, the later stage of infection, the greater the damage to LT structure. Thus, if treatment does not restore the LT structure that supports survival of naïve CD4+ T cells, the LT damage mediated naïve T cell depletion could adversely affect immune reconstitution, even with suppression of viral replication and immune activation by HAART. Conversely, the lesser extent of LT damage in early infection could improve immune reconstitution with HAART, if initiating treatment were to restore LT structure and improve naïve T cell survival.

To test these predictions, we examined the effects of HAART initiated in the acute/early, pre-symptomatic and AIDS stages of infection on LT structure, naïve T cell apoptosis

and restoration of naïve CD4+ T cell populations. Because loss of the FRC network and fibrosis are less in the acute/early stage than at later stages of HIV infection (Figure 3-1), we would expect that the preservation of LT structure in acute/early HIV infection would result in decreased apoptosis and greater increases in naïve T cells if HAART is initiated at this stage. We indeed found that the loss of the FRC network and collagen deposition prior to initiating HAART are associated with significantly increased naïve T cell apoptosis after 6 months of HAART (p=0.0016 and p=0.0292 respectively) (Figure 3-4A-B). Furthermore, the level of naïve T cell apoptosis both before and after treatment is significantly associated with fewer naïve T cells in LTs (p=0.0012). Taken together, these data suggest the extent of LT damage is associated with the extent of inhibition of naïve T cell apoptosis after HAART. We note that this now documents in LTs the previously reported predictive relationship between collagen in LTs and naïve CD4+ T cell increases in peripheral blood [146].

We also find that HAART initiated in the acute/early stage infection results in the greatest restoration of FRCs after 6 months of HAART, albeit not to the level in HIV uninfected population (Figure 3-5A-B). The restoration of LT structure is a slow process as even after 36 months of HAART the area occupied by the FRC network increases but still remains significantly less than in HIV uninfected individuals. Minimal recovery of the FRC network is seen in HIV infected patients starting HAART at chronic stages (Figure 3-5A). At 6 months, there is no significant effect on removal of collagen deposition in LTs (Figure 3-5A-B), but there is increased collagen co-localizing with the FRC network, as opposed to collagen deposits outside the network, albeit not to the same levels seen in HIV uninfected individuals where 90 percent of collagen is within the FRC network (Figure 3-5C-D). We further found that the new WHO guidelines for initiating HAART at CD4 counts of 350 cells/ul have a sound rationale in preservation of the FRC network, since only when therapy had been initiated at or above 350 cells/ul could we detect significant improvement of FRCs after 6 month HAART (Figure 3-6).

HAART initiated in acute/early stage of infection is also associated with greatest decreases in apoptosis and optimal restoration of naïve T cell populations in LTs (Figure 3-7). In contrast, naïve T cell numbers in patients who initiated HAART in the AIDS stage of infection did not increase significantly, and apoptosis in naïve T cell populations remained high (Figure 3-7). These stage-related correlations apply as well to peripheral CD4+ T cell counts in patients receiving HAART for 12 months. The increase in peripheral CD4+ T cell counts to the level of counts in HIV uninfected individuals depended on initiating HAART during the acute/early stage of infection (Figure 3-8A). We also found that this stage-dependent restoration of peripheral CD4+ T cells can be predicted by the extent of fibrosis before initiation of HAART, again suggesting that fibrosis is one key factor that limit immune reconstitution after long-term HAART (Figure 3-8B)..

We also assessed the relationships between viral load and the residual Ki67 level to the extent of restoration of naïve T cells when HAART was initiated at different stages. We found that increases in naïve T cells and decreases in apoptosis do not correlate with HAART-mediated suppression of viral replication and immune activation. HAART initiated at all stages of infection can potently and comparably inhibit viral replication and associated chronic immune activation (Figure 3-9A and B). There is therefore no evidence that these processes are playing important roles in the stage-specific effects of time of initiation on apoptosis and recovery of naïve T cells within LTs. We in fact found no significant association between viral load and the number of naïve T cells or the number of apoptotic naïve T cells, nor any association between activation represented by the number of Ki67+ cells and the number of naïve T cells or the number of apoptotic naïve T cells after 6 month HAART (Figure 3-9C-F).

Discussion

It has generally been thought that viral and immune-cell mediated killing of CD4+ T cells and AICD accompanying chronic immune activation are respectively the major direct and indirect mechanisms of CD4+ depletion in HIV infection, and that the slow and

incomplete restoration of naïve CD4+ T cells is a consequence of the restricted capacity of the adult thymus to re-supply naive T cells [68]. Here we describe a novel mechanism that depletes CD4+ T cells, particularly naïve CD4+ T cells before HAART and determines the pace and extent of naïve CD4+ T cell restoration after HAART.

Naïve T cells depend on IL-7 produced and presented by the FRC network for survival. Our IL-7 staining is consistent with a large literature on the FRC network as the site and source of most of the IL-7 [93, 190, 192-193] but different from one reported human IL-7 staining in LTs [155], which probably due to different reagents and methodologies used. As HIV infection advances, collagen deposition increases and the FRC network is destroyed, which decreases the amount of IL-7 available to support T cell survival. As a consequence, increased apoptosis depletes naïve T cells prior to HAART in proportion to the progressive destruction of LT structure from early to later stages of HIV infection. Because of the progressive and cumulative nature of this pathological process, apoptosis of naïve T cells continues at elevated levels after HAART has been initiated, even though HAART can potently suppress viral replication and at least partially normalize immune activation. The elevated apoptosis level in naïve T cell populations is in proportion to pre-existing damage to LT structure, which is greater in the chronic stages of infection. Thus, predictably, early treatment results in better preservation and restoration of LT structure, which leads to improved survival of naïve T cells and greater increases in naïve T cell numbers. While the limited capacity of the thymus in the adult to supply naïve T cells will certainly limit the pace and extent of reconstitution, the LT structure to which thymic emigrants home will also determine their subsequent survival. By analogy to earlier tap-and-drain models [194], restoration of naïve T cells will be dependent not only on thymic output and from homeostatic proliferation of naïve T cell populations in LT, but also on the drain of overall apoptosis in this population. In such a model, the elevated level of apoptosis in naïve T cells in secondary LTs limits both the extent and pace of immune reconstitution.

As the diversity of the naïve T cell repertoire is critical to defend against new infections and malignancies, the loss and slow restoration of the naïve T cell population creates "holes" in the T cell repertoire and therefore impairs host defenses even after HIV replication has largely been suppressed [182, 185-186]. Thus, therapeutic approaches to prevent or moderate damage to the LT niche and restore a functional FRC network could be particularly beneficial in increasing and preserving naïve T cell populations after HAART. The most straightforward way to do this is through earlier treatment. Our findings also suggest the potential clinical benefit of complementing IL-7 treatment during HIV infection in the restoration of naïve T cell population. Indeed, studies have shown that complementing HAART with IL-7 during both SIV and HIV infection significantly increases the circulating naïve CD4+ T cell number [174-176]. Furthermore, it has been shown that IL-7 treatment could normalize the extent of apoptosis in CD4+ and CD8+ T cells from HIV-infected individuals via up-regulation of Bcl-2 levels [177-178]. These data consistently suggest that insufficient IL-7 is a key contributor in the impaired T cell homeostasis in SIV/HIV infection and limits the reconstitution of T cells.

However, the immediate decline of the absolute numbers of both naïve CD4+ and CD8+ T cells after termination of IL-7 therapy [174-176] suggests that complementing IL-7 only provides transient survival benefit for naïve CD4+ and CD8+ T cells and strongly argues for the development of therapeutic interventions to provide long-term survival benefit for naïve T cells. Our findings here clearly suggest that collagen deposition and the consequential loss of FRCs as the major source of IL-7 play critical roles in compromising homeostasis of naïve T cells. Therefore, the restoration of the lymphoid tissue niche could potentially provide long-term survival benefits for naïve T cells. Therefore, the development of adjunctive anti-fibrosis treatment such as pirfenidone and losartan [190, 195-200] might additionally avert or revert the consequences of damage to the LT niche and improve immune reconstitution.

Acknowledgements

We thank C. O'Neill and T. Leonard for help in preparing the manuscript and figures; Ann Sequin and Katelyn Hanneman for help in organizing patients' information. We also thank all of the donor participants in this study.

Author contribution: M.Z., T.W.S. and A.T.H. developed the concept. M.Z. and A.T.H. designed the experiments and prepared the manuscript. M.Z. performed the experiments and analyzed the data. M.Z. and P.J.S. performed *in vitro* co-culture experiment. T.W.S., G. J. B., J. G. C. provided lymphoid tissue samples. C.S.R. performed statistical analysis.

Financial Disclosure: This work was supported in part by NIH research grants AI028246, AI048484 and AI056997 to A.T.H. and AI074340 to T.W.S. The funders had no role in study design, data collection and analysis, decision to publish, or preparation of the manuscript.

Conflict-of-Interest Disclosures: The authors have declared that no conflict of interest exists.

Figure 3-1.

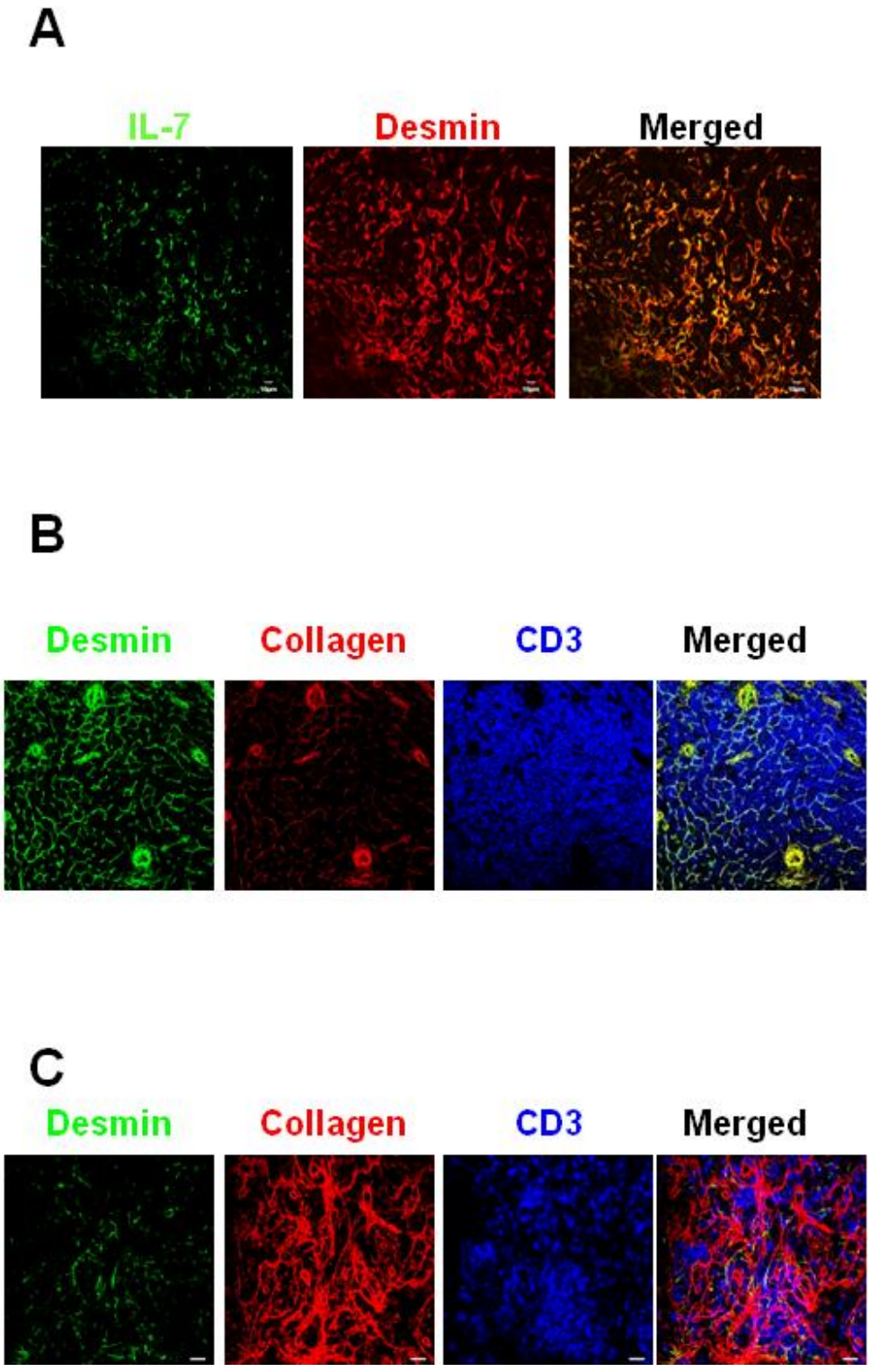
A
IL-7
Desmin
Merged
B
Desmin
Collagen
CD3
Merged
C
Desmin
Collagen
CD3
Merged

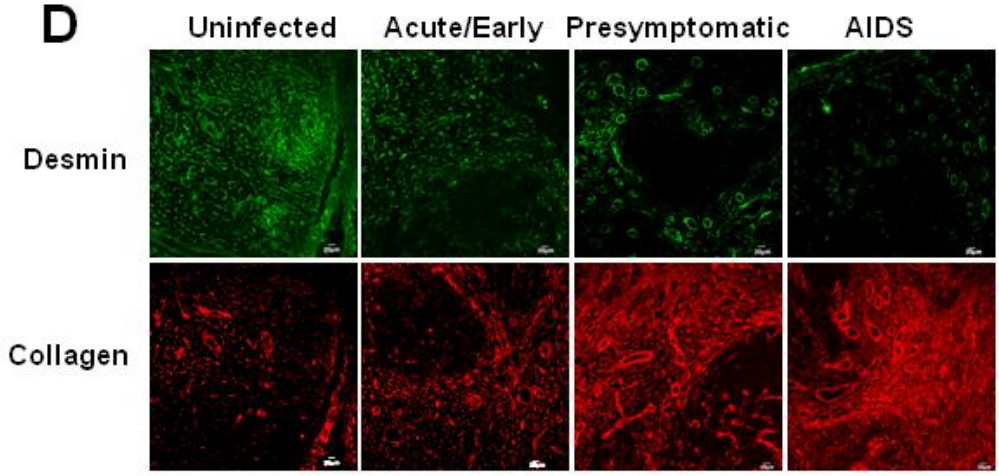
D
Uninfected
Acute/Early
Presymptomatic
AIDS
Desmin
Collagen

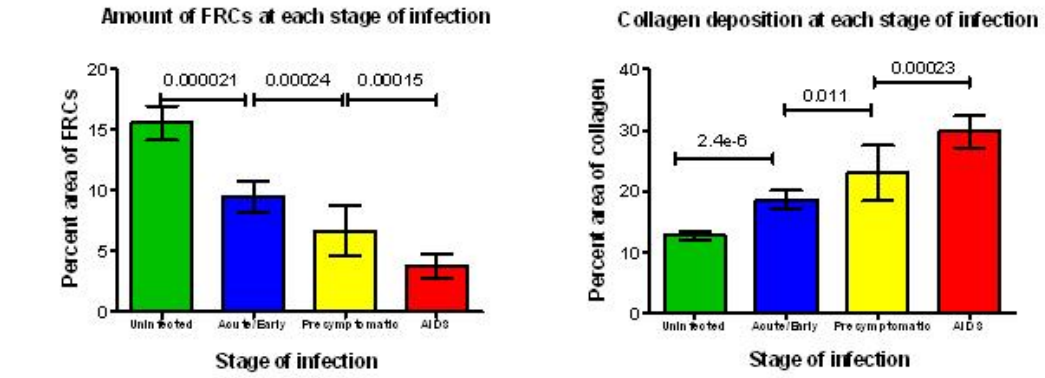
E
Amount of FRCs at each stage of infection
Percent area of FRCs
0.000021
0.00024
0.00015
Uninfected
Acute/Early
Presymptomatic
AIDS
Stage of infection
Collagen deposition at each stage of infection
Percent area of collagen
2.4e-6
0.011
0.00023
Stage of infection

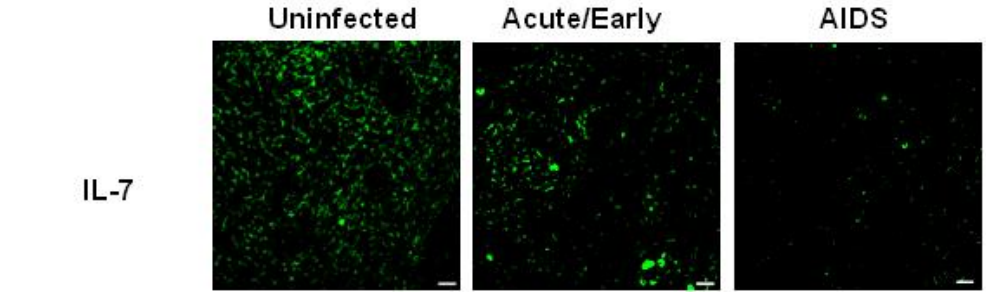
F
Uninfected
Acute/Early
AIDS
IL-7

Figure 3-1. Collagen deposition and loss of the FRC network impede access to and source of IL-7 in HIV infection. (**A**) FRCs are the major producers of IL-7. LN sections (representative image for one HIV negative subject of 5) stained for desmin (red) and IL-7 (green). Merged confocal image shows co-localization of IL-7 and FRCs in T cell area. Scale bar, 10 μm. (**B-C**) Collagen deposition and loss of the FRC network disrupts interaction between T cells and FRCs. Confocal images of LN sections from an uninfected subject (representative image for one subject of 5) immunofluorescently stained for desmin (green), collagen (red) and CD3 (blue). The merged image shows that FRCs colocalize with collagen and T cells are in contact with the FRC network (**B**). Confocal images of LN sections from a subject at AIDS stage (representative image for one subject of 6). The merged image shows that the loss of FRCs and associated collagen deposition leads to loss of the contact between FRCs and T cells, which instead contact mainly extra-FRC collagen. Scale bar, 20 μm (**C**). **(D**) Confocal images of LN sections from HIV negative subjects and from subjects at different stage of HIV infection immunofluorescently stained for desmin (green) and collagen (red), showing the gradual loss of FRCs in the T cell zone within LTs, which is associated with extensive collagen deposition during HIV infection. Scale bar, 20 μm. (**E**) Quantification of average amount of FRCs and collagen deposition at each stage of infection, showing the gradual loss of FRCs and collagen deposition. Error bars represent the s.d. (**F**) Confocal images of LN sections from HIV negative subjects and from subjects at different stage of HIV infection immunofluorescently stained for IL-7 (green), showing that the gradual loss of IL-7 in the T cell zone is associated with gradual depletion of FRCs (**E**). Scale bar, 20 μm.

Figure 3-2.

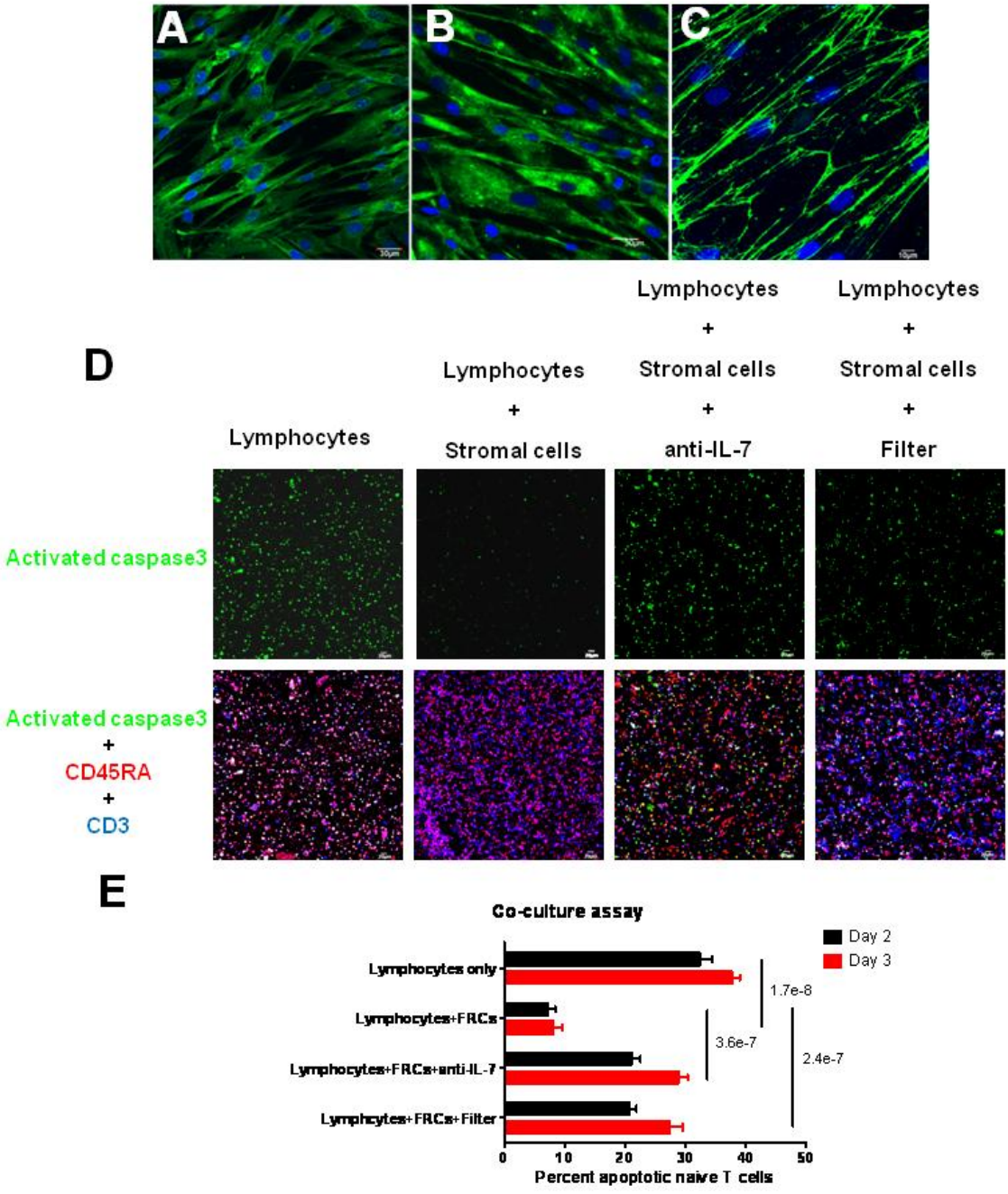
A
B
C
D
Lymphocytes
Lymphocytes + Stromal cells
Lymphocytes + Stromal cells + anti-IL-7
Lymphocytes + Stromal cells + Filter
Activated caspase3
Activated caspase3 + CD45RA + CD3
E
Co-culture assay
Day 2
Day 3
Lymphocytes only
Lymphocytes+FRCs
Lymphocytes+FRCs+anti-IL-7
Lymphcytes+FRCs+Filter
1.7e-8
3.6e-7
2.4e-7
0
10
20
30
40
50
Percent apoptotic naive T cells

Figure 3-2. Naïve T cells need to contact FRCs to get access to IL-7 for survival. (**A-C**) IL-7 is produced and presented on the surface of stromal cells. (**A-B)** Confocal images of monolayer of fixed and permeablized stromal cells isolated from human tonsil immunofluorescently stained for (**A**) IL-7 (green) or (**B**) desmin (green) and DAPI (blue) at one-day post passage. Scale bar, 30 μm. C. Confocal image of live stromal cells (DAPI: blue) staining showing the IL-7 (green) on the surface of stromal cells. Scale bar, 10 μm. (**D-E**) FRC-like stromal cells enhance the survival of naïve T cells via IL-7. (**D**) Triple fluorescently stained activated caspase 3+ (green), CD45RA+ (red) and CD3+ (blue) cells in an ex vivo culture system showing that stromal cells enhance the survival of naïve T cell by mechanisms dependent on IL-7 and cell contact. $2x10^5$ lymphocytes from human tonsil were cultured with or without stromal cells for 2-3 days. Naïve T cell apoptosis is reduced in co-cultures with stromal cells (+stromal cells) compared to cultures without stromal cells. Apoptosis in the naïve T cell population increases with IL-7 blocking antibody (anti-IL-7) or when lymphocytes are separated from stromal cells by a transwell filter (Filter) compared to co-cultures with stromal cells. Scale bar, 60 μm. (**E**) Quantification of the percentages of activated caspase 3+CD45RA+CD3+ naïve T cells in total T cell population at day 2 and day 3 cultures. Values are the mean of the percent apoptotic naïve T cells ± s.d. ANOVA comparison was done on the average percentages of day 2 and day 3.

Figure 3-3.

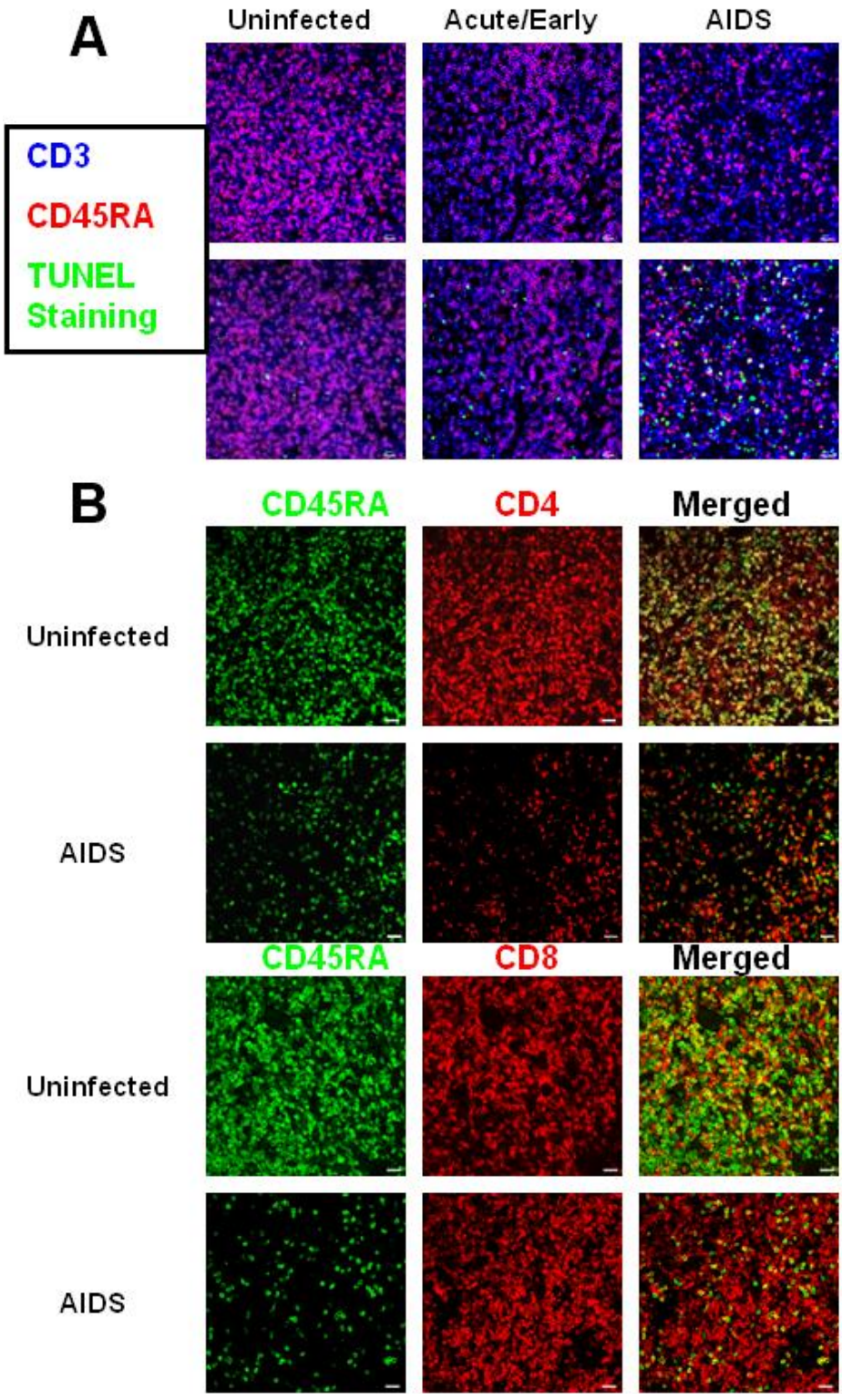
A
Uninfected
Acute/Early
AIDS
CD3
CD45RA
TUNEL
Staining
B
CD45RA
CD4
Merged
Uninfected
AIDS
CD45RA
CD8
Merged
Uninfected
AIDS

C

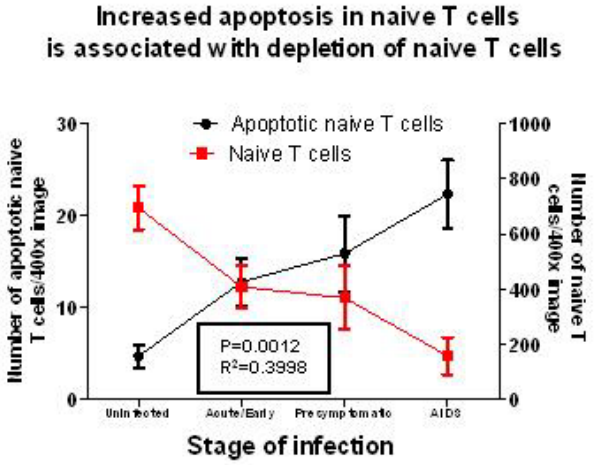
Increased apoptosis in naive T cells
is associated with depletion of naive T cells
Apoptotic naive T cells
Naive T cells
Number of apoptotic naive T cells/400x image
Number of naive T cells/400x image
P=0.0012
R²=0.3998
Uninfected
Acute/Early
Pre symptomatic
AIDS
Stage of infection

D

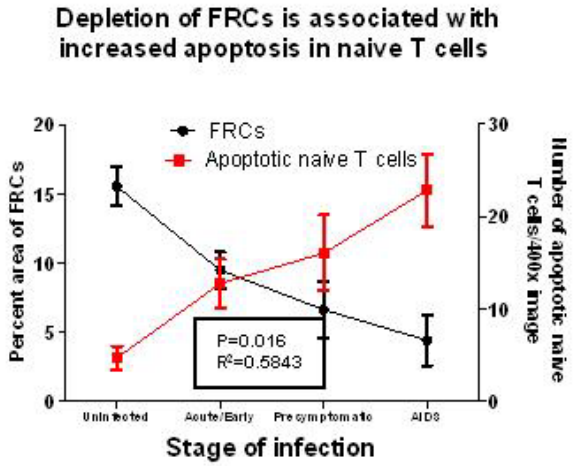
Depletion of FRCs is associated with
increased apoptosis in naive T cells
FRCs
Apoptotic naive T cells
Percent area of FRCs
Number of apoptotic naive T cells/400x image
P=0.016
R²=0.5843
Uninfected
Acute/Early
Pre symptomatic
AIDS
Stage of infection

E

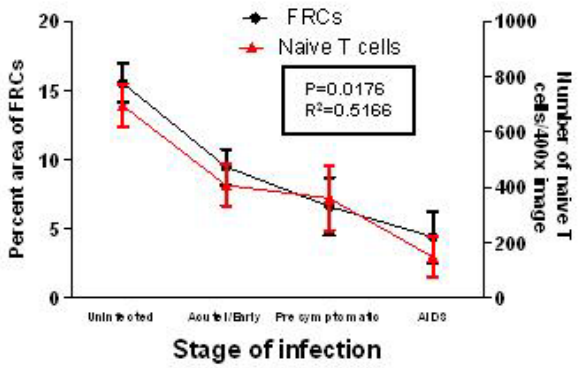
Depletion of FRCs is associated with
depletion of naive T cells before HAART
FRCs
Naive T cells
Percent area of FRCs
Number of naive T cells/400x image
P=0.0176
R²=0.5166
Uninfected
Acute/Early
Pre symptomatic
AIDS
Stage of infection

Figure 3-3. Loss of FRCs is associated with loss of naïve T cells within LTs. (A) Confocal images of LN sections from subjects at different stage of HIV infection triple immunofluorescently stained for TUNEL (green), CD45RA (red) and CD3 (Blue), showing the gradual loss of CD45RA+CD3+ naïve T cells is associated increased apoptosis in the naïve T cell population within LTs during HIV infection. Scale bar, 10 μm. (**B**) Confocal images of LN sections from subjects at different time points post HIV infection double immunofluorescently stained for CD45RA (green) and CD4 or CD8 (red), showing both naïve CD4+ and CD8+ T cells are depleted within LTs. Scale bar, 20 μm. (**C**) Quantitative image analysis of the number of apoptotic naïve T cells and the number of naïve T cells (CD45RA+CD3+), showing that increased apoptosis in the naïve T cell population is associated with depletion of naïve T cells (total n=37, $p<0.0001$, $R^2=0.5373$). (**D**) Quantification of FRCs (the percent area staining positive for desmin in T cell zone) and the number of apoptotic naïve T cells (TUNEL+CD45RA+CD3+), showing that the depletion of FRCs is associated with increased apoptosis in naïve T cell populations (total n=37, $p<0.0001$, $R^2=0.5843$). (**E**) Quantitative image analysis of FRCs and the number of naïve T cells within LTs, showing that the loss of naïve T cells is associated with loss of FRCs (total n=37, $p<0.0001$, $R^2=0.5166$). Values are the mean of measurement ± s.d.

Figure 3-4.

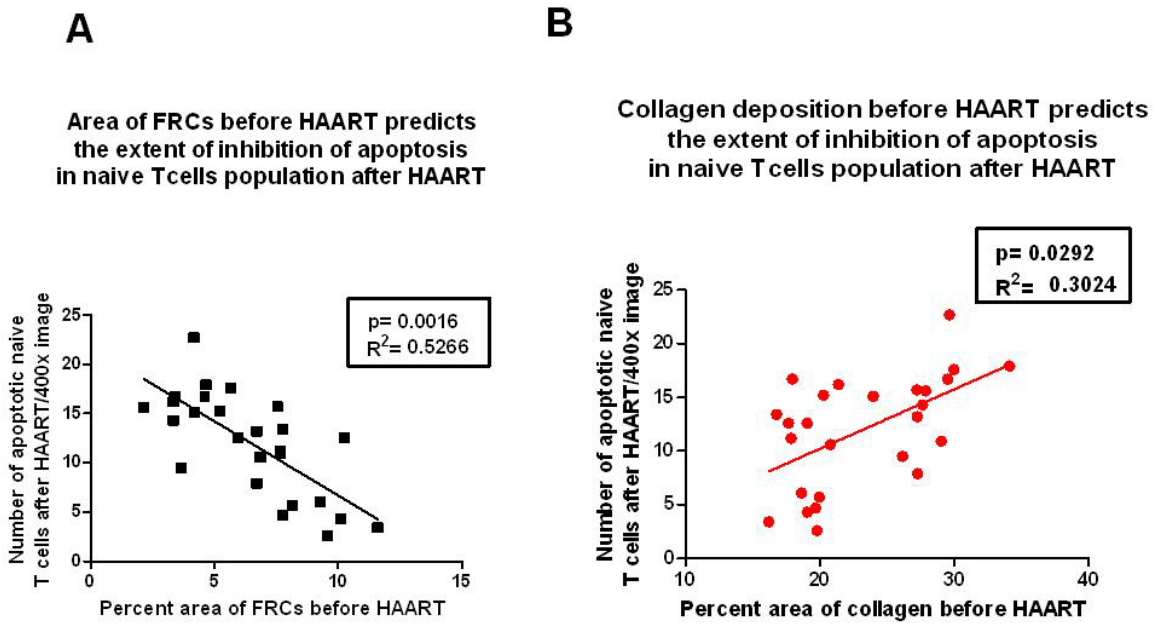
A
Area of FRCs before HAART predicts the extent of inhibition of apoptosis in naive Tcells population after HAART
p= 0.0016
R2= 0.5266
Number of apoptotic naive T cells after HAART/400x image
Percent area of FRCs before HAART
B
Collagen deposition before HAART predicts the extent of inhibition of apoptosis in naive Tcells population after HAART
p= 0.0292
R2= 0.3024
Number of apoptotic naive T cells after HAART/400x image
Percent area of collagen before HAART

Figure 3-4. The extent of LT destruction before HAART predicts the extent of restoration of naïve T cells after HAART. (A) The area that FRCs occupy before HAART is negatively associated with the number of apoptotic naïve T cells after 6 months of HAART. (**B**) The collagen area before HAART is positively associated with the number of apoptotic naïve T cells after 6 months of HAART.

Figure 3-5.

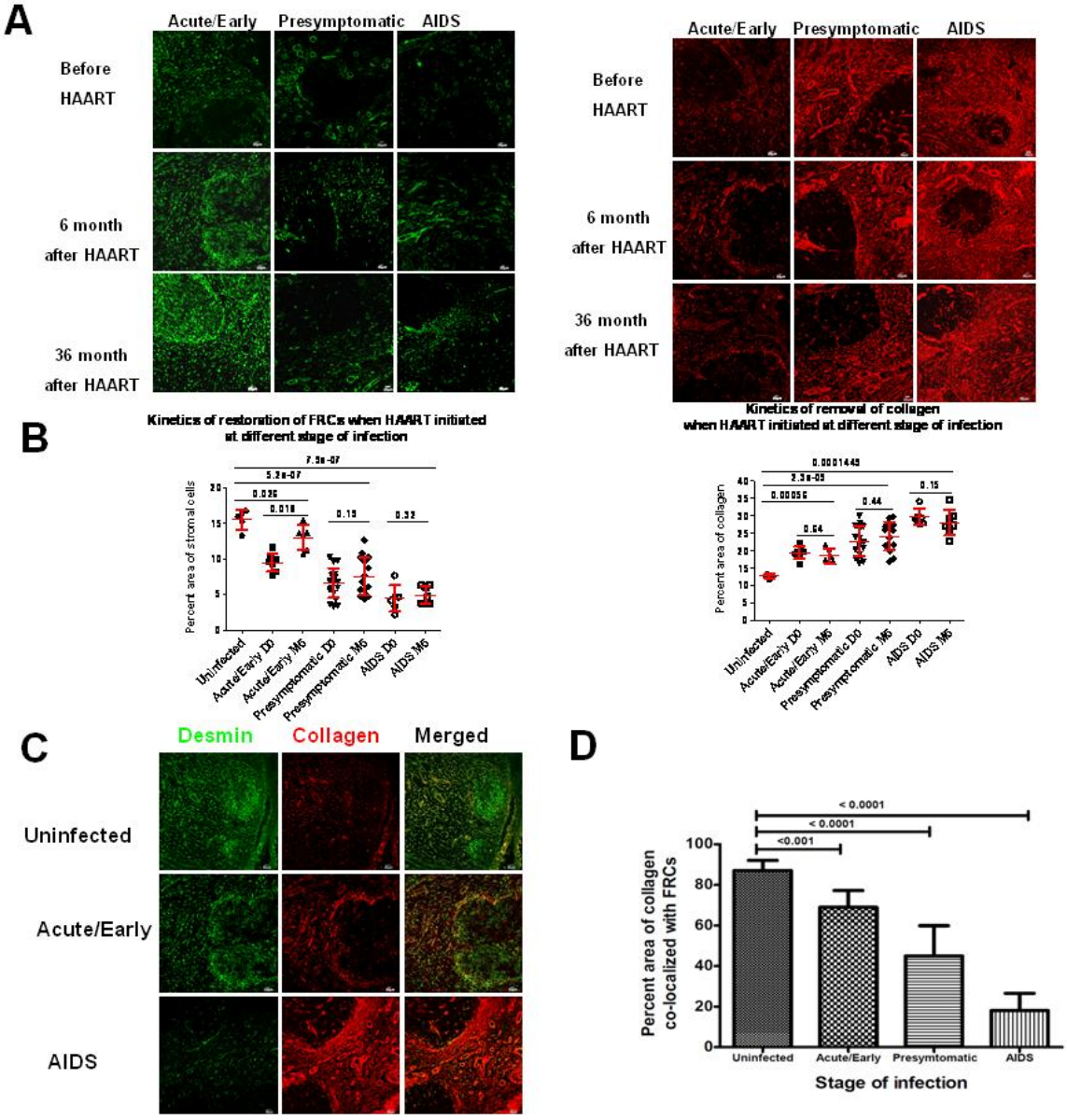
A
Acute/Early
Presymptomatic
AIDS
Before HAART
6 month after HAART
36 month after HAART
Acute/Early
Presymptomatic
AIDS
Before HAART
6 month after HAART
36 month after HAART
B
Kinetics of restoration of FRCs when HAART initiated at different stage of infection
Percent area of stromal cells
Uninfected
Acute/Early D0
Acute/Early M6
Presymptomatic D0
Presymptomatic M6
AIDS D0
AIDS M6
Kinetics of removal of collagen when HAART initiated at different stage of infection
Percent area of collagen
C
Desmin
Collagen
Merged
Uninfected
Acute/Early
AIDS
D
< 0.0001
< 0.0001
<0.001
Percent area of collagen co-localized with FRCs
Uninfected
Acute/Early
Presymtomatic
AIDS
Stage of infection

Figure 3-5. Restoration of LT structure is slow and incomplete after HAART and is associated with the timing of initiation of HAART. (A) Representative confocal images of immunofluorescent staining for desmin (green) and collagen (red), showing the different extent of restoration of stromal cell network and collagen normalization after 6 months of HAART. Scale bar, 20 μm. (**B**) Quantification of the average area of FRCs and collagen before and after 6 months of HAART in patients receiving the HAART at different stages of infection, showing the different extent of restoration of LTs is associated with the timing of initiation of HAART. Error bars represent the s.d. (**C**) Representative confocal images of immunofluorescent staining for desmin (green) and collagen (red), showing that the different extent of restoration of the FRC network and collagen normalization after 6 months of HAART as represented by the percent area not covered by FRCs. Scale bar, 20 μm. (**D**) Quantification of the percent area covered by FRCs.

Figure 3-6.

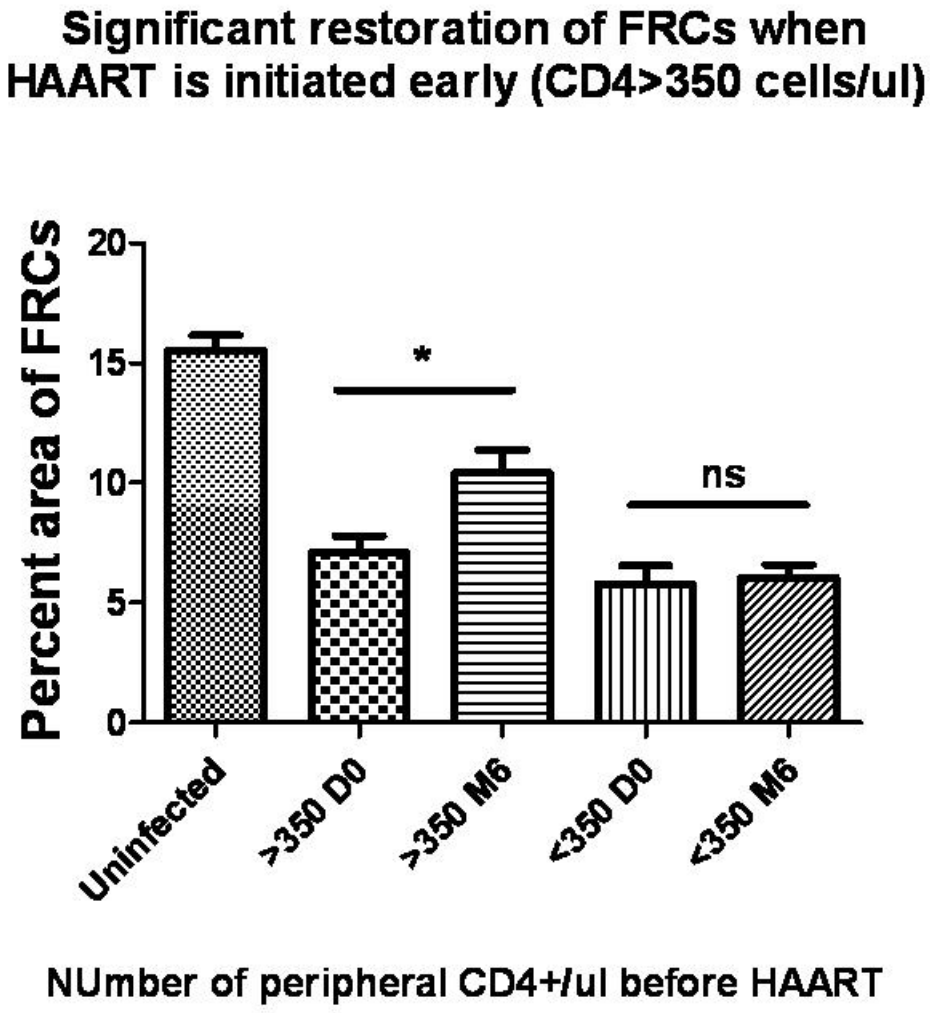
Significant restoration of FRCs when HAART is initiated early (CD4>350 cells/ul)
Percent area of FRCs
20
15
10
5
0
*
ns
Uninfected
>350 D0
>350 M6
<350 D0
<350 M6
NUmber of peripheral CD4+/ul before HAART

Figure 3-6. Significant restoration of FRCs is associated with early initiation of HAART. Bar plot shows that the increase of FRCs is significant when HAART is initiated when peripheral CD4+ T cells is above 350 cells/μl. In contrast to that, the increase of FRCs is insignificant when HAART is started when peripheral CD4+ T cells is below 350 cells/μl (*, $p<0.05$; ns, not significant).

Figure 3-7.

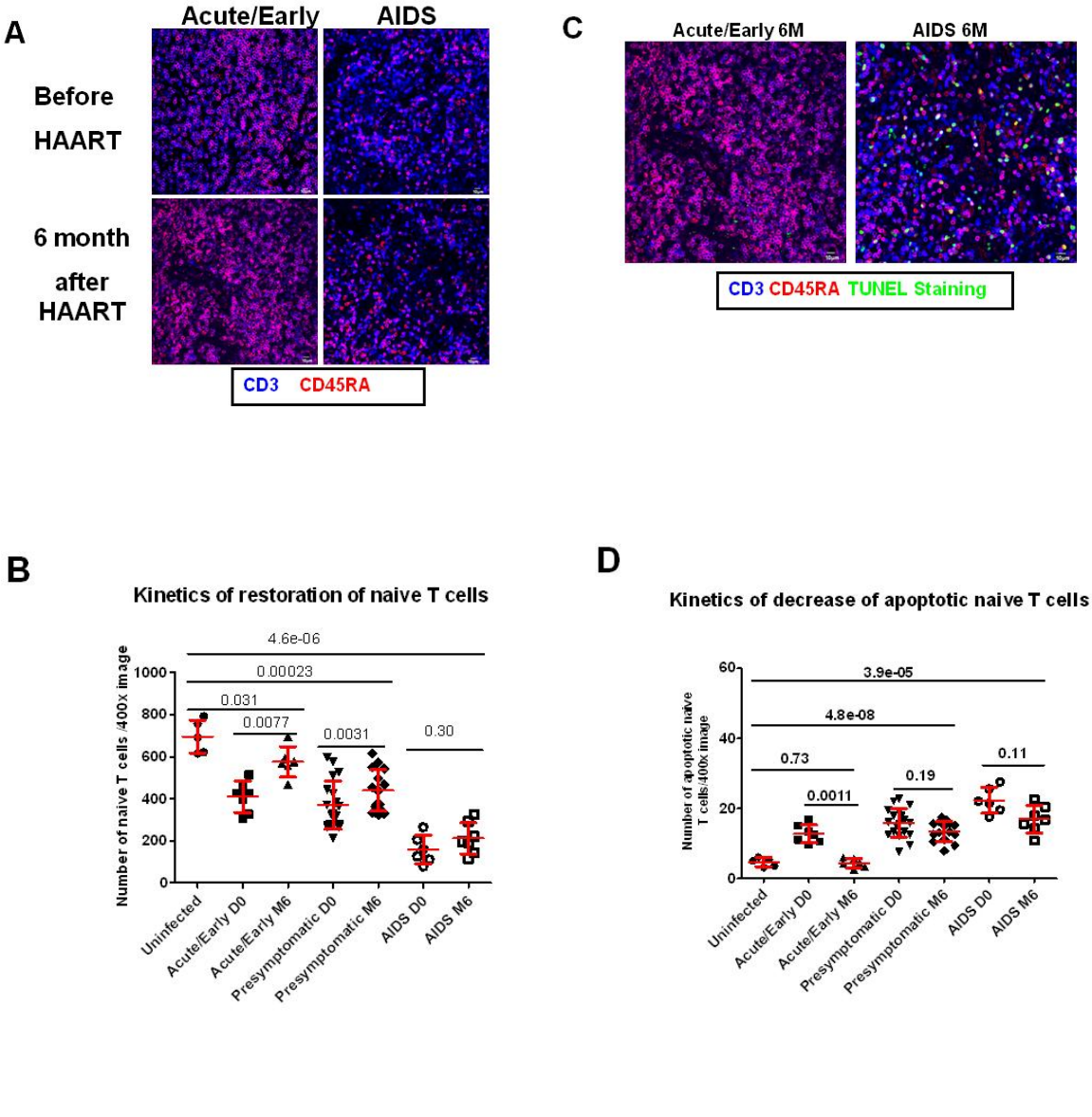
A
Acute/Early
AIDS
Before HAART
6 month after HAART
CD3 CD45RA
C
Acute/Early 6M
AIDS 6M
CD3 CD45RA TUNEL Staining
B
Kinetics of restoration of naive T cells
Number of naive T cells /400x image
4.6e-06
0.00023
0.031
0.0077
0.0031
0.30
Uninfected
Acute/Early D0
Acute/Early M6
Presymptomatic D0
Presymptomatic M6
AIDS D0
AIDS M6
D
Kinetics of decrease of apoptotic naive T cells
Number of apoptotic naive T cells/400x image
3.9e-05
4.8e-08
0.73
0.0011
0.19
0.11

Figure 3-7. Incomplete LT restoration is associated with high level of apoptosis in naïve T cell populations and incomplete restoration of naïve T cells. (A) Confocal images of LN sections from uninfected subjects and patients receiving 6 months of HAART at either acute or AIDS phase of infection, immunofluorescently stained for CD45RA (red) and CD3 (blue), showing the different extent of restoration of naïve T cells. Scale bar, 10 μm. (**B**) Quantification of number of naïve T cells before and after HAART at each stage of infection, showing the different kinetics of restoration of naïve T cells. Error bars represent the s.d. (**C**) Confocal images of LN sections from patients receiving 6 months of HAART at either acute or AIDS phase of infection immunofluorescently stained for CD45RA (red), CD3 (blue) and TUNEL staining of apoptotic cells (green), showing the higher level of apoptosis in naïve T cell populations after 6 months of HAART when HAART was started during chronic phase of infection. Scale bar, 10 μm. (**D**) Quantification of average number of apoptotic naïve T cells before and after HAART at each stage of infection, showing the different kinetics of decrease of apoptotic naïve T cells.

Figure 3-8.

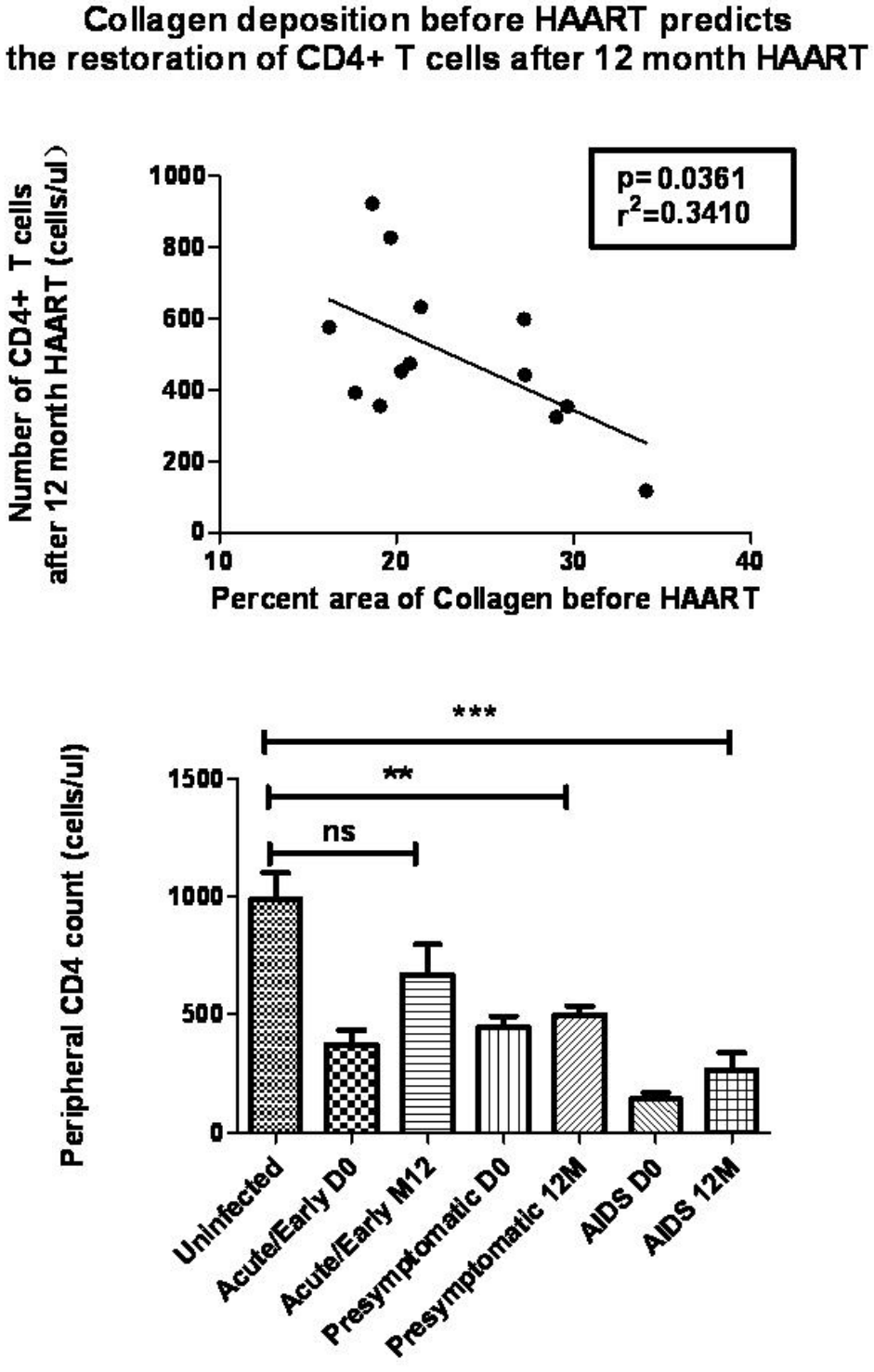
Collagen deposition before HAART predicts
the restoration of CD4+ T cells after 12 month HAART
Number of CD4+ T cells
after 12 month HAART (cells/ul)
1000
800
600
400
200
0
10
20
30
40
p= 0.0361
r2=0.3410
Percent area of Collagen before HAART
Peripheral CD4 count (cells/ul)
1500
1000
500
0
***
**
ns
Uninfected
Acute/Early D0
Acute/Early M12
Presymptomatic D0
Presymptomatic 12M
AIDS D0
AIDS 12M

Figure 3-8. Incomplete restoration of peripheral CD4 count after 12 month HAART is associated with initiation of HAART during chronic stage of infection. (**A**) Plot shows that the level of peripheral CD4 count is not significantly different from that in uninfected subjects when HAART is initiated during acute/early stage of infection after 12 month HAART. In contrast to that, when HAART is started during chronic stage of infection, the level of peripheral CD4 count is still significantly lower than that in uninfected subjects after 12 month HAART (*, $p<0.05$; **, $p<0.01$; ***, $p<0.0001$; ns, not significant). (**B**) The percent area of collagen before HAART is negatively associated with the number of peripheral CD4 count after 12 months of HAART.

Figure 3-9.

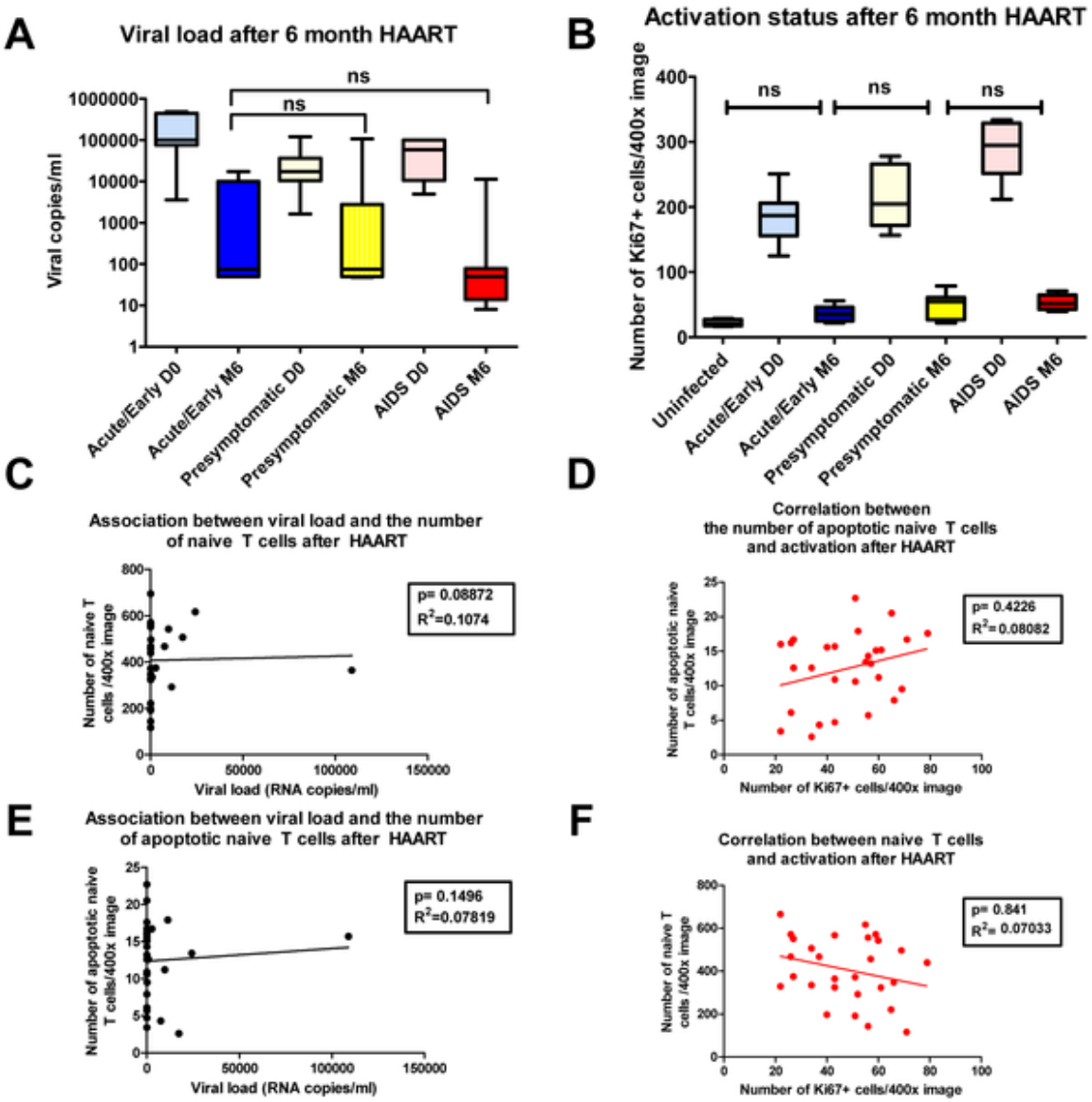
A
Viral load after 6 month HAART
Viral copies/ml
1000000
100000
10000
1000
100
10
1
ns
ns
Acute/Early D0
Acute/Early M6
Presymptomatic D0
Presymptomatic M6
AIDS D0
AIDS M6
B
Activation status after 6 month HAART
Number of Ki67+ cells/400x image
400
300
200
100
0
ns
ns
ns
Uninfected
Acute/Early D0
Acute/Early M6
Presymptomatic D0
Presymptomatic M6
AIDS D0
AIDS M6
C
Association between viral load and the number of naive T cells after HAART
Number of naive T cells /400x image
800
600
400
200
0
p= 0.08872
R2=0.1074
0
50000
100000
150000
Viral load (RNA copies/ml)
D
Correlation between the number of apoptotic naive T cells and activation after HAART
Number of apoptotic naive T cells/400x image
25
20
15
10
5
0
p= 0.4226
R2= 0.08082
0
20
40
60
80
100
Number of Ki67+ cells/400x image
E
Association between viral load and the number of apoptotic naive T cells after HAART
Number of apoptotic naive T cells/400x image
25
20
15
10
5
0
p= 0.1496
R2=0.07819
0
50000
100000
150000
Viral load (RNA copies/ml)
F
Correlation between naive T cells and activation after HAART
Number of naive T cells /400x image
800
600
400
200
0
p= 0.841
R2= 0.07033
0
20
40
60
80
100
Number of Ki67+ cells/400x image

Figure 3-9. The extent of restoration of naïve T cells after HAART is not associated with viral load or immune activation. (A) Viral load before and after HAART in patients receiving HAART at different stages of infection, showing the inhibition of viral replication is similar for patients at different stage of infection. (**B**) Quantification of the number of Ki67+ cells before and after HAART in patients receiving HAART at different stages of infection, showing the inhibition of immune activation by HAART is similar for patients at different stage of infection (ns, not significant). (**C, E**) Association between the viral load and number of naïve T cells and association between viral load and the number of apoptotic naïve T cells after HAART are not significant. (**D, F**) Association between the number of Ki67+ cells and naïve T cells and association between the number of Ki67+ cells and the number of apoptotic naïve T cells after HAART are not significant.

Tables

Table 3-1. Demographic characteristics and clinical information of subjects

Patient	Disease Stage	Time after HAART	Race	Gender	Age	Peripheral Blood CD4+ T Cell Count (Cells/µl)	Plasma HIV RNA Levels (Copies/ml)	Opportunistic Infections (n = none reported)
1292	Uninfected	N/A	Caucasian	Male	28	925	Undetectable	N/A
1476	Uninfected	N/A	Caucasian	Female	28	704	Undetectable	N/A
1472	Uninfected	N/A	Caucasian	Female	52	837	Undetectable	N/A
1425	Uninfected	N/A	Caucasian	Male	43	1351	Undetectable	N/A
1442	Uninfected	N/A	Caucasian	Female	45	1124	Undetectable	N/A
1430	Acute	D0	Caucasian	Male	26	683	3610	n
1430	Acute	M6				702	17400	
1458	Acute	D0	Caucasian	Male	51	400	439000	n
1458	Acute	M6				671	<50	
132	Acute	D0	Cauca	Male	59	370	484694	n

9			sian					
1329	Acute	M6				871	<50	
1329	Acute	M36				789	<50	
1469	Acute	D0	Caucasian	Male	44	180	>100,000	n
1469	Acute	M6				321	7547	
1449	Acute	D0	Caucasian	Male	30	333	>100000	n
1435	Acute	D0	Caucasian	Male	42	410	>100,000	Unknown
1435	Acute	M6				663	<50	
1391	Acute	D0	Black or African American	Male	37	414	24718	n
1391	Acute	M6				765	<50	
1437	AIDS	D0	Caucasian	Male	47	214	656	n
1437	AIDS	M6				235	<50	
1438	AIDS	D0	Caucasian		49	147	4960	n
1438	AIDS	M6				151	<50	
143	AIDS	M36				216	<50	

8								
1406	AIDS	D0	Black or African American	Male	45	188	10684	n
1406	AIDS	M6				209	11438	
1413	AIDS	D0	Black or African American	Male	50	42	59401	Unknown
1413	AIDS	M6				121	8	
1462	AIDS	M6				143	<50	n
1327	AIDS	D0	Black or African American	Female	40	112	12046	n
1327	AIDS	M6				180	14	
1419	AIDS	D0	Caucasian	Male	37	157	61432	n
1419	AIDS	M6				320	79	
146	Pre	D0	Black	Male	23	259	27200	n

3			or Africa n Ameri can					
146 3	Pre	M6				599	<50	
144 7	Pre	D0	Cauca sian	Male	37	640	12100	Unknow n
144 7	Pre	M6				776	24300	
146 8	Pre	D0	Cauca sian	Male	30	875	2150	n
133 5	Pre	D0	Cauca sian	Male	32	400	15284	n
133 5	Pre	M36				458	<50	
142 8	Pre	D0	Cauca sian	Male	30	363	38600	Unknow n
142 8	Pre	M6				379	<50	
147 9	Pre	D0	Cauca sian	Male	42	273	1650	n
147 9	Pre	M6				479	< 75	
146 4	Pre	D0	Cauca sian	Male	34	202	122000	n
146 4	Pre	M6				450	72	
166 9	Pre	D0	Cauca sian	Male	23	434	6506	n
166	Pre	M6				524	85	

9								
1293	Pre	D0	Caucasian	Male	36	905	14225	Unknown
1293	Pre	M6				1842	<50	
1293	Pre	M36				2251	<50	
1408	Pre	D0	Caucasian	Male	39	685	20014	n
1408	Pre	M6				592	9815	
1680	Pre	M6	Caucasian	Male	38	539	<48	n
1448	Pre	D0	Black or African American	Male	51	543	10000	Unknown
1448	Pre	M6				335	2790	
1727	Pre	D0	Caucasian	Male	39	336	17600	n
1436	Pre	D0	Caucasian	Male	63	248	46400	n
1436	Pre	M6				297	893	
1407	Pre	D0	Caucasian	Male	35	372	31922	n
1407	Pre	M6				353	108996	
167	Pre	D0	Cauca	Male	36	620	17388	n

9			sian					
1679	Pre	M6				721	<48	
1317	Pre	D0	Caucasian	Male	31	399	120469	n
1317	Pre	M6				779	303	
1766	Pre	D0	Black or African American	Male	36	389	6810	n
1455	Pre	D0	Black or African American	Male	23	209	19400	n
1455	Pre	M6				324	<50	
1459	Pre	D0	Caucasian	Male	36	286	>100000	n

Note: Definition of classification of HIV infection stage: Acute/Early stage: patients are RNA+ and antibody negative or have serologic proof of infection within the previous 4 months. AIDS stage: patients whose CD4 count is <200cells/μL. Presymptomatic stage: patients between acute/early stage and AIDS stage.

Table 3-2. List of primary antibodies and antigen retrieval methodologies

Antibody	Clone/ Manufacturer & Catalog #	Antigen-retrieval Pretreatment	Antibody Dilution	Species
Desmin	D33 / Lab Vision & # MS-376-S1	Diva Decloaker; High pressure cooker for 30 seconds at 125°C.	1/200	Mouse
Desmin	Polyclonal / Lab Vision & # RB-9014-P1	Diva Decloaker; High pressure cooker for 30 seconds at 125°C.	1/200	Rabbit
CD3	MCA147 / AbD Serotec & # MCA1477	Diva Decloaker; High pressure cooker for 30 seconds at 125°C.	1/200	Rat
CD3	SP7 / Thermo Scientific & # RM-9107-S1	Diva Decloaker; High pressure cooker for 30 seconds at 125°C.	1/100	Rabbit
IL-7	7417 / R & D Systems & # MAB207	Diva Decloaker; High pressure cooker for 30 seconds at 125°C. Proteinase K treatment for 15 min	1/100	Mouse
CD45RA	4KB5 / Dako & # M0754	Diva Decloaker; High pressure cooker for 30 seconds at 125°C.	1/100	Mouse

Activated Caspase-3	8G10 / Cell Signaling Tech. & # 9665	1mm EDTA (ph 8); High pressure cooker for 30 seconds at 125°C.	1/100	Rabbit
Collagen 1	COL-1 / Sigma & # C2456	Diva Decloaker; High pressure cooker for 30 seconds at 125°C. Protease K (10 µg/ml).	1/100	Mouse
Collagen I	Polyclonal / Abcam & # ab292	Diva Decloaker; High pressure cooker for 30 seconds at 125°C. Protease K (10 µg/ml).	1/200	Rabbit
CD4	Polyclonal / R & D Systems & # AF-379-NA	Diva Decloaker; High pressure cooker for 30 seconds at 125°C.	1/100	Goat
CD4	1F6 / Novacastra & # NCL-CD4–1F6	Diva Decloaker; High pressure cooker for 30 seconds at 125°C.	1/100	Mouse
CD8	SP16 / Neomarkers & # RM-9116-s	Diva Decloaker; High pressure cooker for 30 seconds at 125°C.	1/100	Rabbit
Ki-67	SP6 / Neomarkers & # RM-9106-S1	Diva Decloaker; High pressure cooker for 30 seconds at 125°C.	1/200	Rabbit

IgG Isotype Controls	Dako, Jackson ImmunoResearch	Diva Decloaker; High pressure cooker for 30 seconds at 125°C. Protease K (10 µg/ml).	1/50-1/200	Mouse, Rabbit, Rat, Goat

A list of ID numbers for genes and proteins used in the paper: Desmin: 1674, CD3: 916, Interleukin-7: 3574, CD45RA: 151460, Caspase3: 600636, Collagen Type I: 120150, CD4: 186940, CD8: 925, Ki-67: 176741.

Chapter 4

"This research was originally published in Blood Online. Zeng M, Paiardini M, Engram JC, et al. Critical role for CD4 T cells in maintaining lymphoid tissue structure for immune cell homeostasis and reconstitution. Blood. Prepublished May 21, 2012; DOI 10.1182/blood-2012-03-418624."

Critical role for CD4 T cells in maintaining lymphoid tissue structure for immune cell homeostasis and reconstitution

Ming Zeng,[1] Mirko Paiardini,[2] Jessica C. Engram,[3] Timothy W. Schacker,[4] Guido Silvestri,[2] and Ashley T. Haase[1]

[1]Department of Microbiology, Medical School, University of Minnesota, Minneapolis, MN, USA, 55455; [2]Yerkes National Primate Research Center and Emory University, Atlanta, GA, USA, 30329; [3]University of Pennsylvania School of Medicine, Philadelphia, PA, USA, 19104; and [4]Department of Medicine, Medical School, University of Minnesota, Minneapolis, MN, USA, 55455

Address correspondence to: Ashley T. Haase, Department of Microbiology, University of Minnesota, MMC 196, 420 Delaware Street S.E., Minneapolis, Minnesota 55455, USA. Phone: (612) 624-4442; Fax: (612) 626-0623; E-mail: haase001@umn.edu

Introduction

Highly active anti-retroviral therapy (HAART) has had a great beneficial impact on suppressing human immunodeficiency virus (HIV) replication to undetectable levels in peripheral blood, and the associated increases in peripheral CD4+ T cell counts are correlated with decreased morbidity and mortality in HIV infection [34]. However, controlling viral replication has not necessarily led to full reconstitution of the immune system. More than a quarter of the patients after years of HAART still have CD4 T cell counts not significantly increased from pre-treatment levels and/ or below the critical threshold of 200 cell/mm^3, and even in patients with significant increases in peripheral CD4 T cell counts, few reach the levels in uninfected populations after long-term HAART [40-42, 44-45, 84, 183, 201-202]. Limited immune reconstitution is most prevalent in patients starting HAART in the chronic stage of disease (CD4<350 cells/μl) and in patients with older age, and this failure strongly correlates with significantly higher morbidity and mortality [40, 44-45, 73-75, 203]. Further, the magnitude of CD4+ T cell reconstitution in peripheral blood does not necessarily reflect the real magnitude of immune reconstitution in lymphoid tissues (LTs) where these cells mostly reside. Compared to the pace and extent of restoration of peripheral blood CD4+ T cells, the normalization of peripheral blood CD4+ T cell is significantly slower and less significant [48, 77-79, 145, 204-206]. There are several important functional immunologic abnormalities that accompany the limited restoration of T cells including: 1) persistently poor vaccine responses [80-81] and 2) increased frequency of reactivation of latent herpes simplex infection and human papilloma virus infections [82-84]. These persistent defects in immune function likely contribute to the increasing incidence of non-AIDS related clinical events such as cardiovascular disease, liver disease and non-AIDS-related cancer [85-88, 185, 207], and increased susceptibility to bacterial infections [89]. These enduring and pervasive defects in immune surveillance despite the great benefits conferred by suppression of viral replication point to the importance of understanding the mechanisms that limit immune reconstitution after HAART to devise strategies to improve outcomes.

Within the LTs, HIV and SIV infections have their greatest impact on naïve T cell populations in depletion and immune reconstitution and this is also the case in immunodeficiencies caused by chemotherapy and irradiation treatment of cancer or patients receiving allogeneic hematopoietic stem cell transplantation [46, 48, 144, 208-213]. In these conditions, the loss of naïve T cells is greater than in other T cell populations, and the restoration of naïve T cells is slower and to lower levels than other T cell subsets with HAART or cessation of cancer treatments [48, 144, 208-209, 212-214].

While the mechanisms underlying depletion and impaired immune reconstitution particularly of naïve T cells have yet to be fully defined, damage to LT structure plays an important role because naive T cells within secondary LTs rely for their survival on interacting with the fibroblastic reticular cell (FRC) network in the T cell zone (TZ) to supply factors such as interleukin-7 (IL-7) and self-antigen-major histocompatibility complex signals [93, 118-119, 124, 149]. We previously showed that LT damage due to the losses of the FRC network and collagen deposition in HIV and pathogenic SIV infection of rhesus macaques (*Macaca mulatta;* RM) leads to loss of production of IL-7 and limits the access of naïve T cells to the source of IL-7, thereby impairing the survival of naïve T cells [190, 214]. We also found that the damaged LT structure recovers very slowly and incompletely after 3 year HAART when HAART is initiated during the chronic stage of infection, which perpetuates the elevated level of apoptosis in naïve T cells to thereby limit the reconstitution of naïve T cells after HAART [214].

These findings suggest that restoration of LT structure is critical for the successful immune reconstitution. However, little is known about what contributes to the loss of FRC networks during HIV infection. Lymphotoxin beta (LTbeta) is a key factor that together with lymphotoxin alpha (LTalpha) can trigger the LTbeta receptor signaling pathway to maintain the stromal FRC network in TZ and follicular dendritic cell (FDC) network in B cell follicles [157, 190, 215-219]. We previously found that the T cell-derived LTbeta significantly decreased during SIV infection in RMs and the loss of LT beta correlated with depletion of FRC network [190]. These data created a model in which loss of T cell-derived LTbeta during HIV infection leads to loss of FRC network,

which in turn depletes the naïve T cells population and the interdependencies between T cells and stromal cell networks perpetuate the cycle of loss of both networks and T cells [190].

To test this model and dissect the causal relationship between T cell depletion and loss of FRC network, we used anti-CD4 and anti-CD8 antibody depletion of CD4+ and CD8+ T cells in non-human primate models to understand how each subset affects FRC networks. We first showed that LTbeta is mainly produced by naïve CD4+ T cells. The depletion of CD4+ T cells but not CD8+ T cells in RMs reproduces the depletion of FRC network in SIV infected RMs and HIV infection. Interestingly, the depletion of CD4+ T cells also leads to the depletion of FDCs, suggesting that FDCs also rely on CD4+ T cells for their maintenance. Furthermore, we found that in the non-pathogenic model of SIV infection of sooty mangabeys (*Cercocebus atys*) (SMs), despite similar levels of viral replication compared to SIV infection of RMs [65, 220], the maintenance of CD4+ T cells in SMs correlated with maintenance of FRC network. When CD4+ T cells are depleted by antibody in uninfected SMs, the FRC and FDC networks are also significantly depleted, which reproduce the pathogenic effect in SIV infected RMs. The loss of FRC network leads to loss of production of IL-7, which further affects the survival of CD8 T cells. We also found that the loss of CD4+ T cells in LTs correlates with the depletion of FRC network before HAART and also correlates with the extent of restoration after HAART. Last, we extend the conclusions to the more general case of CD4+ T cell depletion induced by chemotherapy and irradiation in cancer patients. We thus provide in vivo evidence to show depletion of CD4+ T cells leads to loss of stromal cell networks in various immunodeficiency conditions and these insights point to potential therapeutic approaches to restore LT structure and improve immune reconstitution.

Materials and methods

Ethics statement

This human study was conducted according to the principles expressed in the Declaration of Helsinki. The study was approved by the Institutional Review Board of the University

of Minnesota. All patients provided written informed consent for the collection of samples and subsequent analysis.

LN biopsy specimens

Inguinal LN (LN) biopsies from HIV negative individuals and HIV-infected individuals at different clinical stages (7 at acute/early stage, 18 at presymptomatic stage and 8 at AIDS stage.) [214] were obtained for this University of Minnesota Institutional Review Board-approved study. Viral load measurements were obtained the same day as biopsies. Each LN biopsy was immediately placed in fixative (4% neutral buffered paraformaldehyde or Streck's tissue fixative) and paraffin embedded. LN biopsies from cancer patients are provided by the University of Minnesota Biological Materials Procurement Network (BioNet).

Animals, SIV infection, & LN biopsy specimens

Adult RMs and SMs used in these studies were housed in accordance with the regulations of the American Association of Accreditation of Laboratory Animal Care and the standards of the Association for Assessment and Accreditation of Laboratory Animal Care International; all protocols and procedures were approved by All animal studies were approved by the University of Pennsylvania and Emory University Institutional Animal Care and Use Committees. For the chronically infected RM and SM study, LTs were obtained in longitudinal studies from five RMs who were inoculated intravenously (i.v.) with 10,000 $TCID_{50}$ of SIVmac239 (generous gift from R. Desrosiers), additional LTs from 5 RMs obtained in previously described cross-sectional studies [151, 190]. Infection of five SMs by i.v. innoculation with 1 ml of plasma from an experimentally SIVsmm-infected SM sampled at day 11 post infection with a viral load of 1×10^7 copies/mL of plasma. In addition, 4 naturally SIV-infected and 3 uninfected SMs were included in the cross-sectional analysis. Blood collection was performed by venipuncture. Each LN biopsy was immediately placed in fixative (4% neutral buffered paraformaldehyde or Streck's tissue fixative) and paraffin embedded. For the CD4+ and CD8+ T cell depletion study, the animals and LTs isolation were previously described in

detail [221]. Briefly, depletion of CD4+ and CD8+ lymphocytes was76 performed using 10 mg/Kg intravenous anti-CD4 mAb (OKT4A) on day -10 and 5 mg/Kg on days -7, -3, and 0, while for CD8+ lymphocyte depletion animals were treated with 4 mg/Kg intravenous anti-CD8 mAb (OKT8F) on days -2, -1, and 0, a protocol that has been shown to deplete CD4+ and CD8+ lymphocytes in vivo in both RMs and SMs [221]. Blood and LN collection were performed at baseline and at different time points after the last antibody administration. Each LN biopsy was immediately place into 70% ethanol immediately upon collection, then 24 hours later transferred to 4% PFA or Streck fixativeplaced in fixative (4% neutral buffered paraformaldehyde) and paraffin embedded.

Immunofluorescence staining, immunohistochemistry staining and quantitative image analysis (QIA)

All staining procedures were performed as previously described using 5-10 μm tissue sections mounted on glass slides [151, 214]. Tissues were deparaffinized in 60°C incubator for 2 hours and rehydrated through graded ethanols and rehydrated in deionized water. Heat-induced epitope retrieval was performed using a high-pressure cooker (125^{o}C) in either DIVA Decloaker or EDTA Decloaker (Biocare Medical), followed by cooling to room temperature. Tissue sections were washed with PBS with 0.5% tween 20 (Sigma-Aldrich) and then blocked with Fc receptor blocker (Innovex) for 30min and SNIPER Blocking Reagent (Biocare Medical) for 30 min at room temperature. Primary antibodies were diluted in TNB (0.1M Tris-HCl, pH 7.5; 0.15M NaCl; 0.05% Tween 20 with Dupont blocking buffer) and incubated overnight at 4^{o}C. After the primary antibody incubation, sections were washed with phosphate buffered saline (PBS) with 0.5% tween 20 for 3 times and then incubated with fluorochrome-conjugated secondary antibodies (Alexa-fluor 488, 586, and 647-conjugated antibodies) in TNB for 2 hr at room temperature. Finally, sections were washed with PBS, nuclei were counterstained blue with DAPI, and mounted using Aqua Poly/Mount (Polysciences Inc.). Immunofluorescent micrographs were taken at room temperature using an Olympus

FV1000 Fluoview confocal microscope with the following objectives: x20 (0.75 NA), x40 (0.75 NA), and x60 (1.42 NA).

For immunohistochemistry staining. After overnight incubation of primary antibody at 4^{o}C, tissues were then washed with PBS with 0.5% tween 20 for 3 times. Endogenous peroxidase inactivated with 3% (v/v) H_2O_2 in PBS for 10 min. Tissues were then washed with PBS with 0.5% tween 20 for 3 times. Primary antibody was detected with Mach-3 (Biocare Medical) and DAB kits (Vector). Stained sections were examined by light microscopy at ambient temperatures. Light micrographs were taken at room temperature using an Olympus BX60 upright microscope with the following objectives: x10 (0.3 NA), x20 (0.5 NA), and x40 (0.75 NA); images were acquired using a Spot color mosaic camera (model 11.2) and Spot acquisition software (version 4.5.9; Diagnostic Instruments).

Isotype-matched negative control antibodies in all instances yielded negative staining results (see Table 1, which lists the primary antibodies and antigen retrieval methodologies).

QIA was performed using 10–20 randomly acquired, high-powered images (X200 or X400 magnification) by either manually counting the cells in each image or by determining the percentage of LT area occupied by positive fluorescence signal using an automated action program in Adobe Photoshop CS with tools from Reindeer Graphics.

Statistical analysis

Data analysis using a Student's *t*-test, one-way analysis of variance with a Bonferroni correction and linear regression analysis was performed using GraphPad Prism (GraphPad Software, San Diego, CA).

Results

Naïve CD4+ T cells are the major producers of LTβ

As LTbeta has been shown *in vitro* to be critical for the maintenance of FRC networks [157, 190], we first tested which subsets of T cells are the major producers of LTbeta within secondary LTs in vivo. We found that about 60-70% of the LTbeta is produced by CD4+ T cells and it is mainly produced by CD45RA+ naïve subset (Figure 4-1), which is consistent with previous findings on LTalpha, suggesting that naïve CD4+ T cells are the key cell subset for the maintenance of FRC network [156]. However, given the fact that a minor subset of memory CD4 T cells (~1%) are also expressing CD45RA, this minor memory population might also composes as a potential minor source of lymphotoxin-beta [222].

Sparing of FRC and FDC networks in SIV-infected SM and loss of both networks with CD4+ T cell depletion

To evaluate this hypothesis, we used antibodies to desmin to label the FRC network in the TZ of LNs [120, 124], and antibodies to CD35 to label the FDC network in the B cell follicles [223]. In support of the hypothesis that CD4+ T cells are critical for the maintenance of the FRC network, we found that the FRC network was destroyed in pathogenic SIV infection of RMs, which correlates with the depletion of CD4+ T cells within LTs. Interestingly, there is a parallel depletion of the FDC network in the B cell follicles after CD4+ T cell depletion due to SIV infection, suggesting that FDC network also relies on CD4+ T cells for their maintenance. By contrast, the FRC and FDC networks were maintained in the non-pathogenic animal model of SIV-infected SMs in which CD4+ T cell counts are preserved despite the similar level of viral replication to SIV-infected RMs (Figure 4-2). To further test the hypothesis that CD4+ T cells are necessary for the maintenance of the FRC and FDC networks, we depleted CD4+ T cells in uninfected SMs and RMs with anti-CD4 antibodies, with the prediction that this would result in the loss of both networks. We had previously reported that the majority of CD4+ T cells in both peripheral blood and LTs could be depleted by repeated treatment of animals with CD4+ T cell depleting antibody, assessed by flow cytometric analysis [221], and we now show by immune-fluorescence analysis of tissue sections from these animals that 1) the CD4+ T cells in the TZ and B cell follicles are both severely depleted

(Figure 4-3A); and that 2) depletion of CD4+ T cells leads to the loss of both FDC and FRC networks and loss of IL-7 production in RMs and SMs (Figure 4-3A). In contrast to CD4+ depletion, the depletion of CD8+ T cells with CD8-depleting-antibody did not significantly affect FDC and FRC networks (Figure 4-3B), further supporting the hypothesis that the CD4+ T cell population is playing the principal role in the preservation of the FRC and FDC networks.

Consequences of loss of the FRC network for CD4+ T cell restoration and depletion of CD8+ T cells

The FRC network is critical for the maintenance of homeostasis of T cell populations by providing critical survival factors such as IL-7, so that the concomitant loss of the network and IL-7 (Figure 4-3A) should slow the restoration of CD4+ T cell populations after termination of CD4 depleting antibody treatment. We indeed found that there was no significant increase of CD4+ T cells within LTs 28 days after the last administration of CD4 depleting antibody (Figure 4-4A), and there was also little restoration of the FRC network in SMs and RMs (Figure 4-4A and B). Since IL-7 is a survival factor particularly critical for both naïve CD4+ and CD8+ T cells [93, 118-119], the loss of the FRC network and IL-7 would also be expected to be associated with depletion of CD8+ T cells through increased apoptosis. We indeed found that CD8+ T cells are also significantly depleted within LTs in both CD4+ T cell depleted RMs and SMs coincident with increased apoptosis (Figure 4-5, A and B), which was sustained to account for continued lower CD8+ T cell counts 30 days after the end of the CD4+ T cell depleting treatments (Figure 4-5B).

Depletion of CD4+ T cells and FRCs and FDCs in HIV infection and other immunodeficiency conditions

In support of the hypothesized CD4-depletion mediated mechanism of depletion of FRC and FDC networks, we found that the number of CD4+ T cells significantly correlated with the sizes of the FRC and FDC networks in HIV infection before the initiation of

anti-retroviral therapy (ART), and that the slow restoration of CD4+ T cells after initiation of ART correlated with the slow restoration of FRC and FDC networks (Figure 4-6).

Amongst the significant issues in chemotherapy and irradiation for cancer treatment are 1) severe depletion of CD4+ T cells and other lymphocytes and 2) the slow and incomplete immune reconstitution, particularly for naïve T cells after cessation of therapy [209, 224]. Since we have found that these same major impacts on T cell homeostasis in HIV infection are related to the "health" of the supportive FCR network, we tested the hypothesis that chemotherapy and irradiation lead to loss of FRC networks to thereby deplete T cells and restrict immune reconstitution after the cessation of the therapy. To test this hypothesis, we examined effects of chemoradiotherapy on depletion of FDCs and FRCs in cancer patients receiving chemoradiotherapy compared to age, gender and cancer type matched patients without chemoradiotherapy. We found that chemotherapy and irradiation depleted CD4+ T cells and diminished FRC and FDC networks in treated cancer patients compared to patients who had not been treated (Figure 4-7). These findings again strongly support the model that loss of lymphocytes, particularly CD4+ T cells, leads to LT structure damage including loss of FRC network, which in turn impairs the survival of lymphocytes and restricts their restoration.

Discussion

The depletion of naïve CD4 T has been well documented during HIV and SIV infections [46, 48, 225-228]. Studies showed that this depletion strongly correlates with the depletion of memory CD4 T cell population and disease progression [227, 229-230], increasing incidence of non-AIDS related clinical events such as cardiovascular disease, liver disease and non-AIDS-related cancer [85-88, 185, 207, 229] and increased susceptibility to bacterial infections [89]. These suggest that naïve T cells might play a critical role in the pathogenesis of HIV infection. In support of this view, it has been recently reported in a non-human primate model that naïve T cell depletion markedly impaired SIV-specific CD4+ T cell responses, SIV env-specific antibody responses, SIV-

specific CD8+ T cell responses but did not affect the homeostasis of the memory T cell population [231]. This suggests that the depletion of naïve T cell population may have a broader negative impact on the other arms of immune functions during HIV infection.

Therefore, given the importance of naïve T cells in immune defense and immuocompetency, it is extremely critical to understand the mechanisms that lead to naïve T cells depletion during HIV infection. We have previously shown that there is a vicious cycle mechanism of CD4+ T cell depletion in SIV infection of RM in which 1) collagen deposition impedes access of naïve T cells to IL-7 on the FRC network and loss of IL-7 production by loss of FRC network itself, leading to the depletion of naïve T cells through increased apoptosis; and 2) depletion of naïve T cells as the source of LTbeta on which the FRC network depends for survival, leads to loss of the network, thereby amplifying and perpetuating the cycle of depletion of both naïve T cells and stromal cells [190, 214]. Since both CD4+ and CD8+ T cells were depleted in infected RMs, we could not unequivocally identify the source (s) of LTbeta and other FRC survival factors, and therefore in the studies we now report we compared the FRC network in pathogenic and non pathogenic models of SIV infection in which CD4+ T cells are depleted or preserved, analyzed changes in the FRC network in uninfected animals depleted of CD4+ and CD8+ T cells with antibodies, and examined the general relationships between CD4+ T cells and the FRC network in HIV infection and cancer patients.

We show that 1) preservation of CD4+ T cells in SIV-infected SMs correlates with the maintenance of FRC network; 2) depletion of CD4+ T cells, but not CD8+ T cells, in uninfected SMs and RMs by antibody recapitulates the LT damage occurring in pathogenic SIV infection in RMs; and 3) CD4+ T cell depletion in HIV infection or chemotherapy and irradiation in cancer patients is associated with loss of the FRC network. Taken together, these findings support the general concept that naïve CD4+ T cell population are the source for LTbeta and other FRC survival factors that are critical for the maintenance of FRC network and the depletion of naïve CD4+ T cells thereby leads to the loss of FRC network during immunodeficiency conditions.

The link established here between CD4+ T cell depletion and damage to the LT niche clearly argues that therapeutic approaches for maintaining and restoring functional stromal cell networks should be beneficial in improving immune reconstitution. Because the CD4+ T cell depletion and damage to the stromal cell networks operate cumulatively during HIV infection, the most straightforward way to do this would be through earlier initiation of HAART to limit the depletion of both CD4+ T cells and FRC (and FDC) networks. Furthermore, these findings strongly suggest that activation of lymphotoxin-beta receptor signaling pathway might be helpful for the restoration of stromal cell network during HAART. With availability of reagents such as the soluble form of lymphotoxin-alpha1beta2 or with a specific anti- lymphotoxin-beta receptor agonistic monoclonal antibody [232], it will be worth to test if the treatment of these reagents in SIV-infected rhesus macaques could improve the restoration of LTs. Lastly, devising treatment regimens that minimize CD4 T cell loss and that preserve/restore LT structure may also help to improve immune reconstitution for other immune cell subsets, including naïve CD8 T cell populations and B cell populations. Taken together, our findings have identified a novel mechanism by which HIV infection depletes FRC and FDC networks, and pointed potential therapeutic approaches to restore the functional stromal cell networks needed for immune reconstitution.

Acknowledgements

We thank C. O'Neill and T. Leonard for help in preparing the manuscript and figures; Ann Sequin and Katelyn Hanneman for their help in organizing patient information; Dr. Stephen Schmechel and Sarah Bowell from University of Minnesota Biological Materials Procurement Network (BioNet) for their help in preparing patients' tissues; Dr. Katherine A. Staskus for her critical and thoughtful suggestions and discussion. We also thank all of the donor participants in this study. This study utilized BioNet histology and digital imaging core facilities, which are supported by NIH grants P30-CA77598 (D Yee), P50-CA101955 (D Buchsbaum) and KL2-RR033182 (B Blazar), and by the University of Minnesota Academic Health Center. This work was supported in part by a University of Minnesota Doctoral Dissertation Fellowship (M.Z.), grants from the National Institutes of

Health (R37 AI028246, R01 AI048484 and R01 AI056997) (A.T.H.), grants from Yerkes National Primate Research Center (P51 00165, R21 AI054234 and R01 HL075766) (G. S.) and in part by federal funds from the National Cancer Institute, National Institutes of Health, under Contract No. HHSN261200800001E.

Contributions: Conceived and designed the tissue analysis experiments: M.Z. and A.T.H. Performed the tissue analysis experiments: M.Z. Contributed reagents/materials/analysis tools: G.S. designed and supervised the experiments of CD4+ lymphocyte depletion in primates; M.P. contributed to the design and supervision of the CD4+ lymphocyte depletion experiments; J.C.E. conducted the experiments of CD4+ lymphcoyte depletion; T.W.S. provided the HIV infected patients tissue sample and CD4 count data. M.Z. and A.T.H. wrote the paper.

Conflict-of-Interest Disclosures: The authors declare no competing financial interests.

Correspondence: Ashley T. Haase, Department of Microbiology, University of Minnesota, Box 196, 420 Delaware Street S.E., Minneapolis, MN 55455; e-mail: haase001@umn.edu.

Figure 4-1.

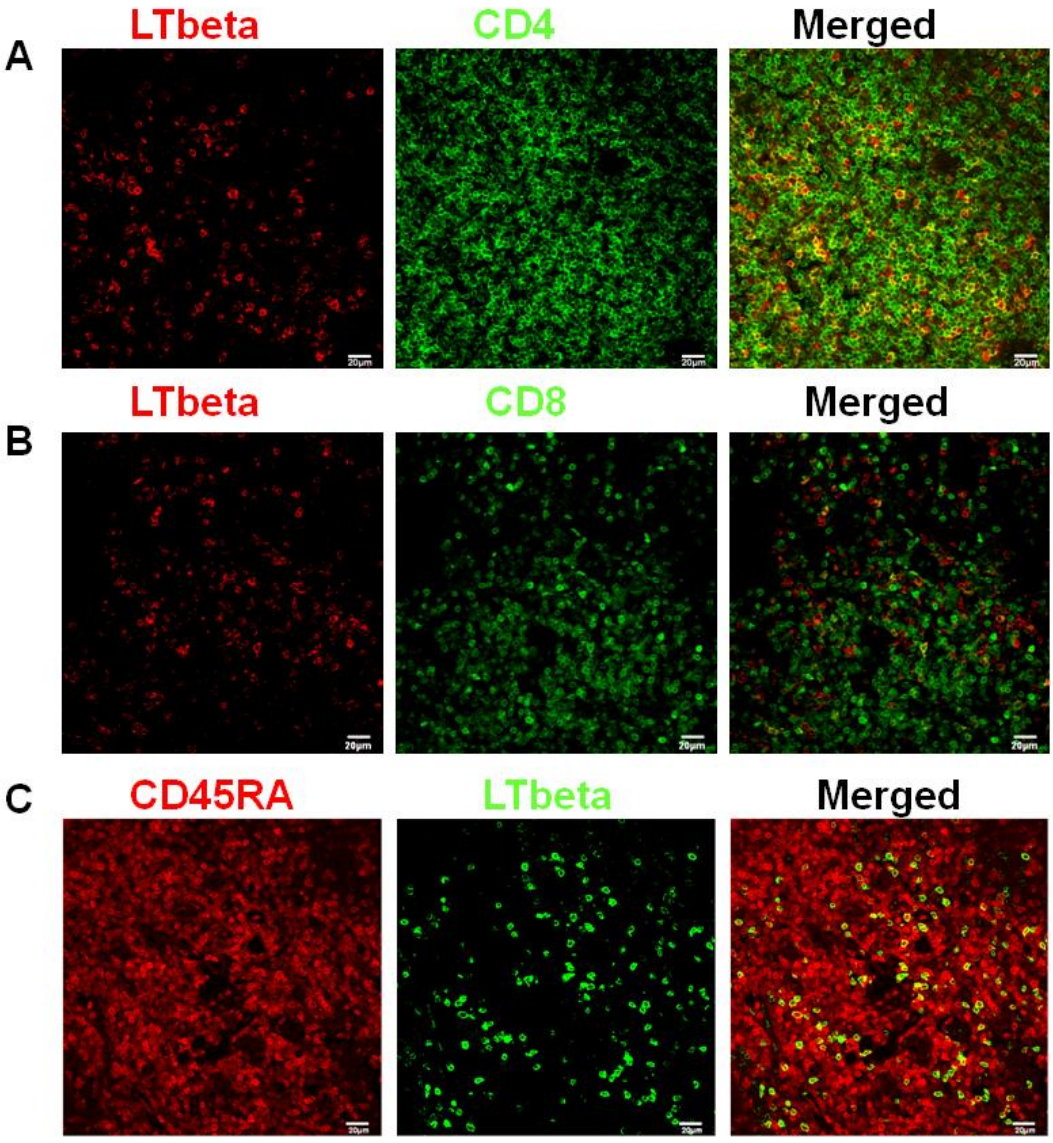
A
LTbeta
CD4
Merged
B
LTbeta
CD8
Merged
C
CD45RA
LTbeta
Merged

Figure 4-1. CD4+ T cells are the major producers of LTbeta. (A-B) Immunofluorescent staining of LTbeta (Red), CD4 or CD8 (Green) in in LNs from RMs, showing that LTbeta is mainly expressed by CD4+ T cells. (C) Immunofluorescent staining of CD45RA (Red), LTbeta (Green) in LNs from RMs, showing that LTbeta is mainly expressed by naive T cells.

Figure 4-2.

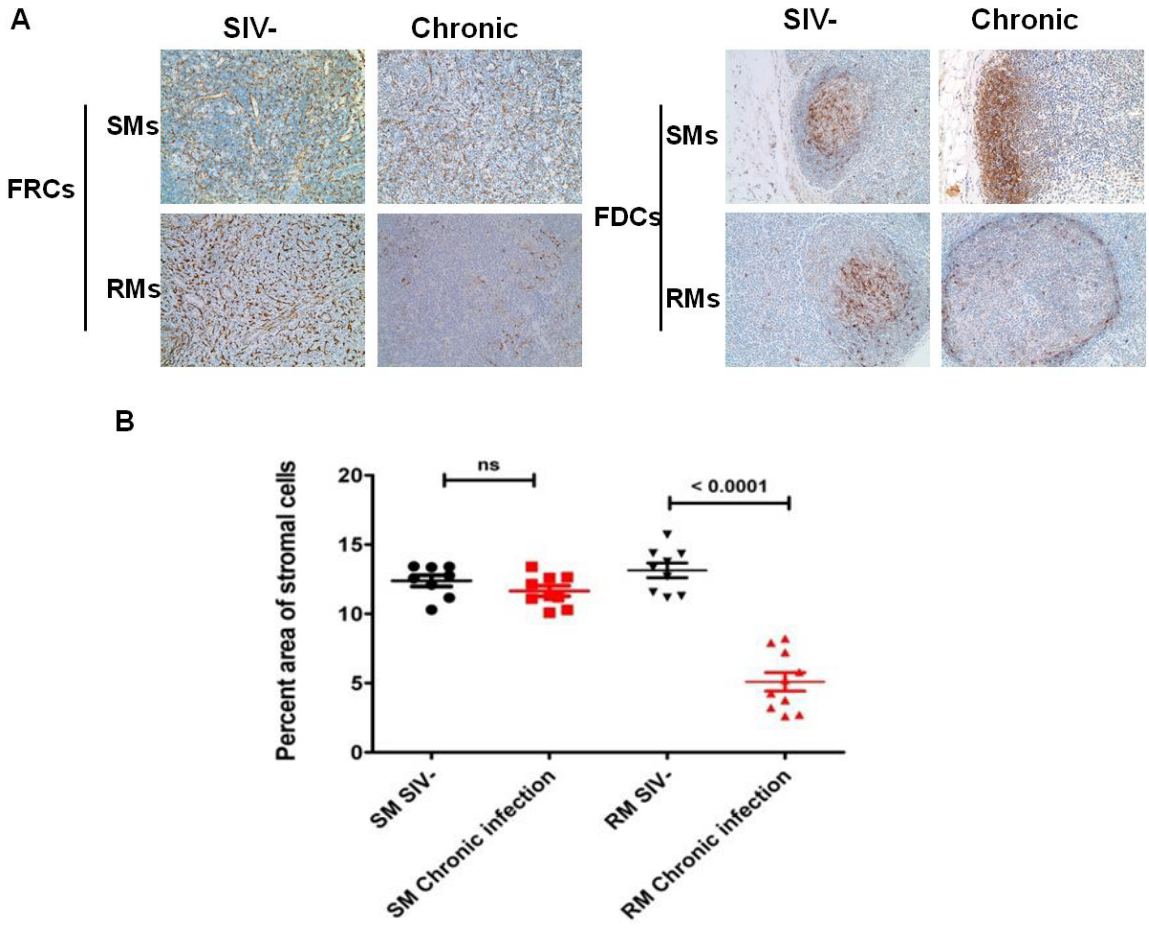
A
SIV-
Chronic
SIV-
Chronic
FRCs
SMs
RMs
FDCs
SMs
RMs
B
Percent area of stromal cells
20
15
10
5
0
ns
< 0.0001
SM SIV-
SM Chronic infection
RM SIV-
RM Chronic infection

Figure 4-2. Maintenance of FRC and FDC networks within LTs in chronically SIV infected sooty mangabeys (SMs) but not in rhesus macaques (RMs). (A) Immunohistochemical staining of desmin (left panel) and CD35 (right panel) in LNs from uninfected and chronically infected SMs and RMs, showing the intact FRC and FDC network in SMs during chronic infection compared to RMs. Original magnification x200. (B) Quantitative image analysis of the percent area of stromal cells, showing the preservation of both FDC and FRC networks in SMs but not in RMs. Bars represent the mean ± s.e.m.

Figure 4-3.

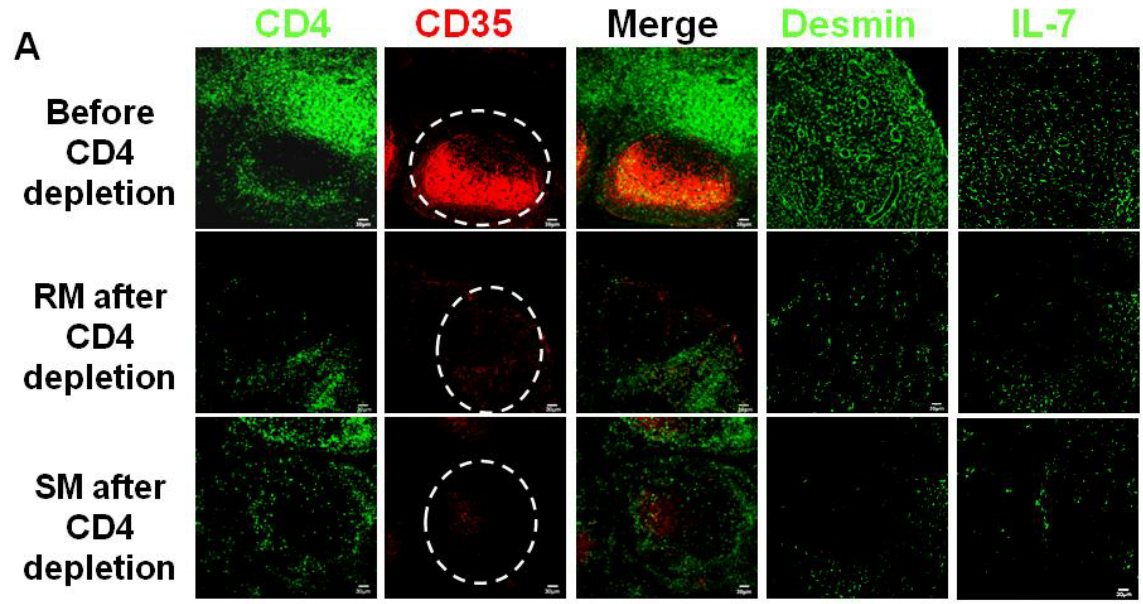
A
CD4
CD35
Merge
Desmin
IL-7
Before CD4 depletion
RM after CD4 depletion
SM after CD4 depletion

B

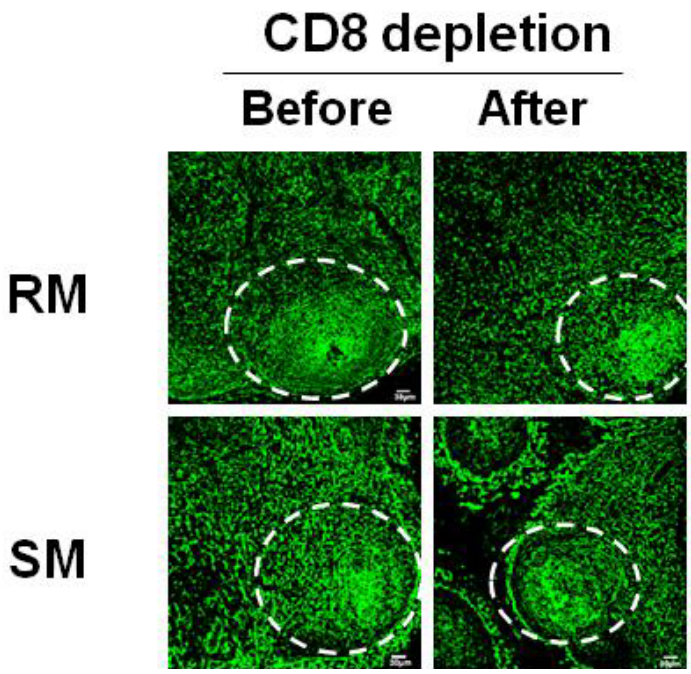
CD8 depletion
Before
After
RM
SM

Figure 4-3. Depletion of CD4+ T cells leads to depletion of both FDC and FRC networks in both RMs and SMs. (A) Immunofluorescent staining of CD4, CD35, desmin and IL-7 in LNs from RMs and SMs before and after CD4+ T cells depletion, showing that CD4+ T cell depletion leads to depletion of FRC and FDC networks and loss of IL-7 production in both SMs and RMs. Dotted circles represents the position of B cell follicles. (B) Immunofluorescent staining of desmin, a marker for both FRCs and FDCs in LNs from RMs and SMs before and after CD8+ T cell depletion, showing that the preservation of FDC and FRC networks after CD8+ T cell depletion in both RMs and SMs. Dotted circles represent the position of B cell follicles.

Figure 4-4.

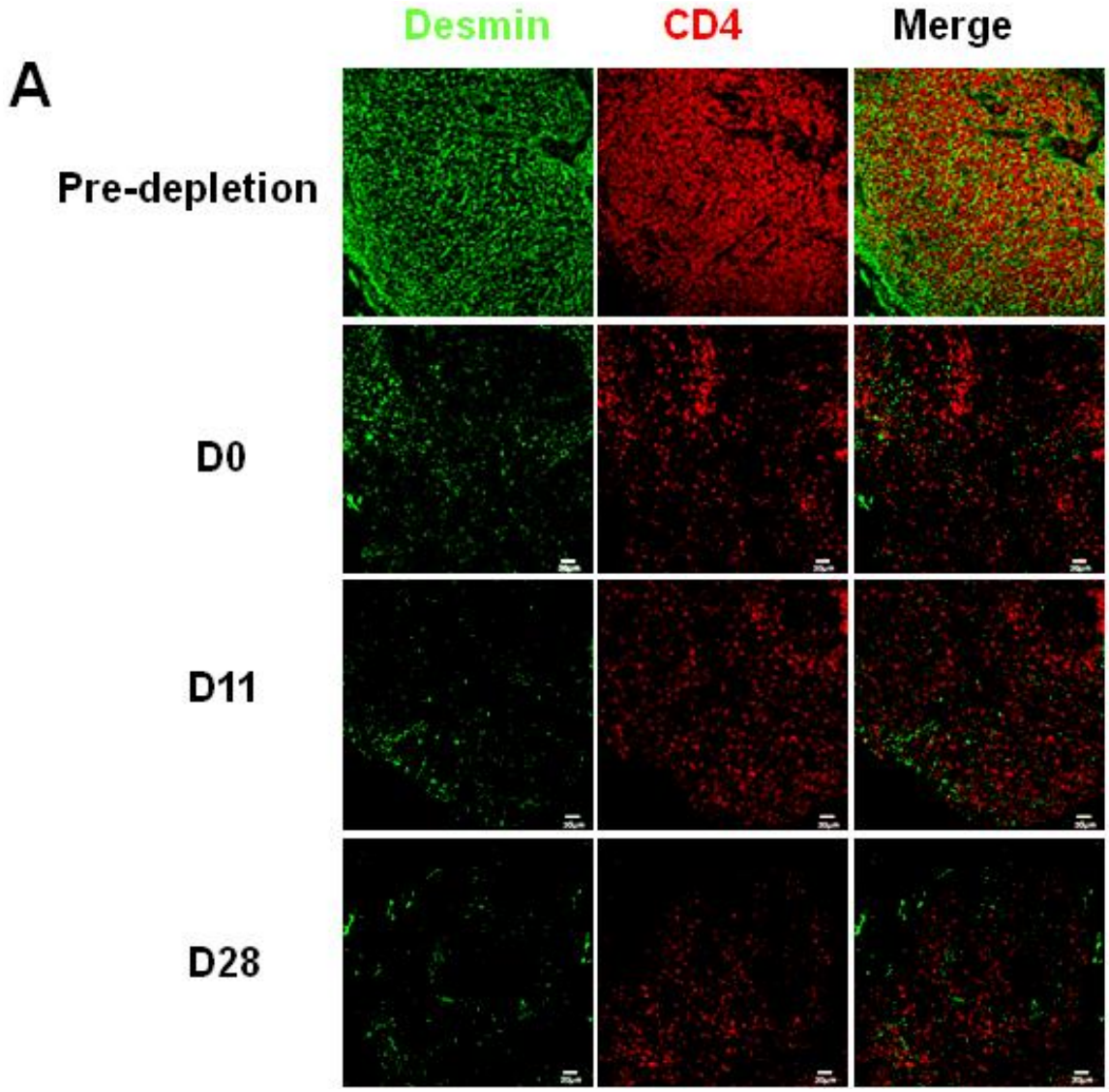

Figure 4-4. Slow restoration of CD4+ T cells correlates with slow restoration of FRC and FDC networks. (A) Immunofluorescent staining of CD4 and desmin in LNs from RMs before and at different time points after stopping CD4 depleting antibody treatment, showing that the slow restoration of CD4+ T cells after stopping antibody treatment correlates with slow restoration of FRC and FDC networks.

Figure 4-4B.

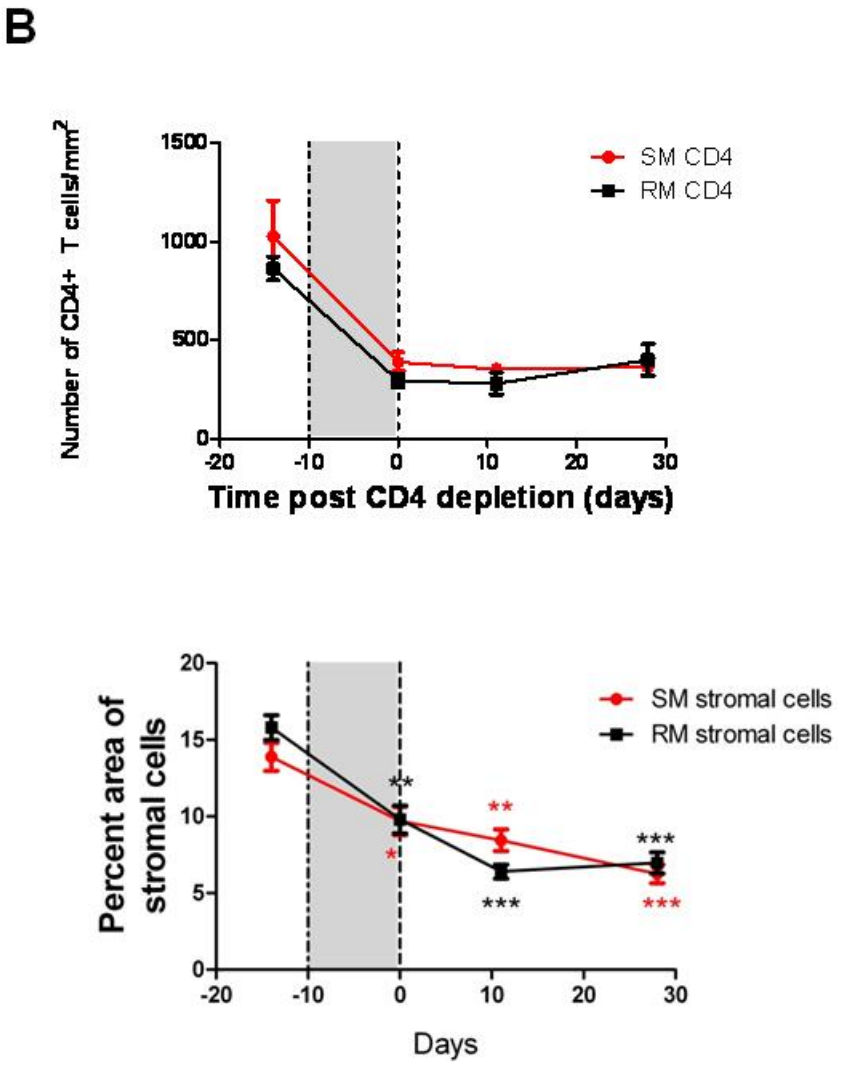
B
Number of CD4+ T cells/mm2
1500
1000
500
0
-20
-10
0
10
20
30
Time post CD4 depletion (days)
SM CD4
RM CD4
Percent area of stromal cells
20
15
10
5
0
Days
SM stromal cells
RM stromal cells
*
**
***

Figure 4-4. Slow restoration of CD4+ T cells correlates with slow restoration of FRC and FDC networks. (B) Quantitative image analysis of the number of CD4+ T cells in LNs and the percent area of stromal cells, showing the slow restoration of both CD4+ T cells and stromal cells. Bars represent the mean ± s.e.m and the dotted lines indicate the timing of anti-CD4 antibody administrations. All the comparisons are made between labeled time point and pre-depletion. Star color matches line color. **P*<0.05. ***P*<0.01. ****P*<0.001.

Figure 4-5.

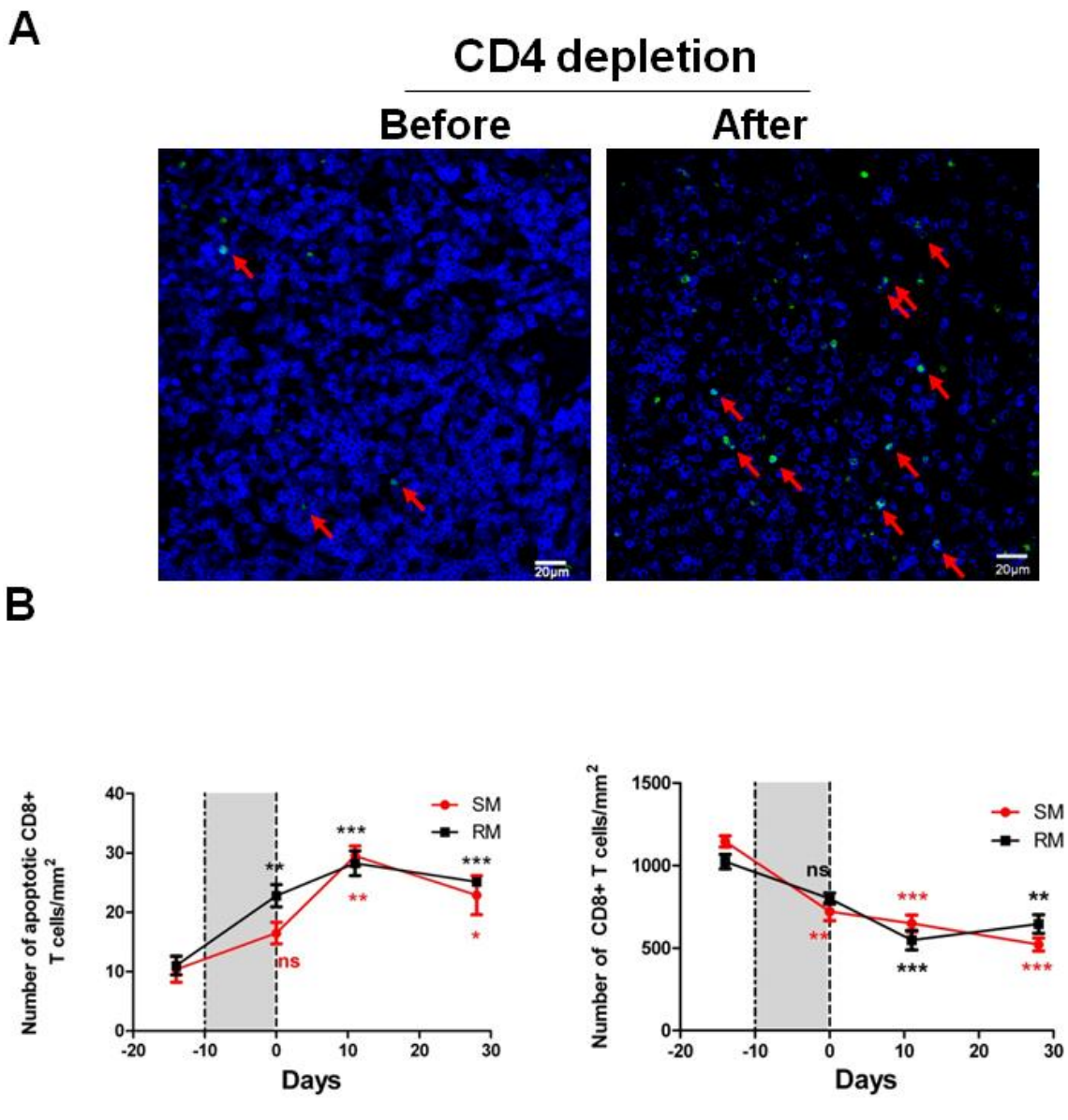
A
CD4 depletion
Before
After
20μm
20μm
B
Number of apoptotic CD8+ T cells/mm2
SM
RM
ns
Days
Number of CD8+ T cells/mm2
SM
RM
ns
Days

Figure 4-5. Depletion of both FDC and FRC networks leads to depletion of CD8+ T cells in both RMs and SMs. (A) Immunofluorescent staining of CD8 (blue) and TUNEL (green) in LNs before and after CD4+ T cells depletion, showing that apoptosis level in CD8 population within LTs is elevated after CD4+ T cell depletion, which correlates with depletion of blue staining CD8+ T cells. (B) Quantitative image analysis of the number of apoptotic CD8+ T cells (left panel) and the number of CD8+ T cells (right panel) in RMs and SMs before and after receiving CD4-depleting-antibody , showing that CD4+ T cell depletion leads to increased apoptosis in CD8+ T cell populations therefore depleting CD8+ T cells. Bars represent the mean ± s.e.m and the dotted lines indicate the timing of anti-CD4 antibody. All the comparisons are made between labeled time point and pre-depletion. Star color matches line color. ns, not significant. *P<0.05. **P<0.01. ***P<0.001.

Figure 4-6.

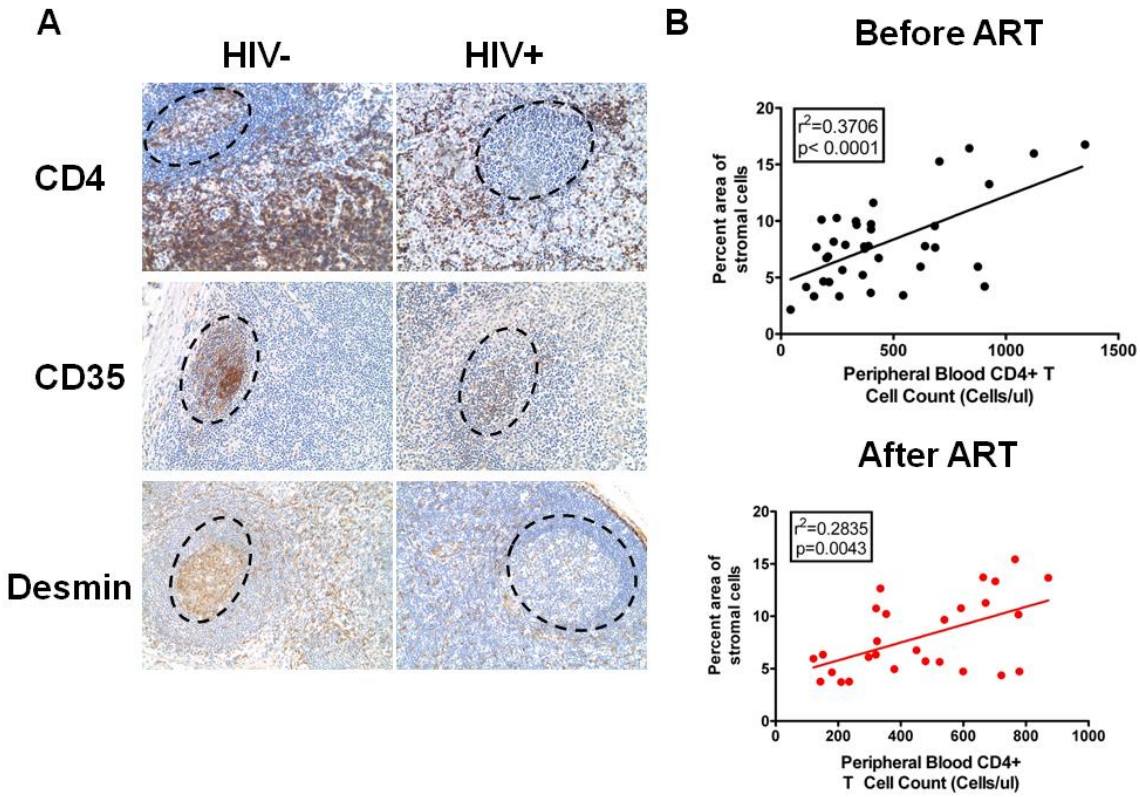
A
HIV-
HIV+
CD4
CD35
Desmin
B
Before ART
r2=0.3706
p< 0.0001
Percent area of stromal cells
Peripheral Blood CD4+ T Cell Count (Cells/ul)
After ART
r2=0.2835
p=0.0043
Percent area of stromal cells
Peripheral Blood CD4+ T Cell Count (Cells/ul)

Figure 4-6. Depletion of CD4+ T cells correlates with depletion of FRC and FDC networks in HIV infection. (A) Immunohistochemical staining of CD4, CD35 and desmin in LNs from uninfected and chronically HIV infected subjects, showing the depletion of CD4+ T cells in B cell follicles and TZ correlates with depletion of FDCs and FRCs in B cell follicles and TZ. Dotted circles represent the position of B cell follicles. Original magnification x200. (B) Correlation between the percent area of stromal cells and peripheral blood CD4+ T cell counts (cells/ul) before (upper panel) and after (lower panel) the initiation of ART.

Figure 4-7.

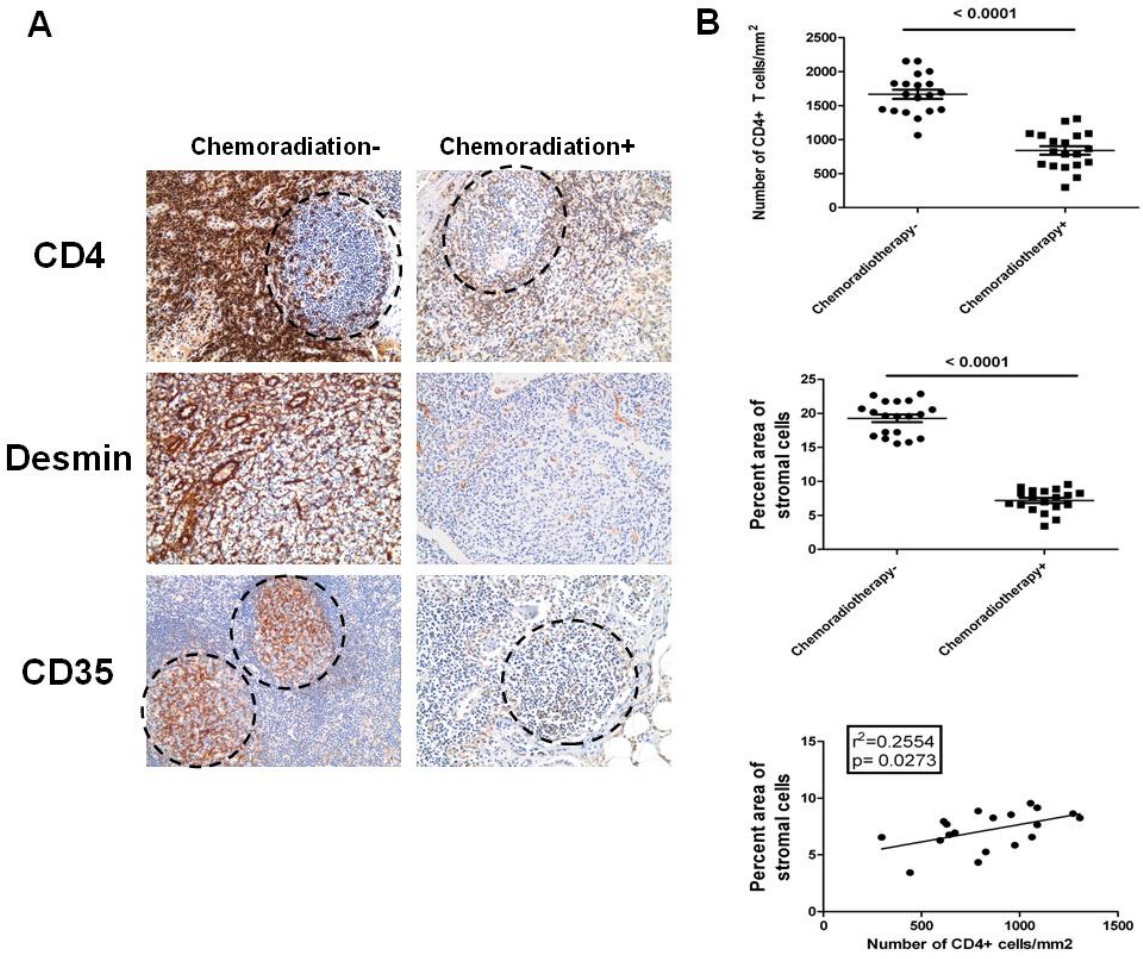
A
Chemoradiation-
Chemoradiation+
CD4
Desmin
CD35
B
< 0.0001
Number of CD4+ T cells/mm2
2500
2000
1500
1000
500
0
Chemoradiotherapy-
Chemoradiotherapy+
< 0.0001
Percent area of stromal cells
25
20
15
10
5
0
Chemoradiotherapy-
Chemoradiotherapy+
r2=0.2554
p= 0.0273
Percent area of stromal cells
15
10
5
0
0
500
1000
1500
Number of CD4+ cells/mm2

Figure 4-7. Depletion of CD4+ T cells by chemoradiotherapy leads to depletion of FRC and FDC networks in cancer patients. (A) Immunohistochemical staining of CD4, CD35 and desmin in LNs from chemoradiotherapy treated patients and untreated patients, showing the depletion of CD4+ T cells in B cell follicles and T cell zone correlates with depletion of FDCs and FRCs. Dotted circles represent the position of B cell follicles. Original magnification x200. (B) Quantitative image analysis of number of CD4+ T cells (upper panel) and amount of stromal cells (middle panel) within LNs of chemoradiotherapy treated patients and untreated patients, showing that both CD4+ T cells and stromal cells are depleted during chemoradiotherapy. The depletion of CD4+ T cells significantly correlates with the depletion of stromal cells within chemoradiotherapy treated patients.

Table 4-1 List of primary antibodies and antigen retrieval methodologies

Antibody	Clone/ Manufacturer & Catalog #	Antigen-retrieval Pretreatment	Antibody Dilution	Species
Desmin	D33 / Lab Vision & # MS-376-S1	Diva Decloaker; High pressure cooker for 30 seconds at 125°C.	1/200	Mouse
Desmin	Polyclonal / Lab Vision & # RB-9014-P1	Diva Decloaker; High pressure cooker for 30 seconds at 125°C.	1/200	Rabbit
CD35	Ber-MAC-DRC / Dako & # M0846	Diva Decloaker; High pressure cooker for 30 seconds at 125°C.	1/100	Mouse
CD21	1F8 / Dako / # M0784	Diva Decloaker; High pressure cooker for 30 seconds at 125°C.	1/100	Mouse
IL-7	7417 / R & D Systems & # MAB207	Diva Decloaker; High pressure cooker for 30 seconds at 125°C. Proteinase K treatment for 15 min	1/100	Mouse
Lymphotoxin -beta	135105 / R & D Systems & # MAB1684	Diva Decloaker; High pressure cooker for 30 seconds at 125°C.	1/100	Mouse
CD4	Polyclonal / R & D Systems &	Diva Decloaker; High pressure cooker	1/100	Goat

	# AF-379-NA	for 30 seconds at 125°C.		
CD4	1F6 / Novacastra & # NCL-CD4–1F6	Diva Decloaker; High pressure cooker for 30 seconds at 125°C.	1/100	Mouse
CD8	SP16 / Neomarkers & # RM-9116-s	Diva Decloaker; High pressure cooker for 30 seconds at 125°C.	1/100	Rabbit
Lymphotoxin -β	Polyclonal / Santa Cruz Biotech. & # sc-23561	Diva Decloaker; High pressure cooker for 30 seconds at 125°C.	1/100	Goat
In Situ Cell Death Detection Kit	Roche Applied Science Cat. No. 1 684 817			
IgG Isotype Controls	Dako, Jackson ImmunoResearch	Diva Decloaker; High pressure cooker for 30 seconds at 125°C. Protease K (10 µg/ml).	1/100	Mouse, Rabbit, Goat

Table 4-2. Demographic characteristics and clinical information of subjects

Patient ID	Disease (grade)	Chemotherapy drugs history (drug doses)	Radiation therapy dose	Time since chemo-therapy and radiation	Races	Gender	Age
Breast carcinoma-Chemotherapy group							
4915	Breast carcinoma (T2, N1/2, M0)	4 cycles of Adriamycin (105mg) + Cytoxan (1050mg)	N/A	18 weeks	Caucasian	Female	70
8871	Breast carcinoma (Grade 1)	4 cycles of Adriamycin (103 mg) + Cytoxan (1000 mg), followed by 4 cycles of Taxol (300mg) and Neulasta (6mg)	N/A	25 weeks	Caucasian	Female	49
4700	Breast carcinoma (T3, N1, M0)	4 cycles of Adriamycin + Cytoxan (performed off-site and the dosing information was	N/A	14 weeks	Unknown	Female	57

		not available)					
9942	Breast carcinoma (T4, N1c, M0)	4 cycle so fIdamycin + Cytoxan (performed off-site and the dosing information was not available)	N/A	14 weeks	Caucasian	Female	59
9576	Breast carcinoma (stage not available)	4 cycles of Fluorouracil (280 mg) + Epirubicin (140mg) + Cytoxan (920mg) + Herceptin (140mg). Followed by weekly Herceptin (140mg) + Taxol (150mg) for 12 weeks	N/A	30 weeks	Caucasian	Female	38
9493	Breast carcinoma (T2, N1, M0)	3 cycles of Taxol dose 2 (300mg) + Neulasta (6mg), followed by Adriamyacin (102mg) + Cytoxan	N/A	25 weeks	Caucasian	Female	51

		(1020mg) + Neulasta (6mg)					
1594	Breast carcinoma (T3, N3c, M0)	4 cycles of Adriamyacin and Cytoxan + Neulasta (6mg), followed one Taxol (175 mg/m^2)	N/A	16 weeks	Unknown	Female	36
7204	Breast carcinoma (T2, N0, M0)	4 cycles of Taxotere (130mg) and Cytoxan (1044mg) + Neulasta (6mg)	N/A	22 weeks	Caucasian	Female	68
4060	Breast carcinoma (T2, N1)	Femar 2.5 mg/day for 13 weeks, followed by 1 cycle of Taxotere (130mg) Cytoxan (1000mg) and 1 cycle of Nuelasta (6mg)	N/A	23 weeks	Caucasian	Female	64
3438	Breast carcinoma (T3, N1, grade 2)	4 cycles of Adriamycin Cytoxan (the dosing information was not available),	N/A	26 weeks	Caucasian	Female	42

		followed by 12 doses of weekly Paclitaxel (the dosing information was not available), followed by 1 cycle of Neulasta (6mg), followed by weekly Taxol (122mg) for 12 weeks.					
Breast carcinoma-Control group (no chemoradiotherapy before lymph node biopsy)							
4914	Breast carcinoma (T2.5, N0, M0)	N/A	N/A	N/A	Caucasian	Female	32
3873	Breast carcinoma (T2, N0, M0)	N/A	N/A	N/A	Caucasian	Female	40
9492	Breast carcinoma (pT1c, N0, M0)	N/A	N/A	N/A	Caucasian	Female	47
5333	Breast carcinoma (T1c, N0, Mx)	N/A	N/A	N/A	Caucasian	Female	76

4197	Breast carcinoma (T2, N0, M0)	N/A	N/A	N/A	Black	Female	51
4934	Breast carcinoma (T2, N0, M0)	N/A	N/A	N/A	Caucasian	Female	39
2021	Breast carcinoma (grade 1)	N/A	N/A	N/A	Caucasian	Female	62
1979	Breast carcinoma (T1c, N0, M0)	N/A	N/A	N/A	Caucasian	Female	57
1626	Breast carcinoma (pT1c, N0(i-)(sn), MX)	N/A	N/A	N/A	Caucasian	Female	42
4131	Breast carcinoma pTis, N0, MX G2)	N/A	N/A	N/A	Caucasian	Female	44
Esophageal carcinoma-Chemoradiotherapy group							
5491	Esophageal carcinoma (stage not available)	Treatment was performed off-site and the information was not available	N/A	11 weeks	Caucasian	Male	46

3445	Esophageal adeno-carcinoma (stage not available)	Cisplatin and infusional 5FU (performed off-site and the dosing information was not available)	N/A	Unknown	Unknown	Male	66
9921	Adeno-carcinoma of the gastro-esophageal junction (T3, N0, M0)	Epirubicin (50 mg/m2), Oxaliplatin (130 mg/m2) and Xeloda (625 mg/m2), followed by one cycle Neulasta (6mg)	N/A	23 weeks	Caucasian	Male	75
2670	Distal esophageal adeno-carcinoma (T3, N0, M0)	Two cycles of concurrent chemotherapy (performed off-site and the drug information was not available)	Area of tumor involve-ment and regional lymph nodes received a dose of 4500 cGy in 25 fractions using	11 weeks	Caucasian	Male	56

			a four field technique with 10 MV photons				
2409	Adeno-carcinoma of the gastro-esophageal junction (T3, N1-2)	4 cycles of cisplatin (75mg/m2), 5-FU (2300mg/day)	25 fractions1.8 Gy to gastro-esophageal junction, regional lymph nodes and margin. 50.4 Gy total dose to primary site	27 weeks	Caucasian	Male	40
7852	Esophageal carcinoma (stage not available)	3 cycles carboplatin, taxol and 5-FU, followed by concurrent	Dosing information was not availab	Unknown	Caucasian	Male	51

		cisplatin and 5-FU (performed off-site and the dosing information was not available)	le				
5595	Esophageal carcinoma (stage not available)	Treatment was performed off-site and the information was not available	Dosing information was not available	22 weeks	Caucasian	Male	59
2341	Esophageal adeno-carcinoma (T3, N1, MX)	2 cycles of Cisplatin (75 mg/m2), 5-FU (100mg/m2)	Dosing information was not available	26 weeks	Caucasian	Male	78
7932	Esophageal adeno-carcinoma (T3, N1, M0)	3 cycles of Carboplatin (658 mg), Taxol (125mg)	Radiation 25 fractions with dose of 45 Gy	31 weeks	Caucasian	Male	54
Esophageal carcinoma-Control group (no chemoradiotherapy before lymph node biopsy)							
6669	Moderately differentiated adeno-carcinoma. (T1, N0)	N/A	N/A	N/A	Caucasian	Male	55

4818	Esophageal leiomyoma (T3, N0)	N/A	N/A	N/A	Caucasian	Male	48
4917	Adeno-carcinoma, moderately to poorly differentiated (T2, N0)	N/A	N/A	N/A	Caucasian	Male	75
4307	Adeno-carcinoma, poorly differentiated, with papillary and clear cell features (T2, N0)	N/A	N/A	N/A	Caucasian	Female	78
5924	Adeno-carcinoma, poorly differentiated (stage not available)	N/A	N/A	N/A	Caucasian	Female	44
3159	Moderately differentiated adeno-	N/A	N/A	N/A	Caucasian	Male	57

	carcinoma (T1, N0)						
6067	Moderately to poorly differentiated adeno-carcinoma (stage not available)	N/A	N/A	N/A	Not available	Female	67
4602	Multifocal high-grade dysplasia (stage not available)	N/A	N/A	N/A	Caucasian	Male	51
6669	Moderately differentiated adeno-carcinoma. (T1, N0)	N/A	N/A	N/A	Caucasian	Male	55

Note: If the patients also had radiation therapy, the lymph node biopsy is included in the radiation field.

Text in this chapter extracted from paper originally published by Trends in Immunology. Volume 33, Issue 6, June 2012, Pages 306–314

Chapter 5 Medical Implications and Future Directions

Introduction

Despite the potent suppression of viral replication by HAART, limited immune reconstitution represents an important clinical issue.. Here we show that LT damage plays an important role in depletion of naïve T cells and limited immune reconstitution after HAART.

Naïve T cells need to physically interact with the FRC network to access to survival factors such as IL-7 presented by the FRC network [93, 124, 190]. Conversely, the FRC network must also physically interact with T cells to receive lymphotoxin signals from CD4+ T cells to activate the lymphotoxin beta (LTβ) receptor-mediated signaling required to maintain the FRC network (Chapter 4) [156-157, 190, 233]. These interdependencies between the FRC network and CD4+ T cells set in motion a vicious cycle in HIV/SIV infection:, TGF-β1+ regulatory T cells stimulate collagen deposition within LTs (Chapter 2); collagen deposition in the T- cell zone (TZ) disrupts FRC network and limits T cells' access to IL-7, leading to increased apoptosis of T cells, particularly naïve T cells (Chapter 2 and 3); this leads to depletion of LTβ+ T cells that in turn, deprives the FRC network of LTβ+ on which the network depends. This, along with the collagen-restricted access of LTβ+ T cells to the FRC network (Chapter 3 and 4), results in loss of the FRC network and further decreases in IL-7 availability for T cells. Thus, a positive loop mechanism is established that progressively and cumulatively causes T cell depletion, particularly in the naïve T cell populations and FRC network (Figure 5-1).

Implications of the LT damage vicious circle model for improving immune reconstitution

This model suggests that the most straightforward way to improve immune reconstitution is by initiating HAART in early infection. In fact, early treatment does correlate with better restoration of naïve T cell populations and lower morbidity and mortality [74, 214, 234-235].

This model also suggests the potential benefit of IL-7 as an adjunctive treatment in HIV infection. Indeed, studies have shown that complementing HAART with IL-7 during both SIV and HIV infection significantly increases naïve CD4+ T cell numbers [174, 176]. Furthermore, *ex vivo* and *in vivo* studies with T cells from HIV infected patients showed that IL-7 treatment could significantly up-regulate Bcl-2 levels to lessen the extent of apoptosis in CD4+ and CD8+ T cells from HIV-infected individuals [177-178]. These data consistently suggest that insufficient IL-7 is a key contributor in the impaired T cell homeostasis in SIV/HIV infection. However, the immediate decline of the absolute numbers of both naïve CD4+ and CD8+ T cells after termination of IL-7 therapy [174, 176] suggests that complementing IL-7 only provides transient survival benefit for naïve CD4+ and CD8+ T cells and strongly argues for the development of therapeutic interventions to inhibit fibrosis thereby restoring a functional FRC network to provide long-term survival benefit for naïve T cells.

There are several therapeutic targets that could be exploited in an effort to prevent or reduce fibrosis to preserve or restore the integrity of the FRC network during HIV infection. It has been shown that therapeutic interventions directed at the TGFβ signaling pathway could potentially avert or moderate this pathological process. Agents that can interfere or block the TGFβ pathway in animal models of fibrosis have been shown to be able to successfully prevent the development of fibrosis in various tissues or organs. TGFβ itself can be blocked by decorin, an endogenous glycoprotein capable of inactivating TGFβ by preventing access to its receptor [236]. The latent activation of TGFβ can be blocked by antibodies against the alphavbeta6 integrin, which is critical for the activation of TGFβ [237]. TGFβ signal transduction can be prevented by Imatinib mesylate and related tyrosine kinase inhibitors [238-239]. We recently identified that an

anti-fibrotic drugs called pirfenidone, which is currently in a phase II clinical trial in the treatment of pulmonary fibrosis (See: http://clinicaltrials.gov/ct2/show/NCT00080223), can potently block the TGFβ signaling pathway in an *ex vivo* model (Figure 2-15 and 2-18). Our preliminary data in SIV infected RMs showed that treatment by pirfenidone can indeed preserve LT FRC network (Figure 5-2) and correlates with better CD4 reconstitution (Estes J. et al. manuscript submitted). Another important parameter that has been shown to determine the amount of collagen is the degradation of collagen determined by matrix metalloproteases (MMPs) and their inhibitor tissue Inhibitor of metalloproteinases (TIMPs), which has been shown to be also dysregulated during HIV infection [48] and may also contribute to collagen deposition during HIV infection [76-79]. Therefore, exploring strategies to restore the balance between MMPs and TIMPs may also help to remove the collagen deposition within LTs during HIV infection [76-79].

Besides inhibition of fibrosis, another key therapeutic target is the disrupted FRC network. It has been shown that accumulation of CD4+CD3- lymphoid tissue inducer (LTi) cells in secondary LTs helps restore the FRC network after virus-mediated FRC network damage [240]. We have tested whether the LTi cells can help restore damaged LT structure in an *ex vivo* co-culture system. We found that the co-culture of autologous CD4+CD3- LTi cells and LT pieces helps restore FRC and FDC networks. This rescuing impact is dependent on the LTβ expressed by CD4+CD3- LTi cells and the physical interactions between CD4+CD3- LTi cells and LT stroma as LTβ blocking antibody or physical isolation of CD4+CD3- LTi cells from LT pieces by transwell can abolish this rescuing impact (Figure 5-3). This preliminary study suggests that CD4+CD3- LTi have a strong capability in re-initiating the generation of the FRC network. Therefore it would be worthwhile to explore whether this population of LTi cells could additionally restore the stromal cell network in SIV infected RMs model.

Concluding remarks

The LT niche is critical for the homeostasis of naïve T cell population and damage to the niche contributes to the loss of naïve T cell during HIV infection and limits immune reconstitution after initiation of HAART. Thus, therapeutic interventions targeting these damaged niches could facilitate the restoration of HIV infected patients' immune systems. Further elucidation of the molecular mechanisms underlying the finely regulated pathways involved in collagen formation, deposition, and degradation and the understanding of the molecular and cellular mechanisms that dictate the differentiation of FRC network will be crucial for developing potential LT structure-based therapies to improve immune reconstitution for HIV infected patients. Furthermore, the understanding of the impact LT damage on host immune function will provide more insights into the role of these pathological processes in the pathogenesis of HIV infection.

Figure 5-1:

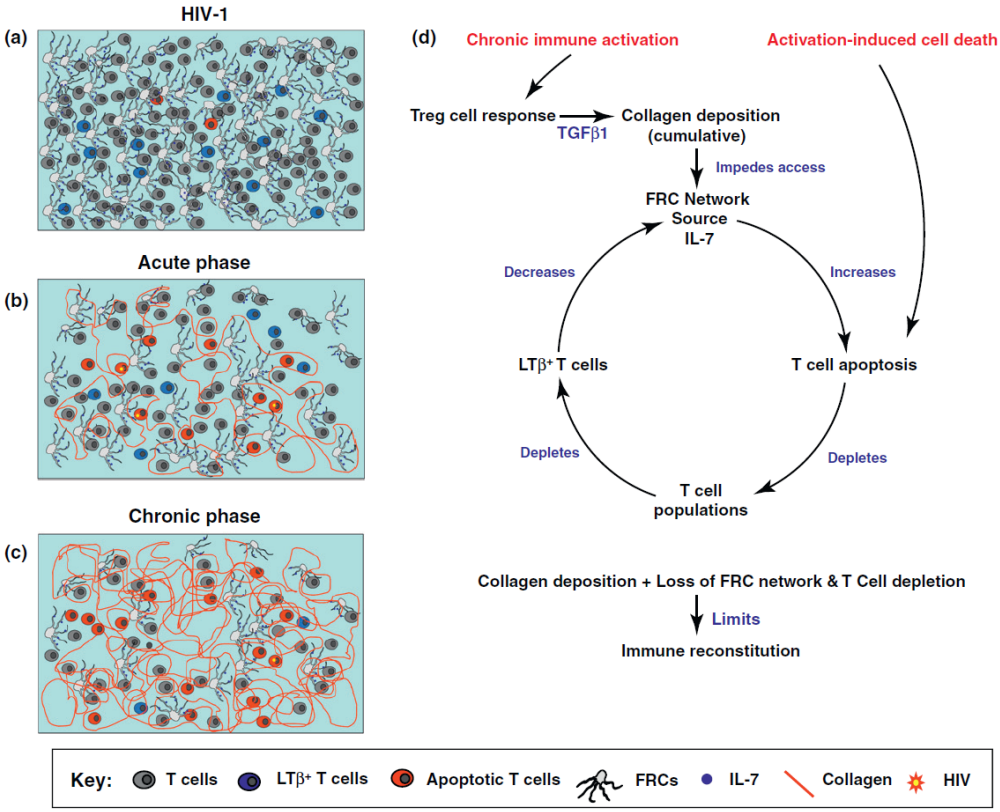
HIV-1
(a)
Acute phase
(b)
Chronic phase
(c)
(d)
Chronic immune activation
Activation-induced cell death
Treg cell response
TGFβ1
Collagen deposition
(cumulative)
Impedes access
FRC Network
Source
IL-7
Decreases
Increases
LTβ+ T cells
T cell apoptosis
Depletes
Depletes
T cell
populations
Collagen deposition + Loss of FRC network & T Cell depletion
Limits
Immune reconstitution
Key:
T cells
LTβ+ T cells
Apoptotic T cells
FRCs
IL-7
Collagen
HIV

Figure 5-1. Collagen deposition and damage to the FRC network in HIV infection. (a) In the TZ of LN, naïve T cell survival depends on interacting with IL-7 produced and "posted" on the surface of FRC network. (b) During the acute phase of HIV infections, T cells are depleted due to direct viral killing and other mechanisms such as activation induced cell death (AICD). But immune activation also elicits a T regulatory response that activates TGFβ signaling in fibroblasts resulting in cumulative collagen deposition. Collagen deposition disrupts the FRC network and impedes access of T cells to the survival factor IL-7 on the FRC network, thereby causing increased apoptosis in naïve T cell populations, which, along with AICD, depletes T cells. (c) As infection progresses, depletion of T cells decreases LTβ, which, compounded by collagen-impeded access to LTβ for FRC network, results in further loss of FRC network and IL-7. Loss of the FCR network leads to further T cell depletion, particularly in the naïve T cell populations. (d) This vicious cycle of survival interdependencies and collagen deposition cause progressive T cell depletion, particularly in the naïve T cell populations during the course of infection. (e) HAART can suppress the loss of CD4+ T cells due to the direct effects of infection and normalize immune activation to reduce losses of CD4+ T cells due to AICD. However, pre-existing collagen deposition, loss of FRC network and T cell depletion will limit immune reconstitution by the continued cyclical mechanisms shown in (d). Reproduced by permission from Trends in Immunology.

Figure 5-2:

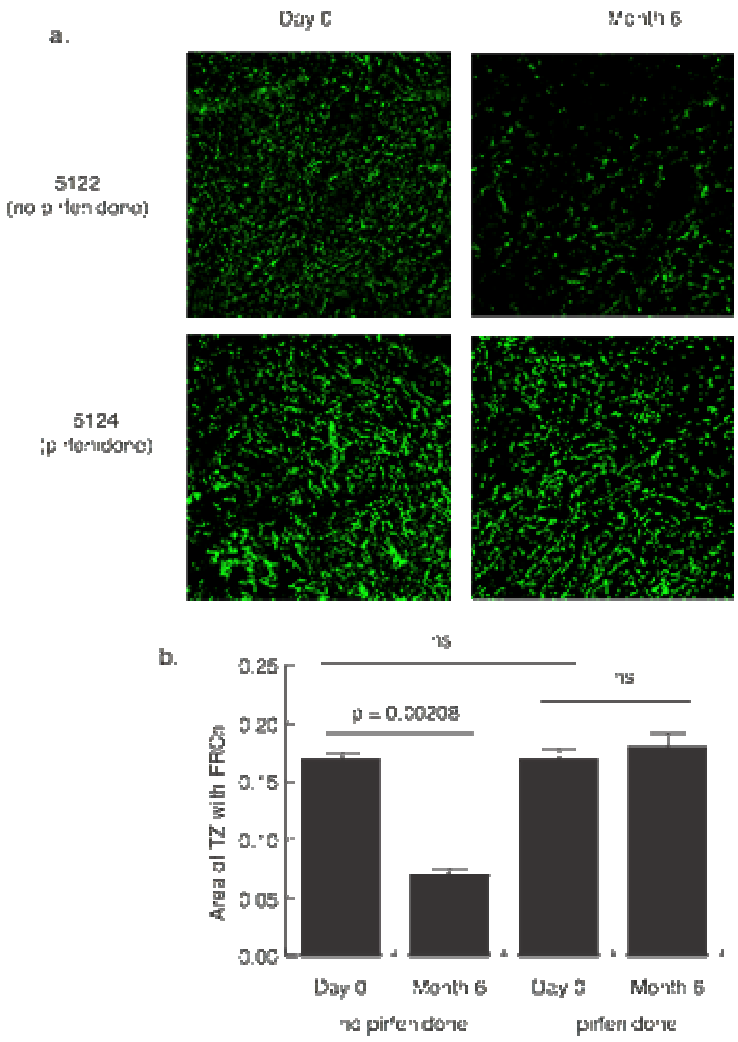

Figure 5-2. Preservation of the FRC network with pirfenidone treatment. (a) Representative image of LN sections stained with anti-desmin antibody. These images are from RM that received pirfenidone and an RM that did not. (b) Quantitative amount of FRCs in perfenidone-treated RMs and control RMs showing pirfenidone treatment helps to preserve FRC network..

Figure 5-3:

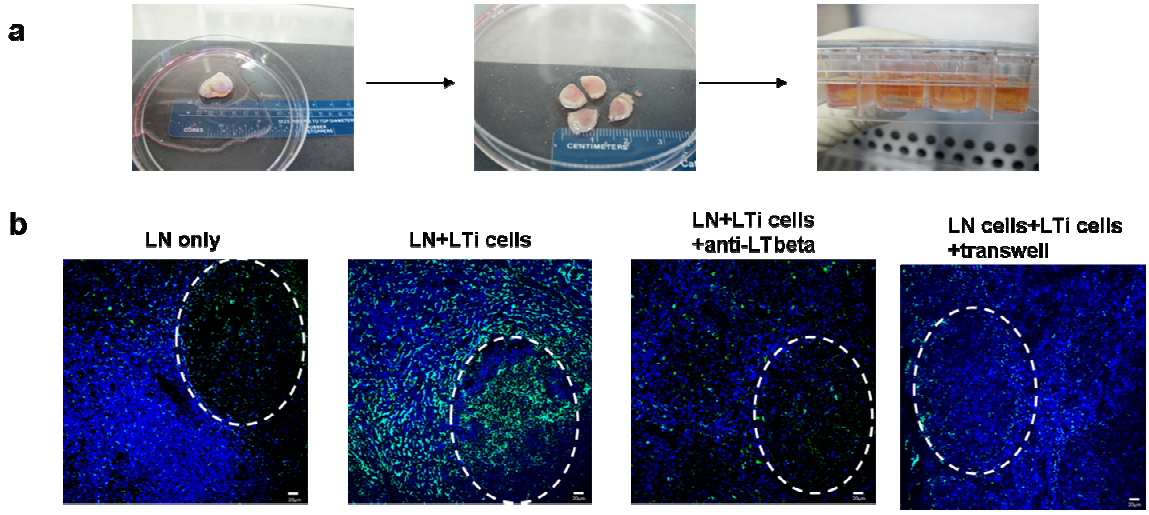
a
b
LN only
LN+LTi cells
LN+LTi cells
+anti-LTbeta
LN cells+LTi cells
+transwell

Figure 5-3. LTi cells partially rescue the damaged FRC and FDC networks. (a) Experimental design of ex vivo co-culture of LTi cells with damaged LNs taken from chronically SIV infected RMs. (b) Immunofluorescent staining of desmin (green) and CD3 (blue) in LNs from chronically SIV infected RMs, showing LTi cells can partially rescue the depleted FDC and FRC networks in B-cell follicles and TZ (second panel compared to first panel). This rescue is dependent on LT beta and contact as blocking LTβ signaling pathway by anti- LTβ antibody or isolating from LTi cells from LN by transwell diminishes the rescuing effect. Dotted circles represent the position of B cell follicles.

Bibliography

1 Barre-Sinoussi, F.*, et al.* (1983) Isolation of a T-lymphotropic retrovirus from a patient at risk for acquired immune deficiency syndrome (AIDS). *Science* 220, 868-871
2 Gallo, R.C.*, et al.* (1983) Isolation of human T-cell leukemia virus in acquired immune deficiency syndrome (AIDS). *Science* 220, 865-867
3 Abdool Karim, S.S.*, et al.* (2007) Global epidemiology of HIV-AIDS. *Infect Dis Clin North Am* 21, 1-17, vii
4 UNAIDS. 2009 AIDS Epidemic update. Geneva (Switzerland): Joint United Nations Programme on HIV/AIDS, D.A.a.h.w.u.o.e.m.u.c.d.
5 (2006) The devastating effects of HIV/AIDS on children. *Lancet* 368, 424
6 Piatak, M., Jr.*, et al.* (1993) Determination of plasma viral load in HIV-1 infection by quantitative competitive polymerase chain reaction. *AIDS* 7 Suppl 2, S65-71
7 Piatak, M., Jr.*, et al.* (1993) High levels of HIV-1 in plasma during all stages of infection determined by competitive PCR. *Science* 259, 1749-1754
8 Little, S.J.*, et al.* (1999) Viral dynamics of acute HIV-1 infection. *J Exp Med* 190, 841-850
9 Fiebig, E.W.*, et al.* (2003) Dynamics of HIV viremia and antibody seroconversion in plasma donors: implications for diagnosis and staging of primary HIV infection. *AIDS* 17, 1871-1879
10 Mellors, J.W.*, et al.* (1996) Prognosis in HIV-1 infection predicted by the quantity of virus in plasma. *Science* 272, 1167-1170
11 Kahn, J.O. and Walker, B.D. (1998) Acute human immunodeficiency virus type 1 infection. *N Engl J Med* 339, 33-39
12 Holmes, C.B.*, et al.* (2003) Review of human immunodeficiency virus type 1-related opportunistic infections in sub-Saharan Africa. *Clin Infect Dis* 36, 652-662
13 Powderly, W.G. and Mayer, K.H. (2003) Centers for Disease Control and Prevention revised guidelines for human immunodeficiency virus (HIV) counseling, testing, and referral: targeting HIV specialists. *Clin Infect Dis* 37, 813-819
14 Guss, D.A. (1994) The acquired immune deficiency syndrome: an overview for the emergency physician, Part 2. *J Emerg Med* 12, 491-497
15 Guss, D.A. (1994) The acquired immune deficiency syndrome: an overview for the emergency physician, Part 1. *J Emerg Med* 12, 375-384
16 Weiss, R.A. (1996) Retrovirus classification and cell interactions. *J Antimicrob Chemother* 37 Suppl B, 1-11
17 Weiss, R.A. (1993) How does HIV cause AIDS? *Science* 260, 1273-1279
18 Levy, J.A. (1993) HIV pathogenesis and long-term survival. *AIDS* 7, 1401-1410
19 JM Coffin, S.H., HE Varmus (Eds.), Retroviruses, Cold Spring Harbor Laboratory Press, Plainview, NY, USA (1997)
20 Chan, D.C. and Kim, P.S. (1998) HIV entry and its inhibition. *Cell* 93, 681-684
21 Wyatt, R. and Sodroski, J. (1998) The HIV-1 envelope glycoproteins: fusogens, antigens, and immunogens. *Science* 280, 1884-1888
22 Zheng, Y.H.*, et al.* (2005) Newly identified host factors modulate HIV replication. *Immunol Lett* 97, 225-234

23 Delelis, O., *et al.* (2008) Integrase and integration: biochemical activities of HIV-1 integrase. *Retrovirology* 5, 114
24 Hiscott, J., *et al.* (2001) Hostile takeovers: viral appropriation of the NF-kappaB pathway. *J Clin Invest* 107, 143-151
25 Zhu, T., *et al.* (1993) Genotypic and phenotypic characterization of HIV-1 patients with primary infection. *Science* 261, 1179-1181
26 Gelderblom, H. R (1997). "Fine structure of HIV and SIV". In Los Alamos National Laboratory (ed.). HIV Sequence Compendium. Los Alamos, New Mexico: Los Alamos National Laboratory. pp. 31–44
27 Gheysen, D., *et al.* (1989) Assembly and release of HIV-1 precursor Pr55gag virus-like particles from recombinant baculovirus-infected insect cells. *Cell* 59, 103-112
28 Ivanchenko, S., *et al.* (2009) Dynamics of HIV-1 assembly and release. *PLoS Pathog* 5, e1000652
29 Adamson, C.S. and Freed, E.O. (2007) Human immunodeficiency virus type 1 assembly, release, and maturation. *Adv Pharmacol* 55, 347-387
30 Lazzarin, A., *et al.* (2003) Efficacy of enfuvirtide in patients infected with drug-resistant HIV-1 in Europe and Australia. *N Engl J Med* 348, 2186-2195
31 Lalezari, J.P., *et al.* (2003) Enfuvirtide, an HIV-1 fusion inhibitor, for drug-resistant HIV infection in North and South America. *N Engl J Med* 348, 2175-2185
32 Dybul, M., *et al.* (2002) Guidelines for using antiretroviral agents among HIV-infected adults and adolescents. Recommendations of the Panel on Clinical Practices for Treatment of HIV. *MMWR Recomm Rep* 51, 1-55
33 Guidelines for the use of antiretroviral agents in HIV-1-infected adults and adolescents. United States Department of Health and Human Services. p. i. http://www.aidsinfo.nih.gov/ContentFiles/AdultandAdolescentGL.pdf. Retrieved 2010-10-12.
34 Palella, F.J., Jr., *et al.* (1998) Declining morbidity and mortality among patients with advanced human immunodeficiency virus infection. HIV Outpatient Study Investigators. *N Engl J Med* 338, 853-860
35 Simon, V., *et al.* (2006) HIV/AIDS epidemiology, pathogenesis, prevention, and treatment. *Lancet* 368, 489-504
36 Mocroft, A., *et al.* (1998) Changing patterns of mortality across Europe in patients infected with HIV-1. EuroSIDA Study Group. *Lancet* 352, 1725-1730
37 Hogg, R.S., *et al.* (1998) Improved survival among HIV-infected individuals following initiation of antiretroviral therapy. *JAMA* 279, 450-454
38 Walensky, R.P., *et al.* (2006) The survival benefits of AIDS treatment in the United States. *J Infect Dis* 194, 11-19
39 Mocroft, A., *et al.* (2003) Decline in the AIDS and death rates in the EuroSIDA study: an observational study. *Lancet* 362, 22-29
40 Robbins, G.K., *et al.* (2009) Incomplete reconstitution of T cell subsets on combination antiretroviral therapy in the AIDS Clinical Trials Group protocol 384. *Clin Infect Dis* 48, 350-361
41 Valdez, H. (2002) Immune restoration after treatment of HIV-1 infection with highly active antiretroviral therapy (HAART). *AIDS Rev* 4, 157-164

42 Valdez, H.*, et al.* (2002) Limited immune restoration after 3 years' suppression of HIV-1 replication in patients with moderately advanced disease. *AIDS* 16, 1859-1866
43 Florence, E.*, et al.* (2003) Factors associated with a reduced CD4 lymphocyte count response to HAART despite full viral suppression in the EuroSIDA study. *HIV Med* 4, 255-262
44 Moore, R.D. and Keruly, J.C. (2007) CD4+ cell count 6 years after commencement of highly active antiretroviral therapy in persons with sustained virologic suppression. *Clin Infect Dis* 44, 441-446
45 Kelley, C.F.*, et al.* (2009) Incomplete peripheral CD4+ cell count restoration in HIV-infected patients receiving long-term antiretroviral treatment. *Clin Infect Dis* 48, 787-794
46 Roederer, M.*, et al.* (1995) CD8 naive T cell counts decrease progressively in HIV-infected adults. *J Clin Invest* 95, 2061-2066
47 Roederer, M.*, et al.* (1997) HIV does not replicate in naive CD4 T cells stimulated with CD3/CD28. *J Clin Invest* 99, 1555-1564
48 Zhang, Z.Q.*, et al.* (1998) Kinetics of CD4+ T cell repopulation of lymphoid tissues after treatment of HIV-1 infection. *Proc Natl Acad Sci U S A* 95, 1154-1159
49 Giorgi, J.V.*, et al.* (1999) Shorter survival in advanced human immunodeficiency virus type 1 infection is more closely associated with T lymphocyte activation than with plasma virus burden or virus chemokine coreceptor usage. *J Infect Dis* 179, 859-870
50 Douek, D.C.*, et al.* (2009) Emerging concepts in the immunopathogenesis of AIDS. *Annu Rev Med* 60, 471-484
51 Brenchley, J.M.*, et al.* (2006) Microbial translocation is a cause of systemic immune activation in chronic HIV infection. *Nat Med* 12, 1365-1371
52 Raffatellu, M.*, et al.* (2008) Simian immunodeficiency virus-induced mucosal interleukin-17 deficiency promotes Salmonella dissemination from the gut. *Nat Med* 14, 421-428
53 Estes, J.D.*, et al.* (2010) Damaged intestinal epithelial integrity linked to microbial translocation in pathogenic simian immunodeficiency virus infections. *PLoS Pathog* 6, e1001052
54 Racz, P. (1988) Molecular, biologic, immunohistochemical, and ultrastructural aspects of lymphatic spread of the human immunodeficiency virus. *Lymphology* 21, 28-35
55 Fauci, A.S.*, et al.* (2005) NK cells in HIV infection: paradigm for protection or targets for ambush. *Nat Rev Immunol* 5, 835-843
56 Moir, S. and Fauci, A.S. (2009) B cells in HIV infection and disease. *Nat Rev Immunol* 9, 235-245
57 Hellerstein, M.K. and McCune, J.M. (1997) T cell turnover in HIV-1 disease. *Immunity* 7, 583-589
58 Day, C.L.*, et al.* (2006) PD-1 expression on HIV-specific T cells is associated with T-cell exhaustion and disease progression. *Nature* 443, 350-354
59 Petrovas, C.*, et al.* (2006) PD-1 is a regulator of virus-specific CD8+ T cell survival in HIV infection. *J Exp Med* 203, 2281-2292

60 Trautmann, L.*, et al.* (2006) Upregulation of PD-1 expression on HIV-specific CD8+ T cells leads to reversible immune dysfunction. *Nat Med* 12, 1198-1202
61 Gougeon, M.L. and Piacentini, M. (2009) New insights on the role of apoptosis and autophagy in HIV pathogenesis. *Apoptosis* 14, 501-508
62 Bower, M.*, et al.* (2006) AIDS-related malignancies: changing epidemiology and the impact of highly active antiretroviral therapy. *Curr Opin Infect Dis* 19, 14-19
63 Douek, D.C.*, et al.* (2003) T cell dynamics in HIV-1 infection. *Annu Rev Immunol* 21, 265-304
64 Grossman, Z.*, et al.* (1998) Multiple modes of cellular activation and virus transmission in HIV infection: a role for chronically and latently infected cells in sustaining viral replication. *Proc Natl Acad Sci U S A* 95, 6314-6319
65 Silvestri, G.*, et al.* (2003) Nonpathogenic SIV infection of sooty mangabeys is characterized by limited bystander immunopathology despite chronic high-level viremia. *Immunity* 18, 441-452
66 Bosinger, S.E.*, et al.* (2009) Global genomic analysis reveals rapid control of a robust innate response in SIV-infected sooty mangabeys. *J Clin Invest* 119, 3556-3572
67 Paiardini, M.*, et al.* (2009) Lessons learned from the natural hosts of HIV-related viruses. *Annu Rev Med* 60, 485-495
68 Haase, A.T. (1999) Population biology of HIV-1 infection: viral and CD4+ T cell demographics and dynamics in lymphatic tissues. *Annu Rev Immunol* 17, 625-656
69 Bonyhadi, M.L.*, et al.* (1993) HIV induces thymus depletion in vivo. *Nature* 363, 728-732
70 Douek, D.C.*, et al.* (1998) Changes in thymic function with age and during the treatment of HIV infection. *Nature* 396, 690-695
71 Giorgi, J.V.*, et al.* (2002) Predictive value of immunologic and virologic markers after long or short duration of HIV-1 infection. *J Acquir Immune Defic Syndr* 29, 346-355
72 Hazenberg, M.D.*, et al.* (2003) Persistent immune activation in HIV-1 infection is associated with progression to AIDS. *AIDS* 17, 1881-1888
73 Butler, S.L.*, et al.* (2011) Disease-modifying therapeutic concepts for HIV in the era of highly active antiretroviral therapy. *J Acquir Immune Defic Syndr* 58, 297-303
74 Sterne, J.A.*, et al.* (2009) Timing of initiation of antiretroviral therapy in AIDS-free HIV-1-infected patients: a collaborative analysis of 18 HIV cohort studies. *Lancet* 373, 1352-1363
75 Reuter, S.*, et al.* (2012) Risk factors associated with older age in treatment-naive HIV-positive patients. *Intervirology* 55, 147-153
76 Schacker, T.W.*, et al.* (2002) Persistent abnormalities in lymphoid tissues of human immunodeficiency virus-infected patients successfully treated with highly active antiretroviral therapy. *J Infect Dis* 186, 1092-1097
77 Estes, J.*, et al.* (2008) Collagen deposition limits immune reconstitution in the gut. *J Infect Dis* 198, 456-464
78 Estes, J.D.*, et al.* (2008) The role of collagen deposition in depleting CD4+ T cells and limiting reconstitution in HIV-1 and SIV infections through damage to the secondary lymphoid organ niche. *Semin Immunol* 20, 181-186

79 Guadalupe, M.*, et al.* (2003) Severe CD4+ T-cell depletion in gut lymphoid tissue during primary human immunodeficiency virus type 1 infection and substantial delay in restoration following highly active antiretroviral therapy. *J Virol* 77, 11708-11717
80 Tedaldi, E.M.*, et al.* (2004) Hepatitis A and B vaccination practices for ambulatory patients infected with HIV. *Clin Infect Dis* 38, 1478-1484
81 Rodriguez-Barradas, M.C.*, et al.* (2003) Response of human immunodeficiency virus-infected patients receiving highly active antiretroviral therapy to vaccination with 23-valent pneumococcal polysaccharide vaccine. *Clin Infect Dis* 37, 438-447
82 Schacker, T.*, et al.* (1998) Frequency of symptomatic and asymptomatic herpes simplex virus type 2 reactivations among human immunodeficiency virus-infected men. *J Infect Dis* 178, 1616-1622
83 Posavad, C.M.*, et al.* (2004) Frequent reactivation of herpes simplex virus among HIV-1-infected patients treated with highly active antiretroviral therapy. *J Infect Dis* 190, 693-696
84 Piketty, C.*, et al.* (2004) High prevalence of anal squamous intraepithelial lesions in HIV-positive men despite the use of highly active antiretroviral therapy. *Sex Transm Dis* 31, 96-99
85 Engels, E.A.*, et al.* (2008) Cancer risk in people infected with human immunodeficiency virus in the United States. *Int J Cancer* 123, 187-194
86 Baker, J.V.*, et al.* (2008) CD4+ count and risk of non-AIDS diseases following initial treatment for HIV infection. *AIDS* 22, 841-848
87 Phillips, A.N.*, et al.* (2008) The role of HIV in serious diseases other than AIDS. *AIDS* 22, 2409-2418
88 Weber, R.*, et al.* (2006) Liver-related deaths in persons infected with the human immunodeficiency virus: the D:A:D study. *Arch Intern Med* 166, 1632-1641
89 Curran, A.*, et al.* (2008) Bacterial pneumonia in HIV-infected patients: use of the pneumonia severity index and impact of current management on incidence, aetiology and outcome. *HIV Med* 9, 609-615
90 Takada, K. and Jameson, S.C. (2009) Naive T cell homeostasis: from awareness of space to a sense of place. *Nat Rev Immunol* 9, 823-832
91 Sprent, J.*, et al.* (2008) T cell homeostasis. *Immunol Cell Biol* 86, 312-319
92 Tan, J.T.*, et al.* (2001) IL-7 is critical for homeostatic proliferation and survival of naive T cells. *Proc Natl Acad Sci U S A* 98, 8732-8737
93 Link, A.*, et al.* (2007) Fibroblastic reticular cells in lymph nodes regulate the homeostasis of naive T cells. *Nat Immunol* 8, 1255-1265
94 Surh, C.D. and Sprent, J. (2008) Homeostasis of naive and memory T cells. *Immunity* 29, 848-862
95 Haynes, B.F.*, et al.* (2000) The role of the thymus in immune reconstitution in aging, bone marrow transplantation, and HIV-1 infection. *Annu Rev Immunol* 18, 529-560
96 den Braber, I.*, et al.* (2012) Maintenance of peripheral naive T cells is sustained by thymus output in mice but not humans. *Immunity* 36, 288-297
97 Haynes, B.F. and Hale, L.P. (1998) The human thymus. A chimeric organ comprised of central and peripheral lymphoid components. *Immunol Res* 18, 175-192

98 Haynes, B.F.*, et al.* (1999) Analysis of the adult thymus in reconstitution of T lymphocytes in HIV-1 infection. *J Clin Invest* 103, 921
99 Wykrzykowska, J.J.*, et al.* (1998) Early regeneration of thymic progenitors in rhesus macaques infected with simian immunodeficiency virus. *J Exp Med* 187, 1767-1778
100 Richardson, M.W.*, et al.* (2004) T-cell receptor excision circles (TREC) in SHIV 89.6p and SIVmac251 models of HIV-1 infection. *DNA Cell Biol* 23, 1-13
101 Hatzakis, A.*, et al.* (2000) Effect of recent thymic emigrants on progression of HIV-1 disease. *Lancet* 355, 599-604
102 Pakker, N.G.*, et al.* (1998) Biphasic kinetics of peripheral blood T cells after triple combination therapy in HIV-1 infection: a composite of redistribution and proliferation. *Nat Med* 4, 208-214
103 Bucy, R.P.*, et al.* (1999) Initial increase in blood CD4(+) lymphocytes after HIV antiretroviral therapy reflects redistribution from lymphoid tissues. *J Clin Invest* 103, 1391-1398
104 Arron, S.T.*, et al.* (2005) Impact of thymectomy on the peripheral T cell pool in rhesus macaques before and after infection with simian immunodeficiency virus. *Eur J Immunol* 35, 46-55
105 Zhang, L.*, et al.* (1999) Measuring recent thymic emigrants in blood of normal and HIV-1-infected individuals before and after effective therapy. *J Exp Med* 190, 725-732
106 Walker, R.E.*, et al.* (1998) Peripheral expansion of pre-existing mature T cells is an important means of CD4+ T-cell regeneration HIV-infected adults. *Nat Med* 4, 852-856
107 Burton, G.F.*, et al.* (1993) Follicular dendritic cells and B cell costimulation. *J Immunol* 150, 31-38
108 Kapasi, Z.F.*, et al.* (1998) Follicular dendritic cell (FDC) precursors in primary lymphoid tissues. *J Immunol* 160, 1078-1084
109 Liu, Y.J.*, et al.* (1992) Germinal centres in T-cell-dependent antibody responses. *Immunol Today* 13, 17-21
110 MacLennan, I.C. (1994) Germinal centers. *Annu Rev Immunol* 12, 117-139
111 MacLennan, I.C. and Gray, D. (1986) Antigen-driven selection of virgin and memory B cells. *Immunol Rev* 91, 61-85
112 Tew, J.G.*, et al.* (1997) Follicular dendritic cells and presentation of antigen and costimulatory signals to B cells. *Immunol Rev* 156, 39-52
113 Thorbecke, G. and Lerman, S.P. (1976) Germinal centers and their role in immune responses. *Adv Exp Med Biol* 73 PT-A, 83-100
114 Gretz, J.E.*, et al.* (1997) Cords, channels, corridors and conduits: critical architectural elements facilitating cell interactions in the lymph node cortex. *Immunol Rev* 156, 11-24
115 Gretz, J.E.*, et al.* (1996) Sophisticated strategies for information encounter in the lymph node: the reticular network as a conduit of soluble information and a highway for cell traffic. *J Immunol* 157, 495-499
116 Kaldjian, E.P.*, et al.* (2001) Spatial and molecular organization of lymph node T cell cortex: a labyrinthine cavity bounded by an epithelium-like monolayer of fibroblastic reticular cells anchored to basement membrane-like extracellular matrix. *Int Immunol* 13, 1243-1253

117 Hayakawa, M.*, et al.* (1988) Direct contact between reticular fibers and migratory cells in the paracortex of mouse lymph nodes: a morphological and quantitative study. *Arch Histol Cytol* 51, 233-240
118 Rathmell, J.C.*, et al.* (2001) IL-7 enhances the survival and maintains the size of naive T cells. *J Immunol* 167, 6869-6876
119 Schluns, K.S.*, et al.* (2000) Interleukin-7 mediates the homeostasis of naive and memory CD8 T cells in vivo. *Nat Immunol* 1, 426-432
120 Sixt, M.*, et al.* (2005) The conduit system transports soluble antigens from the afferent lymph to resident dendritic cells in the T cell area of the lymph node. *Immunity* 22, 19-29
121 Katakai, T.*, et al.* (2004) A novel reticular stromal structure in lymph node cortex: an immuno-platform for interactions among dendritic cells, T cells and B cells. *Int Immunol* 16, 1133-1142
122 Mempel, T.R.*, et al.* (2004) T-cell priming by dendritic cells in lymph nodes occurs in three distinct phases. *Nature* 427, 154-159
123 Gretz, J.E.*, et al.* (2000) Lymph-borne chemokines and other low molecular weight molecules reach high endothelial venules via specialized conduits while a functional barrier limits access to the lymphocyte microenvironments in lymph node cortex. *J Exp Med* 192, 1425-1440
124 Bajenoff, M.*, et al.* (2006) Stromal cell networks regulate lymphocyte entry, migration, and territoriality in lymph nodes. *Immunity* 25, 989-1001
125 Moussion, C. and Girard, J.P. (2011) Dendritic cells control lymphocyte entry to lymph nodes through high endothelial venules. *Nature* 479, 542-546
126 Wendland, M.*, et al.* (2011) Lymph node T cell homeostasis relies on steady state homing of dendritic cells. *Immunity* 35, 945-957
127 Miyasaka, M. and Tanaka, T. (2004) Lymphocyte trafficking across high endothelial venules: dogmas and enigmas. *Nat Rev Immunol* 4, 360-370
128 von Andrian, U.H. and Mempel, T.R. (2003) Homing and cellular traffic in lymph nodes. *Nat Rev Immunol* 3, 867-878
129 Forster, R.*, et al.* (1999) CCR7 coordinates the primary immune response by establishing functional microenvironments in secondary lymphoid organs. *Cell* 99, 23-33
130 Gunn, M.D.*, et al.* (1999) Mice lacking expression of secondary lymphoid organ chemokine have defects in lymphocyte homing and dendritic cell localization. *J Exp Med* 189, 451-460
131 Boyman, O.*, et al.* (2009) Homeostatic proliferation and survival of naive and memory T cells. *Eur J Immunol* 39, 2088-2094
132 Tenner-Racz, K. (1988) Human immunodeficiency virus associated changes in germinal centers of lymph nodes and relevance to impaired B-cell function. *Lymphology* 21, 36-43
133 Graziosi, C.*, et al.* (1993) HIV-1 infection in the lymphoid organs. *AIDS* 7 Suppl 2, S53-58
134 Pantaleo, G. and Fauci, A.S. (1996) Immunopathogenesis of HIV infection. *Annu Rev Microbiol* 50, 825-854

135 Pantaleo, G.*, et al.* (1993) HIV infection is active and progressive in lymphoid tissue during the clinically latent stage of disease. *Nature* 362, 355-358
136 Pantaleo, G.*, et al.* (1993) The role of lymphoid organs in the pathogenesis of HIV infection. *Semin Immunol* 5, 157-163
137 Pantaleo, G.*, et al.* (1993) New concepts in the immunopathogenesis of human immunodeficiency virus infection. *N Engl J Med* 328, 327-335
138 Pantaleo, G.*, et al.* (1993) The role of lymphoid organs in the immunopathogenesis of HIV infection. *AIDS* 7 Suppl 1, S19-23
139 Fauci, A.S.*, et al.* (1996) Immunopathogenic mechanisms of HIV infection. *Ann Intern Med* 124, 654-663
140 Pantaleo, G.*, et al.* (1995) Studies in subjects with long-term nonprogressive human immunodeficiency virus infection. *N Engl J Med* 332, 209-216
141 O'Murchadha, M.T.*, et al.* (1987) The histologic features of hyperplastic lymphadenopathy in AIDS-related complex are nonspecific. *Am J Surg Pathol* 11, 94-99
142 Estes, J.D.*, et al.* (2006) Premature induction of an immunosuppressive regulatory T cell response during acute simian immunodeficiency virus infection. *J Infect Dis* 193, 703-712
143 Estes, J.D.*, et al.* (2007) Simian immunodeficiency virus-induced lymphatic tissue fibrosis is mediated by transforming growth factor beta 1-positive regulatory T cells and begins in early infection. *J Infect Dis* 195, 551-561
144 Schacker, T.W.*, et al.* (2006) Lymphatic tissue fibrosis is associated with reduced numbers of naive CD4+ T cells in human immunodeficiency virus type 1 infection. *Clin Vaccine Immunol* 13, 556-560
145 Schacker, T.W.*, et al.* (2002) Collagen deposition in HIV-1 infected lymphatic tissues and T cell homeostasis. *J Clin Invest* 110, 1133-1139
146 Schacker, T.W.*, et al.* (2005) Amount of lymphatic tissue fibrosis in HIV infection predicts magnitude of HAART-associated change in peripheral CD4 cell count. *AIDS* 19, 2169-2171
147 Diaz, A.*, et al.* (2010) Factors associated with collagen deposition in lymphoid tissue in long-term treated HIV-infected patients. *AIDS*
148 Diaz, A.*, et al.* (2011) Lymphoid tissue collagen deposition in HIV-infected patients correlates with the imbalance between matrix metalloproteinases and their inhibitors. *J Infect Dis* 203, 810-813
149 Fletcher, A.L.*, et al.* (2010) Lymph node fibroblastic reticular cells directly present peripheral tissue antigen under steady-state and inflammatory conditions. *J Exp Med* 207, 689-697
150 Mueller, S.N. and Ahmed, R. (2008) Lymphoid stroma in the initiation and control of immune responses. *Immunol Rev* 224, 284-294
151 Estes, J.D.*, et al.* (2008) Early resolution of acute immune activation and induction of PD-1 in SIV-infected sooty mangabeys distinguishes nonpathogenic from pathogenic infection in rhesus macaques. *J Immunol* 180, 6798-6807
152 Li, Q.*, et al.* (2005) Peak SIV replication in resting memory CD4+ T cells depletes gut lamina propria CD4+ T cells. *Nature* 434, 1148-1152

153 Lawrence, J.B. and Singer, R.H. (1986) Intracellular localization of messenger RNAs for cytoskeletal proteins. *Cell* 45, 407-415
154 St Johnston, D. (1995) The intracellular localization of messenger RNAs. *Cell* 81, 161-170
155 Napolitano, L.A.*, et al.* (2001) Increased production of IL-7 accompanies HIV-1-mediated T-cell depletion: implications for T-cell homeostasis. *Nat Med* 7, 73-79
156 Ohshima, Y.*, et al.* (1999) Naive human CD4+ T cells are a major source of lymphotoxin alpha. *J Immunol* 162, 3790-3794
157 Katakai, T.*, et al.* (2004) Lymph node fibroblastic reticular cells construct the stromal reticulum via contact with lymphocytes. *J Exp Med* 200, 783-795
158 Hulmes, D.J. (2002) Building collagen molecules, fibrils, and suprafibrillar structures. *J Struct Biol* 137, 2-10
159 Lamande, S.R. and Bateman, J.F. (1999) Procollagen folding and assembly: the role of endoplasmic reticulum enzymes and molecular chaperones. *Semin Cell Dev Biol* 10, 455-464
160 Silver, F.H.*, et al.* (2003) Collagen self-assembly and the development of tendon mechanical properties. *J Biomech* 36, 1529-1553
161 Border, W.A. and Noble, N.A. (1994) Transforming growth factor beta in tissue fibrosis. *N Engl J Med* 331, 1286-1292
162 Border, W.A. and Ruoslahti, E. (1992) Transforming growth factor-beta in disease: the dark side of tissue repair. *J Clin Invest* 90, 1-7
163 Gressner, A.M.*, et al.* (2002) Roles of TGF-beta in hepatic fibrosis. *Front Biosci* 7, d793-807
164 Li, Q.*, et al.* (2009) Microarray analysis of lymphatic tissue reveals stage-specific, gene expression signatures in HIV-1 infection. *J Immunol* 183, 1975-1982
165 Bigg, H.F.*, et al.* (2006) The mammalian chitinase-like lectin, YKL-40, binds specifically to type I collagen and modulates the rate of type I collagen fibril formation. *J Biol Chem* 281, 21082-21095
166 Iwata, T.*, et al.* (2009) YKL-40 secreted from adipose tissue inhibits degradation of type I collagen. *Biochem Biophys Res Commun* 388, 511-516
167 Mizoguchi, E. (2006) Chitinase 3-like-1 exacerbates intestinal inflammation by enhancing bacterial adhesion and invasion in colonic epithelial cells. *Gastroenterology* 130, 398-411
168 Recklies, A.D.*, et al.* (2005) Inflammatory cytokines induce production of CHI3L1 by articular chondrocytes. *J Biol Chem* 280, 41213-41221
169 Stanley, S.K.*, et al.* (1993) Human immunodeficiency virus infection of the human thymus and disruption of the thymic microenvironment in the SCID-hu mouse. *J Exp Med* 178, 1151-1163
170 Rabin, R.L.*, et al.* (1995) Altered representation of naive and memory CD8 T cell subsets in HIV-infected children. *J Clin Invest* 95, 2054-2060
171 Woods, T.C.*, et al.* (1997) Loss of inducible virus in CD45RA naive cells after human immunodeficiency virus-1 entry accounts for preferential viral replication in CD45RO memory cells. *Blood* 89, 1635-1641

172 Nie, C.*, et al.* (2009) Selective infection of CD4+ effector memory T lymphocytes leads to preferential depletion of memory T lymphocytes in R5 HIV-1-infected humanized NOD/SCID/IL-2Rgammanull mice. *Virology* 394, 64-72
173 Schnittman, S.M.*, et al.* (1990) Preferential infection of CD4+ memory T cells by human immunodeficiency virus type 1: evidence for a role in the selective T-cell functional defects observed in infected individuals. *Proc Natl Acad Sci U S A* 87, 6058-6062
174 Fry, T.J.*, et al.* (2003) IL-7 therapy dramatically alters peripheral T-cell homeostasis in normal and SIV-infected nonhuman primates. *Blood* 101, 2294-2299
175 Leone, A.*, et al.* (2010) Increased CD4+ T cell levels during IL-7 administration of antiretroviral therapy-treated simian immunodeficiency virus-positive macaques are not dependent on strong proliferative responses. *J Immunol* 185, 1650-1659
176 Levy, Y.*, et al.* (2009) Enhanced T cell recovery in HIV-1-infected adults through IL-7 treatment. *J Clin Invest* 119, 997-1007
177 Sportes, C.*, et al.* (2008) Administration of rhIL-7 in humans increases in vivo TCR repertoire diversity by preferential expansion of naive T cell subsets. *J Exp Med* 205, 1701-1714
178 Vassena, L.*, et al.* (2007) Interleukin 7 reduces the levels of spontaneous apoptosis in CD4+ and CD8+ T cells from HIV-1-infected individuals. *Proc Natl Acad Sci U S A* 104, 2355-2360
179 Site., N.I.o.H.C.T.W. (Updated August 25, 2010) *http://clinicaltrials.gov/ct2/show/NCT00080223* Accessed September 25, 2010
180 Andersson, J.*, et al.* (1998) Early reduction of immune activation in lymphoid tissue following highly active HIV therapy. *AIDS* 12, F123-129
181 Lewden, C.*, et al.* (2005) Causes of death among human immunodeficiency virus (HIV)-infected adults in the era of potent antiretroviral therapy: emerging role of hepatitis and cancers, persistent role of AIDS. *Int J Epidemiol* 34, 121-130
182 Barbaro, G. and Barbarini, G. (2007) HIV infection and cancer in the era of highly active antiretroviral therapy (Review). *Oncol Rep* 17, 1121-1126
183 Martin, M.*, et al.* (2001) Limited immune reconstitution at intermediate stages of HIV-1 infection during one year of highly active antiretroviral therapy in antiretroviral-naive versus non-naive adults. *Eur J Clin Microbiol Infect Dis* 20, 871-879
184 Gea-Banacloche, J.C. and Clifford Lane, H. (1999) Immune reconstitution in HIV infection. *AIDS* 13 Suppl A, S25-38
185 Engels, E.A.*, et al.* (2006) Elevated incidence of lung cancer among HIV-infected individuals. *J Clin Oncol* 24, 1383-1388
186 Grulich, A.E.*, et al.* (2007) Incidence of cancers in people with HIV/AIDS compared with immunosuppressed transplant recipients: a meta-analysis. *Lancet* 370, 59-67
187 Palefsky, J.M.*, et al.* (2005) Anal intraepithelial neoplasia in the highly active antiretroviral therapy era among HIV-positive men who have sex with men. *AIDS* 19, 1407-1414

188 Kaufmann, G.R.*, et al.* (2003) CD4 T-lymphocyte recovery in individuals with advanced HIV-1 infection receiving potent antiretroviral therapy for 4 years: the Swiss HIV Cohort Study. *Arch Intern Med* 163, 2187-2195
189 Sempowski, G.D. and Haynes, B.F. (2002) Immune reconstitution in patients with HIV infection. *Annu Rev Med* 53, 269-284
190 Zeng, M.*, et al.* (2011) Cumulative mechanisms of lymphoid tissue fibrosis and T cell depletion in HIV-1 and SIV infections. *J Clin Invest* 121, 998–1008
191 Kaufmann, G.R.*, et al.* (2002) The extent of HIV-1-related immunodeficiency and age predict the long-term CD4 T lymphocyte response to potent antiretroviral therapy. *AIDS* 16, 359-367
192 Kroncke, R.*, et al.* (1996) Human follicular dendritic cells and vascular cells produce interleukin-7: a potential role for interleukin-7 in the germinal center reaction. *Eur J Immunol* 26, 2541-2544
193 Zhou, Y.W.*, et al.* (2003) Murine lymph node-derived stromal cells effectively support survival but induce no activation/proliferation of peripheral resting T cells in vitro. *Immunology* 109, 496-503
194 Ho, D.D.*, et al.* (1995) Rapid turnover of plasma virions and CD4 lymphocytes in HIV-1 infection. *Nature* 373, 123-126
195 Gao, X.*, et al.* (2009) Angiotensin II increases collagen I expression via transforming growth factor-beta1 and extracellular signal-regulated kinase in cardiac fibroblasts. *Eur J Pharmacol* 606, 115-120
196 Moreno, M.*, et al.* (2010) Reduction of advanced liver fibrosis by short-term targeted delivery of an angiotensin receptor blocker to hepatic stellate cells in rats. *Hepatology* 51, 942-952
197 Yao, H.W.*, et al.* (2006) Losartan attenuates bleomycin-induced pulmonary fibrosis in rats. *Respiration* 73, 236-242
198 Taniguchi, H.*, et al.* (2010) Pirfenidone in idiopathic pulmonary fibrosis. *Eur Respir J* 35, 821-829
199 Azuma, A. (2010) Pirfenidone: antifibrotic agent for idiopathic pulmonary fibrosis. *Expert Rev Respir Med* 4, 301-310
200 Diop-Frimpong, B.*, et al.* (2011) Losartan inhibits collagen I synthesis and improves the distribution and efficacy of nanotherapeutics in tumors. *Proc Natl Acad Sci U S A* 108, 2909-2914
201 Bottieau, E.*, et al.* (2003) Multiple tuberculous brain abscesses in an HIV-infected patient successfully treated with HAART and antituberculous treatment. *Infection* 31, 118-120
202 Benveniste, O.*, et al.* (2005) Mechanisms involved in the low-level regeneration of CD4+ cells in HIV-1-infected patients receiving highly active antiretroviral therapy who have prolonged undetectable plasma viral loads. *J Infect Dis* 191, 1670-1679
203 Piketty, C.*, et al.* (1998) Discrepant responses to triple combination antiretroviral therapy in advanced HIV disease. *Aids* 12, 745-750
204 Guadalupe, M.*, et al.* (2006) Viral suppression and immune restoration in the gastrointestinal mucosa of human immunodeficiency virus type 1-infected patients initiating therapy during primary or chronic infection. *J Virol* 80, 8236-8247

205 Mehandru, S.*, et al.* (2006) Lack of mucosal immune reconstitution during prolonged treatment of acute and early HIV-1 infection. *PLoS Med* 3, e484
206 Brenchley, J.M.*, et al.* (2004) CD4+ T cell depletion during all stages of HIV disease occurs predominantly in the gastrointestinal tract. *J Exp Med* 200, 749-759
207 Engels, E.A. (2007) Infectious agents as causes of non-Hodgkin lymphoma. *Cancer Epidemiol Biomarkers Prev* 16, 401-404
208 Mackall, C.L.*, et al.* (1997) T-cell regeneration: all repertoires are not created equal. *Immunol Today* 18, 245-251
209 Hakim, F.T.*, et al.* (1997) Constraints on CD4 recovery postchemotherapy in adults: thymic insufficiency and apoptotic decline of expanded peripheral CD4 cells. *Blood* 90, 3789-3798
210 Poulin, J.F.*, et al.* (2003) Evidence for adequate thymic function but impaired naive T-cell survival following allogeneic hematopoietic stem cell transplantation in the absence of chronic graft-versus-host disease. *Blood* 102, 4600-4607
211 Patel, D.D.*, et al.* (2000) Thymic function after hematopoietic stem-cell transplantation for the treatment of severe combined immunodeficiency. *N Engl J Med* 342, 1325-1332
212 Williams, K.M.*, et al.* (2007) T cell immune reconstitution following lymphodepletion. *Semin Immunol* 19, 318-330
213 Evans, T.G.*, et al.* (1998) Highly active antiretroviral therapy results in a decrease in CD8+ T cell activation and preferential reconstitution of the peripheral CD4+ T cell population with memory rather than naive cells. *Antiviral Res* 39, 163-173
214 Zeng, M.*, et al.* (2012) Lymphoid Tissue Damage in HIV-1 Infection Depletes Naive T Cells and Limits T Cell Reconstitution after Antiretroviral Therapy. *PLoS Pathog* 8, e1002437
215 Tumanov, A.*, et al.* (2002) Distinct role of surface lymphotoxin expressed by B cells in the organization of secondary lymphoid tissues. *Immunity* 17, 239-250
216 Gommerman, J.L.*, et al.* (2002) Manipulation of lymphoid microenvironments in nonhuman primates by an inhibitor of the lymphotoxin pathway. *J Clin Invest* 110, 1359-1369
217 Mackay, F. and Browning, J.L. (1998) Turning off follicular dendritic cells. *Nature* 395, 26-27
218 Mackay, F.*, et al.* (1997) Lymphotoxin but not tumor necrosis factor functions to maintain splenic architecture and humoral responsiveness in adult mice. *Eur J Immunol* 27, 2033-2042
219 Ngo, V.N.*, et al.* (1999) Lymphotoxin alpha/beta and tumor necrosis factor are required for stromal cell expression of homing chemokines in B and T cell areas of the spleen. *J Exp Med* 189, 403-412
220 Silvestri, G. (2008) AIDS pathogenesis: a tale of two monkeys. *J Med Primatol* 37 Suppl 2, 6-12
221 Engram, J.C.*, et al.* (2010) Lineage-specific T-cell reconstitution following in vivo CD4+ and CD8+ lymphocyte depletion in nonhuman primates. *Blood* 116, 748-758

222 Libri, V.*, et al.* (2011) Cytomegalovirus infection induces the accumulation of short-lived, multifunctional CD4+CD45RA+CD27+ T cells: the potential involvement of interleukin-7 in this process. *Immunology* 132, 326-339
223 Zhang, Z.Q.*, et al.* (1999) Reversibility of the pathological changes in the follicular dendritic cell network with treatment of HIV-1 infection. *Proc Natl Acad Sci U S A* 96, 5169-5172
224 van den Brink, M.R.*, et al.* (2004) Strategies to enhance T-cell reconstitution in immunocompromised patients. *Nat Rev Immunol* 4, 856-867
225 Di Mascio, M.*, et al.* (2006) Naive T-cell dynamics in human immunodeficiency virus type 1 infection: effects of highly active antiretroviral therapy provide insights into the mechanisms of naive T-cell depletion. *J Virol* 80, 2665-2674
226 Connors, M.*, et al.* (1997) HIV infection induces changes in CD4+ T-cell phenotype and depletions within the CD4+ T-cell repertoire that are not immediately restored by antiviral or immune-based therapies. *Nat Med* 3, 533-540
227 Nishimura, Y.*, et al.* (2007) Loss of naive cells accompanies memory CD4+ T-cell depletion during long-term progression to AIDS in Simian immunodeficiency virus-infected macaques. *J Virol* 81, 893-902
228 Khoury, G.*, et al.* (2011) The role of naive T-cells in HIV-1 pathogenesis: an emerging key player. *Clin Immunol* 141, 253-267
229 Rickabaugh, T.M.*, et al.* (2011) The dual impact of HIV-1 infection and aging on naive CD4 T-cells: additive and distinct patterns of impairment. *PLoS One* 6, e16459
230 Prescott, L.M. (1995) Loss of naive T cells may play major role in weakened immune response. *J Int Assoc Physicians AIDS Care* 1, 32
231 Okoye, A.A.*, et al.* (2012) Naive T cells are dispensable for memory CD4+ T cell homeostasis in progressive simian immunodeficiency virus infection. *J Exp Med* 209, 641-651
232 Mackay, F.*, et al.* (1996) Lymphotoxin beta receptor triggering induces activation of the nuclear factor kappaB transcription factor in some cell types. *J Biol Chem* 271, 24934-24938
233 Gramaglia, I.*, et al.* (1999) Lymphotoxin alphabeta is expressed on recently activated naive and Th1-like CD4 cells but is down-regulated by IL-4 during Th2 differentiation. *J Immunol* 162, 1333-1338
234 Kitahata, M.M.*, et al.* (2009) Effect of early versus deferred antiretroviral therapy for HIV on survival. *N Engl J Med* 360, 1815-1826
235 Opravil, M.*, et al.* (2002) Clinical efficacy of early initiation of HAART in patients with asymptomatic HIV infection and CD4 cell count > 350 x 10(6) /l. *AIDS* 16, 1371-1381
236 Giri, S.N.*, et al.* (1997) Antifibrotic effect of decorin in a bleomycin hamster model of lung fibrosis. *Biochem Pharmacol* 54, 1205-1216
237 Munger, J.S.*, et al.* (1999) The integrin alpha v beta 6 binds and activates latent TGF beta 1: a mechanism for regulating pulmonary inflammation and fibrosis. *Cell* 96, 319-328
238 Nakao, A.*, et al.* (1999) Transient gene transfer and expression of Smad7 prevents bleomycin-induced lung fibrosis in mice. *J Clin Invest* 104, 5-11

239 Bonniaud, P.*, et al.* (2005) Progressive transforming growth factor beta1-induced lung fibrosis is blocked by an orally active ALK5 kinase inhibitor. *Am J Respir Crit Care Med* 171, 889-898
240 Scandella, E.*, et al.* (2008) Restoration of lymphoid organ integrity through the interaction of lymphoid tissue-inducer cells with stroma of the T cell zone. *Nat Immunol* 9, 667-675

Appendix

Reprint permissions

Copyright Clearance Center

1 PAYMENT 2 REVIEW 3 CONFIRMATION

Step 3: Order Confirmation

Thank you for your order! A confirmation for your order will be sent to your account email address. If you have questions about your order, you can call us at 978-646-2600, M-F between 8:00 AM and 6:00 PM (Eastern), or write to us at info@copyright.com.

Confirmation Number: 10999079
Order Date: 05/21/2012

If you pay by credit card, your order will be finalized and your card will be charged within 24 hours. If you pay by invoice, you can change or cancel your order until the invoice is generated.

Payment Information

Ming Zeng
zengx038@umn.edu
+1 (612)6244649
Payment Method: CC ending in 2019

Order Details

The journal of clinical investigation

Order detail ID:	62473308
ISSN:	0021-9738
Publication year:	2011
Publication Type:	Journal
Publisher:	AMERICAN SOCIETY FOR CLINICAL INVESTIGATION
Rightsholder:	AMERICAN SOCIETY FOR CLINICAL INVESTIGATION
Author/Editor:	Ming Zeng and Ashley Haase
Your reference:	Ming's thesis

Permission Status: Granted

Permission type:	Republish or display content
Type of use:	Republish in a dissertation
Republication title:	Lymphoid Tissue Damage in HIV and SIV Infections Depletes Naive T Cells and Limits Immune Reconstitution after Anti-retroviral Therapy
Republishing organization:	University of Minnesota
Organization status:	Non-profit 501(c)(3)
Republication date:	05/31/2012
Circulation/ Distribution:	10
Type of content:	Full article/chapter
Description of requested content:	Portion of text and all figures
Page range(s):	998-1008
Translating to:	No Translation
Requested content's publication date:	03/01/2011

Rightsholder terms apply (see terms and conditions)

$ 3.50

ELSEVIER LICENSE
TERMS AND CONDITIONS

May 30, 2012

This is a License Agreement between Ming Zeng ("You") and Elsevier ("Elsevier") provided by Copyright Clearance Center ("CCC"). The license consists of your order details, the terms and conditions provided by Elsevier, and the payment terms and conditions.

All payments must be made in full to CCC. For payment instructions, please see information listed at the bottom of this form.

Supplier	Elsevier Limited The Boulevard,Langford Lane Kidlington,Oxford,OX5 1GB,UK
Registered Company Number	1982084
Customer name	Ming Zeng
Customer address	University of Minnesota Minneapolis, MN 55455
License number	2918961054923
License date	May 30, 2012
Licensed content publisher	Elsevier
Licensed content publication	Trends in Immunology
Licensed content title	Lymphoid tissue structure and HIV-1 infection: life or death for T cells
Licensed content author	Ming Zeng,Ashley T. Haase,Timothy W. Schacker
Licensed content date	June 2012
Licensed content volume number	33
Licensed content issue number	6
Number of pages	9
Start Page	306
End Page	314
Type of Use	reuse in a thesis/dissertation
Portion	full article
Format	both print and electronic
Are you the author of this	Yes

Elsevier article?	
Will you be translating?	No
Order reference number	
Title of your thesis/dissertation	Lymphoid Tissue Damage in HIV and SIV Infections Depletes Naive T Cells and Limits Immune Reconstitution after Anti-retroviral Therapy
Expected completion date	May 2012
Estimated size (number of pages)	200
Elsevier VAT number	GB 494 6272 12
Permissions price	0.00 USD
VAT/Local Sales Tax	0.0 USD / 0.0 GBP
Total	0.00 USD
Terms and Conditions	